International Journal of

Communications, Network and System Sciences

ISSN: 1913-3715

Volume 2, Number 4, July 2009

www.scirp.org/journal/ijcns/

Scientific Research

JOURNAL EDITORIAL BOARD

ISSN 1913-3715 (Print) ISSN 1913-3723 (Online)
Http://www.scirp.org/journal/ijcns/

Int. J. Communications, Network and System Sciences, **2009, 4, 249-324**
Published Online July 2009 in SciRes (http://www.SciRP.org/journal/ijcns/).

TABLE OF CONTENTS

Volume 2 Number 4 July 2009

International Journal of Communications, Network and System Sciences (IJCNS)

Journal Information

SUBSCRIPTIONS

The *International Journal of Communications, Network and System Sciences* (Online at Scientific Research Publishing, www.SciRP.org) is published monthly by Scientific Research Publishing, Inc., USA.

E-mail: ijcns@scirp.org

Subscription rates: Volume 2 2009
Print: $50 per copy.
Electronic: free, available on www.SciRP.org.
To subscribe, please contact Journals Subscriptions Department, E-mail: ijcns@scirp.org

Sample copies: If you are interested in subscribing, you may obtain a free sample copy by contacting Scientific Research Publishing, Inc at the above address.

SERVICES

Advertisements
Advertisement Sales Department, E-mail: ijcns@scirp.org

Reprints (minimum quantity 100 copies)
Reprints Co-ordinator, Scientific Research Publishing, Inc., USA.
E-mail: ijcns@scirp.org

COPYRIGHT

PRODUCTION INFORMATION

For manuscripts that have been accepted for publication, please contact:
E-mail: ijcns@scirp.org

Int. J. Communications, Network and System Sciences, **2009, 4, 249-324**
doi:10.4236/ijcns.2009.24027 Published Online July 2009 (http://www.SciRP.org/journal/ijcns/).

Self-Encoded Multiple Access Multiuser Convolutional Codes in Uplink and Downlink Cellular Systems

Jong Hak JUNG, Won Mee JANG, Lim NGUYEN
University of Nebraska-Lincoln, Omaha, NE, USA
Email: *jjung@mail.unomaha.edu*, {*wjang*1, *lnguyen*1}*@unl.edu*
Received March 9, 2009; *revised May* 5, 2009; *accepted June* 20, 2009

ABSTRACT

Self-encoded spread spectrum eliminates the need for traditional pseudo noise (PN) code generators. In a self-encoded multiple access (SEMA) system, the number of users is not limited by the number of available sequences, unlike code division multiple access (CDMA) systems that employ PN codes such as m-, Gold or Kassami sequences. SEMA provides a convenient way of supporting multi-rate, multi-level grades of service in multimedia communications and prioritized heterogeneous networking systems. In this paper, we propose multiuser convolutional channel coding in SEMA that provides fewer cross-correlations among users and thereby reducing multiple access interference (MAI). We analyze SEMA multiuser convolutional coding in additive white Gaussian noise (AWGN) channels as well as fading channels. Our analysis includes downlink synchronous system as well as asynchronous system such as uplink mobile-to-base station communication.

Keywords: Spread Spectrum, Self-Encoded Multiple Access, Multiuser Convolutional Coding, Multiuser Detection

1. Introduction

In CDMA communications, each user is assigned a unique PN spreading sequence that has a low cross-correlation with other users' sequences. This prevents code collisions between the users and controls MAI. PN code generators are typically linear feedback shift register circuits that generate maximal-length or related sequences. These deterministic sequences provide low cross-correlations that are critical for achieving good system performance. Although random codes have often been employed for analysis purposes [1], they present a practical implementation problem because data recovery by the intended receiver requires a prior knowledge of the codes for signal despreading. As a result, the random codes in these studies would remain fixed once they have been generated. In previous work, we have proposed a novel spread spectrum technique that does not use PN codes [2]. The new technique is unique in that traditional transmit and receive PN code generators are not needed.

Our approach abandons the use of PN codes in SEMA that can reduce MAI, and provide a multi-rate and multi-level grade of service for multimedia communications and prioritized networks [3–6]. A realization of the self-encoding principle for a direct sequence spread spectrum systems is illustrated in Figure 1. As the term implies, the spreading code is obtained from the random digital information source itself. At the transmitter, the delay registers are constantly updated from v-tap, serial delay of the data, where v is the code length. The delay registers generate the code chips that switch at v times the data rate for signal spreading. The random nature of the digital information source means that binary symbols can be modeled as independent and identically distributed Bernoulli random variables. Symbol values of +1 and -1 occur equally likely with a probability of 0.5. As a result, the spreading sequences are not only randomly generated and independent of the current symbol, but also dynamically changing from one symbol to the next. This smoothes out the spectrum of the signals and eliminates the spectral lines associated with PN sequences. The self-encoding operation at the transmitter is reversed at the receiver. The recovered data are fed back to the v-tap delay registers, which provide an estimation of the

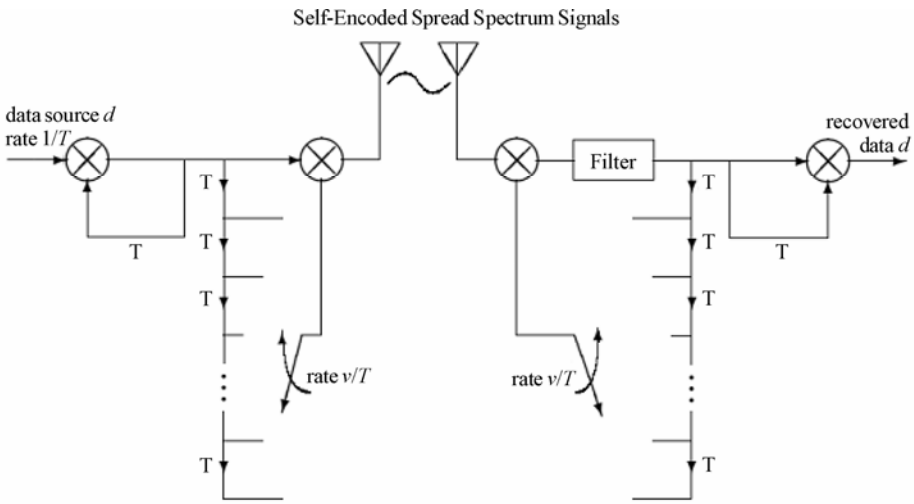

Figure 1. Self-encoded, direct-sequence spread spectrum.

Transmitte's spreading codes required for signal despreading. Data recovery is by means of a correlation detector. Notice that the contents of the delay registers in the transmitter and receiver should be identical at the start of the transmission. This is accomplished as part of the initial synchronization procedure. In the following, we develop SEMA multiuser convolutional coding, and investigate the performance with and without precoding or multiuser detection. Convolutional codes with Viterbi decoding have been studied for decades and applied in practical communication systems such as wide area networks (IS-95, CDMA2000) and local area networks (IEEE 802.11a and b). In order to improve the performance, we present the shift generator matrix concept that provides lower cross-correlations among users and reduces the MAI in the system. We present the performance analysis and simulation both in uplink asynchronous and downlink synchronous channels.

2. System Model

2.1. SEMA System and Multiuser Convolutional Coding

Figure 2 shows the block diagram of SEMA with multiuser detection and channel coding. The SEMA spread block is as illustrated in Figure 1. Notice that the detection errors may accumulate in the delay registers and are the source of self-interference (SI) in the receiver.

Acquisition and tracking of self-encoded sequences can be performed in a similar manner to PN sequences with the proviso that the chip updates are enabled once data transmission has commenced following code acquisition. At the chip rate, the self-encoded chips are latched at the output register by shifting the registers serially, with the output being fed back to the input register. The input feedback is switched to the data during the last chip period of the current symbol for a new chip input. This resembles a simple linear feedback register circuit of length v, with zero valued taps except for the input and output taps, where the input register is updated periodically by the data and the output register provides the spreading sequence.

The conventional convolutional codes in Figure 2 applied to single user self-encoded spread spectrum significantly reduce SI due to detection errors in the despreading registers at the receiver. However, under SEMA these codes generate the same code words for different users and may lead to code collisions. We propose to mitigate this problem with shift generator matrix for SEMA multiuser convolutional coding. For example, if the first user employs the generator matrix given in octal form, G1=[5 7 7], the second and the third user can use G2=[7 5 7] and G3=[7 7 5], respectively. The property of G2 and G3 is identical to G1 in that they have the same weight transfer function and maximum free distance, d_{free}. This method guarantees the maximum free distance per single user and provides lower cross-correlations among the users. Figure 3 compares the cross-correlation of code words from generator matrix G1 and its shift generator matrices, G1 and G2, in two user systems. The plots show that cross-correlations of the codes using the shift generator matrices are smaller than those with the same matrix [4].

2.2. Matched Filter Receiver

For a multiuser system with K +1 users (K interferers), the received signal at the matched filter is

$$r(t) = x(t) + \eta(t) \quad \textbf{(1)}$$

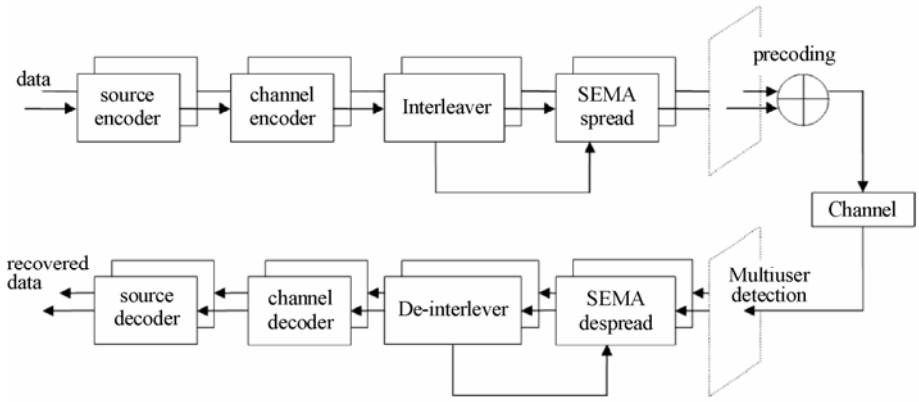

Figure 2. Self-encoded multiple access (SEMA) with channel coding.

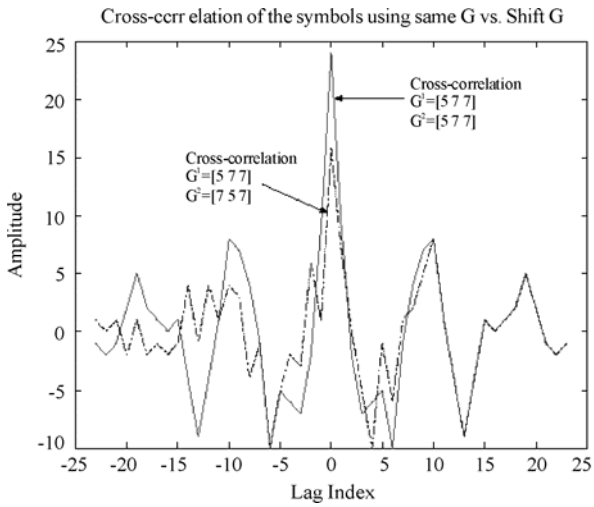

Figure 3. Cross-correlations of the same generator matrix and shifted generator matrices in SEMA.

where x(t) is the transmitted signal, and η(t) is AWGN noise with a two-sided power spectral density of $\delta^2 = N_o/2$. The transmitted signal in Equation (1) is given by

$$x(t) = \sum_{i=-\infty}^{\infty}\sum_{j=0}^{K} A_j s^j(t - iT_s - \tau_j) h_j^i \quad \textbf{(2)}$$

where T_s is the symbol duration and $s^j(t)$ is a spreading sequence during T_s for the jth user. A_j is the amplitudes of the jth user, h_i^j is the encoded symbol of the jth user during the ith symbol interval, and τ_j is the time delay of jth user signal, with $0 \leqslant \tau_j \leqslant T_s$ τ_j is zero for synchronous systems. For simplicity we do not consider carrier offset in uplink asynchronous systems. The output of the convolutional encoder h_i^j for j^{th} user and i^{th} symbol is given by [7]

$$h_i^j = \sum_{l=0}^{m} b_{i-l}^j G_i^{j,(l)} \quad \textbf{(3)}$$

where b_j and $G_i^{j,(l)}$ are the set of the jth user data sequences and the indices denoting the lth column and i^{th} row in the generator matrix, respectively. The generator matrix is

$$G^j = \begin{bmatrix} G_0^{j,(0)} & G_0^{j,(1)} & \cdots & G_0^{j,(m)} \\ G_1^{j,(0)} & G_1^{j,(1)} & \cdots & G_1^{j,(m)} \\ G_r^{j,(0)} & G_r^{j,(1)} & \cdots & G_r^{j,(m)} \end{bmatrix} \quad \textbf{(4)}$$

where m is the memory size in the encoder, and r is the code rate.

Assuming that the signature waveforms have unit energy, the output of the matched filters of the jth user signature waveform during the ith symbol interval is

$$\begin{aligned} y_i^j &= \int_{iT_s+\tau_j}^{(i+1)T_s+\tau_j} r(t) s^j(t - iT_s - \tau_j) dt \\ &= A_j h_i^j + \sum_{p=0, p\neq j}^{K} A_p R_i^{j,p} h_i^p + \delta\eta \end{aligned} \quad \textbf{(5)}$$

Equation (5) consists of the signal $A_j h_i^j$, Gaussian noise $\delta\eta$, and the multiple access interference $\sum A_p R_i^{j,p} h_i^p$. $R_i^{j,P}$ is the cross-correlation of the spreading sequences of the jth user and p^{th} user during the ith symbol interval. In our analysis, the MAI is modeled as noise [8].

At the receiver, the despreading codes are updated by the detected data. If the data are incorrectly recovered, the incoming signals are correlated with an erroneous sequence set. This may lead to additional errors at the receiver and cause SI, which can be serious at a low signal-to-noise ratio (SNR). To combat self-interference, a longer spreading sequence is desired [3]. We will show that powerful error correcting code can also reduce SI.

2.3. Precoding and Multiuser Detection

Precoding: Decorrelating and precoding techniques have been developed for multiuser detections [6,8,9]. Decorrelating detector is used for multiuser detection at the receiver, whereas precoding is employed at the transmitter to eliminate or reduce MAI. To reduce MAI, we examine the precoding system with interleaver. From Equations (1) and (2), we consider a synchronous system and rewrite (2) as

$$x(t)=\sum_{i=0}^{K}A_i s_i(t)h_i=\mathbf{s}^T(t)\mathbf{Ah},\quad 0\leqslant t\leqslant T_b \tag{6}$$

where $\mathbf{s}(t)=\{s_1(t),\cdots s_{K+1}(t)\}^T$ is the signature waveforms vector, and $\mathbf{s}^T(t)$ is the transpose of $\mathbf{s}(t)$. Then, the output of the matched filters can be expressed as

$$y_i=\int_0^{T_b} r_i(t)s_i(t)dt,\quad i=1,\cdots K+1 \tag{7}$$

Equation (7) can be rewritten in a vector form, with $\hat{y}=\{y_1,\cdots y_{K+1}\}$ as follows

$$\hat{\mathbf{y}}=\mathbf{RAbh}+\boldsymbol{\eta} \tag{8}$$

A is the diagonal matrix of amplitudes, **R** is the cross-correlation matrix, and **h** is the vector of the data symbols of K+1 users. The basic concept of precoding is to eliminate MAI at the receiver before transmitting signals. In other words, the transmit signals in Equation (2) become

$$x(t)=\mathbf{s}^T(t)\mathbf{TAh} \tag{9}$$

where the precode matrix **T** is chosen as $\mathbf{T}=\mathbf{R}^{-1}$. Then, the output of the bank of matched filters at the receiver will be

$$\bar{\mathbf{y}}=\mathbf{RTAh}+\boldsymbol{\eta}=\mathbf{Ah}+\boldsymbol{\eta} \tag{10}$$

In order to maintain the average power with precoding the same as without precoding, we modify the precode transformation matrix as [6,8,10]

$$\mathbf{T}=\sqrt{C}\mathbf{R}^{-1} \tag{11}$$

such that

$$C=\frac{\sum_{i=1}^{K+1}A_i^2}{\sum_{i=1}^{K+1}A_i^2R_{i,i}^{-1}} \tag{12}$$

Multiuser Detection: Decorrelation detection is a suboptimal multiuser detection with comparatively low complexity. Receiver-based decorrelator can be found in [11]:

$$\tilde{\mathbf{y}}=\mathbf{R}^{-1}\hat{\mathbf{y}}=\mathbf{R}^{-1}(\mathbf{RAh}+\boldsymbol{\eta})=\mathbf{Ah}+\mathbf{R}^{-1}\boldsymbol{\eta} \tag{13}$$

3. Performance Analysis

3.1. Self-Interference in SEMA

Due to detection errors, the despreading sequence may not be identical to the spreading sequence at the transmitter. Since the recovered symbols are used to despread the signals, a chip error will remain in the shift registers and affect the following symbol decision until it is shifted out of the registers. This results in error propagation and causes SI: the bit error rate (BER) of SEMA is a dynamic quantity that depends on the signal-to-noise ratio (SNR), spreading factor, the number of users and transmitted symbols. The effect of SI is reduced as the spreading factor or the SNR increases.

The average bit error probability, P_b, can be described by a Bernoulli distribution in terms of v and l, where l is the number of chip errors in the despreading registers and v is the spreading length. When v is large, the BER of SEMA can be well approximated by [12,13]

$$P_b=\sum_{l=0}^{v}P_{b|l}\binom{v}{l}P_b^l(1-P_b)^{v-l} \tag{14}$$

where the conditional bit error probability is

$$P_{b|l}=Q\left(\sqrt{\frac{2E_b}{N_o}\left(1-\frac{2l}{v}\right)^2}\right) \tag{15}$$

To ameliorate the effect of error propagation, differential encoding as shown in Figure 1 was proposed and analyzed in [13]. Figure 4 shows the performance with and without differential encoding for a spreading length of 8. The effect of error propagation was analyzed by averaging 100 simulation runs of 10,000 bits, followed by 100, 000 bits. The results demonstrate that differential encoding eliminates the effect of error propagation on the BERs. Figure 5 shows the BER performance with differential encoding for various values of spreading length. We can see that the effect of SI is negligible for $E_b/N_o\geqslant$2dB for the spreading length larger than 4. Since l is equal to the number of bit errors in a v bit se-

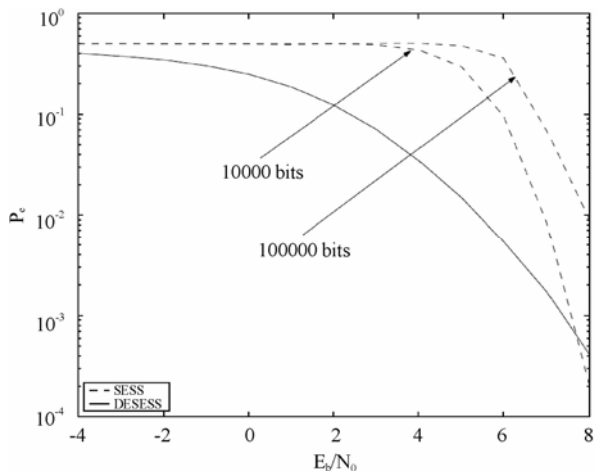

Figure 4. Comparison of BER of Self-encoded spread spectrum (SESS) and differentially encoded SESS (DESESS), reproduced from [13].

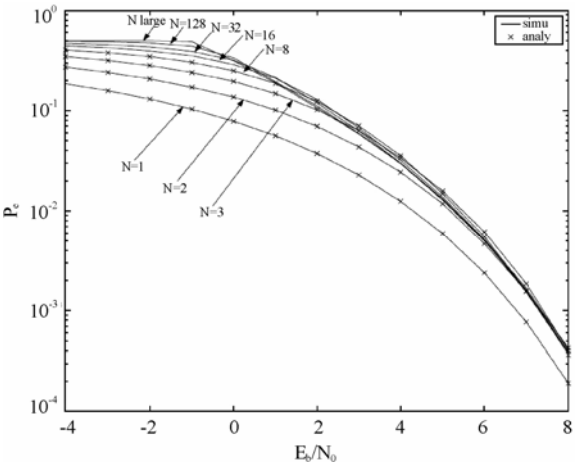

Figure 5. BER of SESS with differential encoding where N is the spreading length, reproduced from [13].

quence, as $v \to \infty$ we have $l/v \to P_b$. Therefore, with differential encoding, the BER for large spreading length approaches the following

$$P_b = Q\left(\sqrt{\frac{2E_b}{N_o}(1-2P_b)^2}\right) \tag{16}$$

3.2. SEMA in AWGN Channels

The downlink cellular system can be described as a synchronous system. The delay in synchronous transmission is zero for all users ($\tau_j = 0$). With the assumptions that the information sequences are independent and identically distributed, the probability density function (pdf) of MAI and noise is [9]

$$f_{sync}(x) = \frac{1}{2^{vK}}\sum_{i=0}^{vK}\binom{vK}{i}\frac{1}{\sqrt{2\pi\delta^2}}e^{\frac{-(x-[(vK-2i)/v]A)^2}{2\delta^2}} \tag{17}$$

with variance [9]

$$\delta_{sync}^2 = \delta^2 + \frac{A^2K}{v} \tag{18}$$

The probability of a bit error in synchronous channels is [9]

$$p \approx Q\left(\sqrt{\frac{2E_b}{N_o}\left(\frac{1}{1+\frac{2E_b}{N_o}\frac{K}{v}}\right)}\right) \tag{19}$$

where $Q(.)$ is $Q(\beta) = \frac{1}{\sqrt{2\pi}}\int_\beta^\infty e^{-x^2/2}dx$. E_b/N_o is the bit energy-to-noise ratio.

Signals in asynchronous systems arrive with different delays for all users as in uplink cellular systems. Thus, when the delay factor for user j is $0 \leqslant \tau_j \leqslant T_s$, the pdf of the MAI and noise is shown to be [14]:

$$\begin{aligned} f_{async}(x) &= \left(\frac{1}{2}\right)^{2vK}\sum_{i=0}^{vK}\binom{vK}{i}^2\frac{1}{\sqrt{2\pi\delta^2}}e^{-\frac{(x-A(vK-2i)/v)^2}{2\delta^2}} \\ &+ \left(\frac{1}{2}\right)^{2vK}\left(\frac{v}{2A}\right)\sum_k\sum_{i\neq j}^{vK}\binom{vK}{i}\binom{vK}{j}\frac{1}{i-j} \\ &\times\left\{Q\left(\frac{x-\left[\frac{(vK-2j)}{v}\right]A}{\delta}\right)-Q\left(\frac{x-\left[\frac{(vK-2i)}{v}\right]A}{\delta}\right)\right\} \end{aligned} \tag{20}$$

In asynchronous systems, the carriers of users are not synchronized. Therefore an additional term, $\cos(\Theta)$, $0 \leqslant \Theta \leqslant 2\pi$, should be included in MAI. However, we do not include the term in our discussion for simple presentation. In fact, incorporating the carrier mismatch will reduce MAI and improve the system performance a little. As a result, our analysis is somewhat conservative.

The variance of MAI and noise in the asynchronous channels is

$$\delta_{async}^2 = \delta^2 + \frac{2}{3}\frac{A^2K}{v} \tag{21}$$

and the probability of a bit error in asynchronous channels is given as

$$p \approx Q\left(\sqrt{\frac{2E_b}{N_o}\left(\frac{1}{1+\frac{4}{3}\frac{E_b}{N_o}\frac{K}{v}}\right)}\right) \tag{22}$$

Notice that from Equations (18) and (21), the variance of asynchronous systems is less than that of synchronous systems, by a factor of 2/3.

3.3. SEMA Multiuser Convolutional Coding

Figure 6 shows the state diagram for r = 1/3, constraint length L = 3 convolutional code with the generator matrix G = [5 7 7]. The state diagram does not change when the generator matrix is shifted, i.e., G = [7 7 5] or [7 5 7]. Figure 7 illustrates the two trellis diagrams of one state to the next with the shift generator matrices. These matrices result in the same state diagram as in Figure 6. In Figure 6, the letters a, b, c, d, and e represent state 00, 01, 10, 11, and returning state 00. On each branch between any two states, the power of D represents the symbol weight of the transition while the

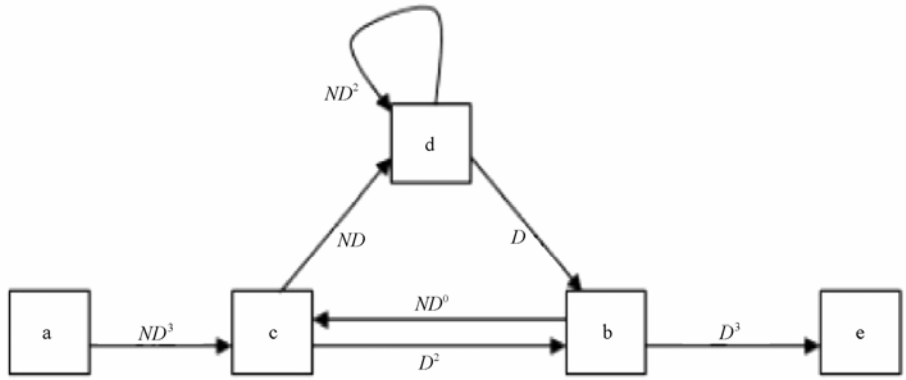

Figure 6. State diagram of *R*=1/3, *L* = 3 convolutional code.

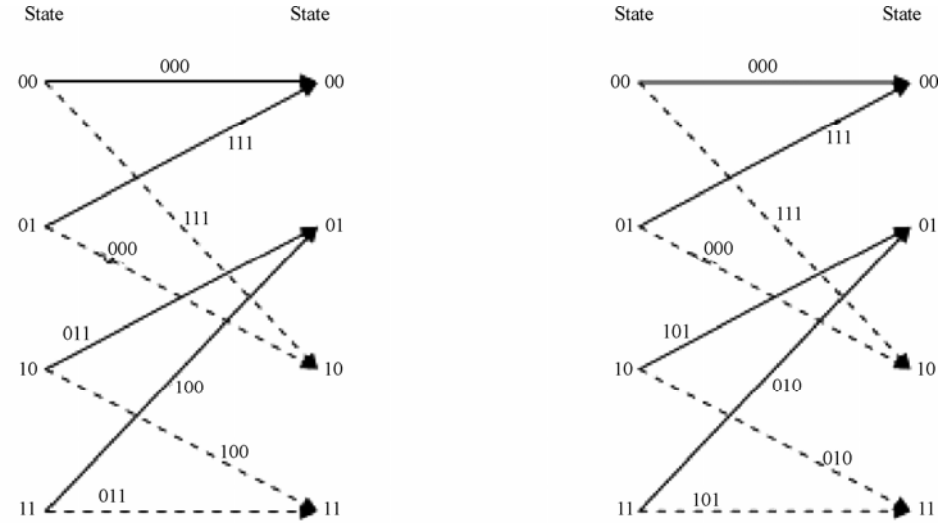

(a) **(b)**

Figure 7. Trellis diagram of *R* =1/3, *L* = 3 convolutional code (a) G1 = [5 7 7] and (b) G2 = [7 5 7].

power of N tells us the weight of the information bit weight. From this diagram, we derive the transfer function using Mason' formula [15]:

$$T(D,N)=\frac{(N+N^2)D^8-N^2D^{10}}{1-(2N+N^2)D^2+N^2D^4} \quad \textbf{(23)}$$

It can be shown from Equation (23) that d_{free} of this system is 8. For the hard-decision maximum likelihood decoder, Viterbi decoding algorithm for the binary symmetric channel (BSC) is used. We apply the transfer function upper bounds derived from the union bound computation for analytical comparison to the simulation results. From [15,16], we obtain the first-event error probability and the bit error probability:

$$P_e < \sum_{d=d_{free}}^{\infty} a_d D^d < T(D,N)\Big|_{D=\sqrt{4P(1-P)},N=1}$$

$$P_b < \frac{\partial T(D,N)}{\partial N}\Big|_{D=\sqrt{4P(1-P)},N=1} \quad \textbf{(24)}$$

where a_b is the coefficient of the transfer function, and p is the probability of a bit error for BSC. The BER can be calculated from Equation (24) by replacing p with (19) and (22) (using symbol energy-to-noise ratio E_s/N_o instead of E_b/N_o) for synchronous and asynchronous systems, respectively. For moderate and high signal-to-noise ratios, it is well known that d_{free} in the union bound for the BER dominates the bound [17]. Thus, we limit the first term in Equation (24) to find the asymptotic BER of our simulations.

3.4. SEMA and Multiuser Detection in Fading Channels

From Equations (11), (12) and (13), the bit error probability for precoding and decorrelating detector, respectively, is given by [10]

$$P_b = Q\left(\sqrt{\left(\frac{2E_b}{N_o}\right)C}\right) \quad \textbf{(25)}$$

$$P_b = Q\left(\sqrt{\left(\frac{2E_b}{N_o}\right)\frac{1}{R_{i,i}^{-1}}}\right) \quad \textbf{(26)}$$

$R_{i,i}^{-1}$ denotes the ith row and j^{th} column of $\mathbf{R}^{-1}$. The performance of SEMA with precoding/multiuser detection and convolutional coding in AWGN channels can be derived from equations (19) and (22) as [8]

$$P_b = Q\left(\sqrt{\frac{2E_b}{N_o}\left(1-\frac{K}{v}\right)}\right) \quad \textbf{(27)}$$

which replaces p in Equation (24) to find the BER. The BER of SEMA with precoding/multiuser detection in Rayleigh fading channel can be obtained as

$$P_b = \int_0^\infty Q\left(\sqrt{\left(\frac{2E_b}{N_o}\right)\gamma\left(1-\frac{K}{v}\right)}\right) f_\Gamma(\gamma)d\gamma$$

$$= \frac{1}{2}\left(1-\sqrt{\frac{(E_b/N_o)(1-K/v)}{(E_b/N_o)(1-K/v)+1}}\right) \quad \textbf{(28)}$$

where $f_\Gamma(\gamma) = e^{-\gamma}$ for Rayleigh fading channels. Equation (28) (using E_s/N_o instead of E_b/N_o) replaces p in Equation (25) to find the BER in fading channels.

4. Simulation Results

In Subsection 3.1, we observed that SI is dominant at low SNR regions with small spreading length. The differential encoding was employed to mitigate the effect of error propagation. In fact, SI becomes negligible under high SNR and with a sufficiently large spreading length. The BER performance then approaches random spread spectrum (RASS). Figure 8 shows the example performance of SEMA with Turbo coding [6]. The plots show that the BER approaches RASS not only asymptotically but also iteratively for $E_b/N_o \geqslant 2.5$ dB. The results indicate that we can ignore SI in examining the asymptotic behavior of the system.

Figure 9 plots the BER of SEMA without interleaving. The performance is clearly unacceptable due to code collisions. The performance of RASS without SI is also shown for comparison: SEMA does not approach RASS even at high SNRs. The performance with interleaving is plotted in Figure 10. The results clearly demonstrate that interleaving is essential in SEMA. Figure 11 compares the performance of SEMA with and without shift generator matrix. At about 10^{-4} BER, the performance with G1 = [5 7 7] applying to both users is approximately 2dB worse than that with shifted matrices G1 = [5 7 7] for user 1 and G2 = [7 5 7] for user 2. Figure 12 shows the BER with the example convolutional code of rate 1/3 and constraint length 4. A larger constraint length is needed for a larger number of users. The BER performance de-

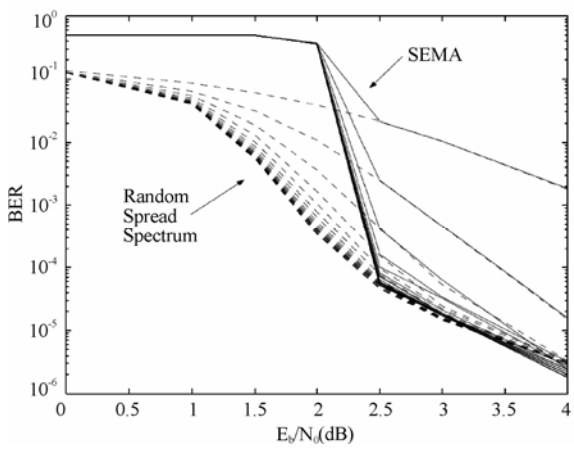

Figure 8. SEMA and random spread spectrum, Turbo coding, two users, *v*= 16 chips/symbol, AWGN, reproduced from [6].

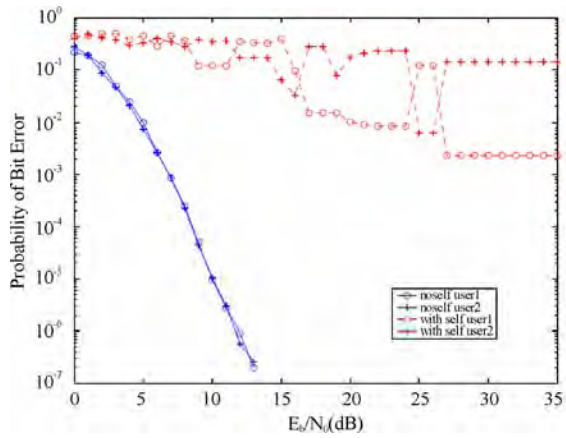

Figure 9. SEMA with and without SI, multiuser convolutional code, G=[5 7 7], *R* = 1/3, *L* = 3, *v* =16 chips/bit, two users, AWGN, no Interleaver.

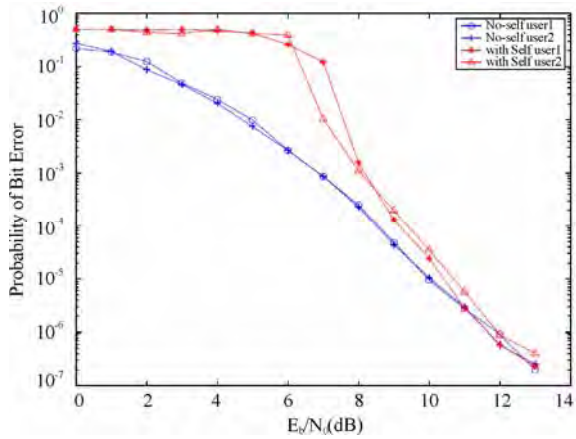

Figure 10. SEMA with and without SI, multiuser convolutional code, G=[5 7 7], *R* = 1/3, *L* = 3, *v* = 16 chips/bit, two users, AWGN, interleaver.

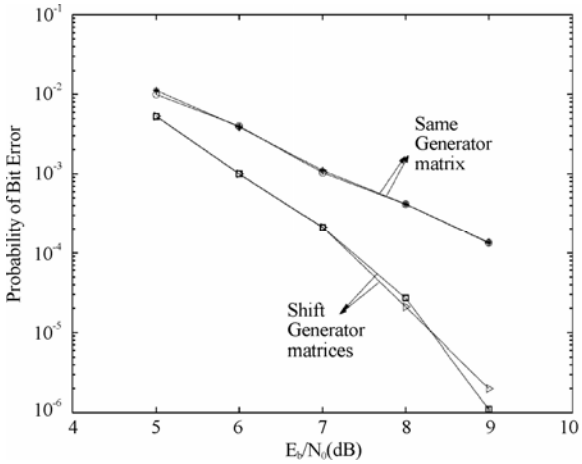

Figure 11. SEMA without SI, multiuser convolutional code, G=[5 7 7], *R* =1/3, *L*=3, *v* =128 chips/symbol, two users, synchronous, AWGN.

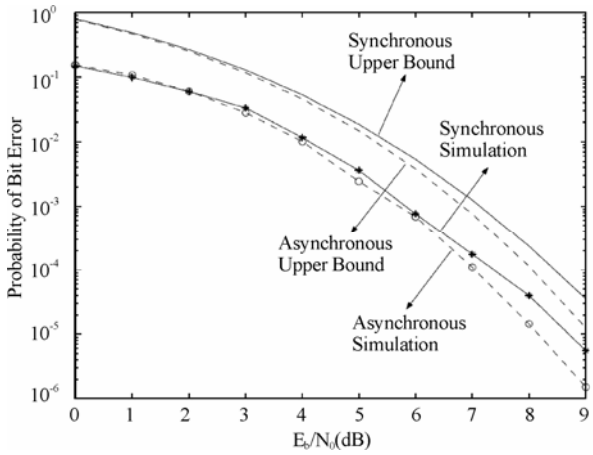

Figure 13. SEMA without SI, multiuser convolutional code, G=[13 15 17], *R* = 1/3, *L* =4, *v* =128 chips/symbol, five users, synchronous and asynchronous, AWGN.

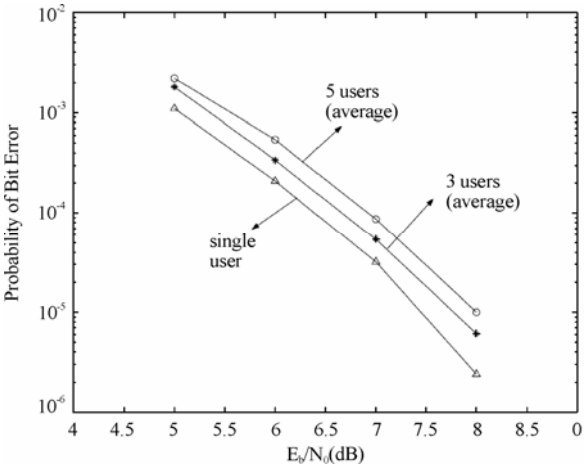

Figure 12. SEMA without SI, multiuser convolutional code, G=[13 15 17], *R* = 1/3, *L* = 4, *v* = 128 chips/symbol, one, three, five users, synchronous, AWGN.

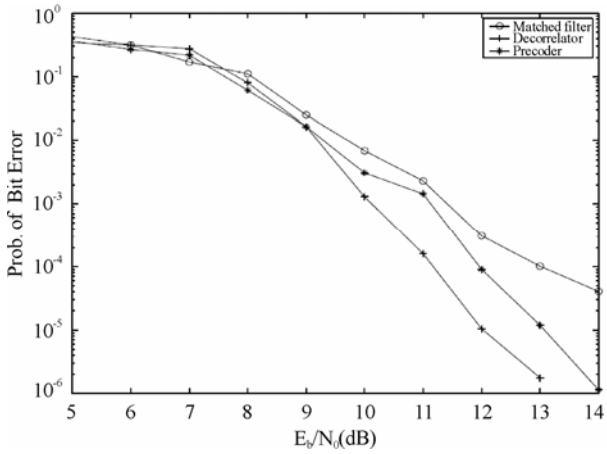

Figure 14. SEMA, multiuser convolutional code, G=[13 15 17], *R* = 1/3, *L* = 8, *v* = 64 chips/symbol, precoding and multiuser detection, two users, Rayleigh fading.

grades by about 0.5dB, indicating that MAI is still manageable for five users with shifted generator matrices.

The plots in Figure 13 indicate that asynchronous system performs better than the synchronous system. About 1 dB difference is observed between the theoretical upper bound and simulations in the synchronous system as well as the asynchronous system. The performance of SEMA in Rayleigh fading channels is shown in Figure 14. The BER of precoding and decorrelating receiver decreases linearly with SNR for $E_b/N_o \geqslant 8$ dB, while the performance of the matched filter receiver starts to saturate at E_b/N_o=12 dB. The results show that precoding and multiuser detection can improve SEMA system performance with additional complexity. Figure 15 compares the analytical calculations to the simulation results of SEMA in Rayleigh fading channels. The performance of precoding and multiuser detection is comparable to each other and is within 2dB of the theoretical results.

5. Conclusions

SEMA provides a feasible implementation of multi-rate transmissions and multi-level grades of service. These are desirable features in multimedia communications and prioritized heterogeneous networking systems. In this paper, we developed multiuser convolutional coding directly applicable to SEMA in synchronous downlink as well as asynchronous uplink cellular systems. We show that SEMA multiuser convolutional coding can improve performance over conventional convolutional coding. The performance analysis shows that the performance of SEMA in the uplink channel is better than the downlink

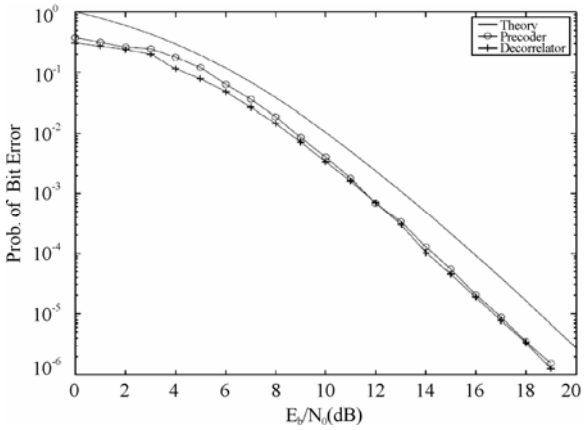

Figure 15. SEMA without SI, multiuser convolutional code, G=[5 7 7], *R* = 1/3, *L* = 3, *v* = 32 chips/symbol, precoding and multiuser detection, three users, Rayleigh fading.

channel. There is a critical SNR at which the self-interference introduced by SEMA becomes negligible and BER improves rapidly. It is important that the operating point of SEMA to be beyond the critical SNR, which depends on channel characteristics and system parameters such as spreading length and the number of users. Beyond the critical SNR, the performance of SEMA is equivalent to the random spread spectrum. The performance of SEMA can be significantly improved by multiuser detection or precoding, as well as channel coding such as multiuser convolutional coding introduced in this paper.

6. Acknowledgements

This work was supported in part by the contract award FA9550-08-1-0393 from the U. S. Air Force Office of Scientific Research. Thanks are due to Dr. J. A. Sjogren whose support has allowed the authors to investigate the field of self-encoded multiple access multiuser convolutional codes.

7. References

[1] T. F. Wong, T. M. Lok, and J. S. Lehnert, "Asynchronous multiple-access interference suppression and chip waveform selection with aperiodic random sequences," IEEE Transactions on Communications, Vol. 47, No. 1, pp. 103−114, January 1999.

[2] J. S. Lehnert and M. B. Pursley, "Error probability for binary direct sequence spread-spectrum communications with random signature sequences," IEEE Transactions on Communications, Vol. COM-35, No. 1, pp. 87−98, January 1987.

[3] L. Nguyen, "Self-encoded spread spectrum and multiple access communications," Proceedings of the IEEE 6th International Conference on Spread Spectrum Technology & Applications, NJIT, NJ, September 2000.

[4] J. Jung, W. M. Jang and L. Nguyen, "Convolutional codes with shift generator matrices in synchronous and asynchronous self-encoded spread spectrum multiple access," Conference on Information Sciences and Systems (CISS'03), The Johns Hopkins University, MD, March, 2003.

[5] J. Jung, W. M. Jang, and L. Nguyen, "Implementation of self-encoded spread spectrum multiple access with convolutional coding," IASTED International Conference WOC, pp. 250−254, July 2002.

[6] W. M. Jang, L. Nguyen, and M. Hempel, "Self-encoded spread spectrum and Turbo coding," Journal of Communications and Networks, Vol. 6, No. 1, pp. 9−18, March 2004.

[7] W. M. Jang and W. Wu, "Distributed and centralized multiuser detection with antenna arrays," IEEE Transactions on Wireless Communications, Vol. 4, No. 3, pp. 855−860, May 2005.

[8] W. M. Jang, L. Nguyen, and M. Hempel, "Precoded random spreading multiple access in AWGN channels," IEEE Transactions on Wireless Communications, Vol. 3, No. 5, pp. 1477−1480, September 2004.

[9] W. M. Jang, L. Nguyen and P. Bidarkar, "MAI and ICI of Synchronous Downlink MC-CDMA with Frequency Offset," IEEE Transactions on Wireless Communications, Vol. 5, No. 3, pp. 693−703, March 2006.

[10] B. Vojcic and W. M. Jang, "Transmitter precoding in synchronous multiuser communications," IEEE Trans. on Commun., Vol. 46, No. 10, October 1998.

[11] S. Verdu, Multiuser Detection, Cambridge Univ. Press, New York, pp. 72, 104−119, 1998.

[12] Y. Kong, L. Nguyen and W. Jang, "On the BER of self-encoded spread spectrum communication system," Proceedings of the IASTED International Conference, Wireless and Optical Communications, Banff, Canada, pp. 202−206, June 27−29, 2001.

[13] Y. Kong, L. Nguyen and W. M. Jang, "Self-encoded spread spectrum modulation with differential encoding," IEEE International Symposium on Spread Spectrum Techniques and Applications, pp. 471−474, September 2−5, 2002.

[14] W. M. Jang, L. Nguyen, and M. W. Lee, "MAI and ICI of asynchronous uplink MC-CDMA with frequency offset," IEEE Transactions on Vehicular Technology, Vol. 57, No. 4, pp. 2164−2179, July 2008.

[15] S. B. Wicker, "Error control systems for digital communication and storage," Prentice Hall, New Jersey, pp. 264−330, 1995.

[16] J. G. Proakis, "Digital communications, 4th Edition, McGraw- Hill, New York, pp. 471−541, 2001.

[17] S. Lin and D. J. Costello, Jr., "Error control coding: fundamentals and applications," Prentice Hall, New Jersey, pp. 287−346, 1983.

Int. J. Communications, Network and System Sciences, **2009, 4, 249-324**
doi:10.4236/ijcns.2009.24028 Published Online July 2009 (http://www.SciRP.org/journal/ijcns/).

True Random Bit Generator Using ZCDPLL Based on TMS320C6416

Qassim NASIR
Department of Electrical and Computer Engineering College of Engineering, University of Sharjah, Sharjah, UAE
Email: *nasir@sharjah.ac.ae*
Received September 4, 2008; *revised December* 8, 2008; *accepted February* 6, 2009

ABSTRACT

A True Random Binary Generator (TRBG) based on a zero crossing digital phase-locked loop (ZCDPLL) is proposed. In order to face the challenges of using the proposed TRBG in cryptography, the proposed TRBG is subjected to the AIS 31 test suite. The ZCDPLL operate as chaotic generator for certain loop filter gains and this has been used to generate TRBs. The generated binary sequences have a good autocorrelation and cross-correlation properties as seen from the simulation results. A prototype of TRBG using ZCDPLL has been developed through Texas Instruments TMS320C6416 DSP development kit. The proposed TRBG successfully passed the AIS 31 test suit.

Keywords: True Random Binary Sequence, Zero Crossing Digital Phase Locked Loop, Spreading Sequences, Cryptography, TMS320C64x

1. Introduction

Random and pseudo-random numbers are used in many areas including test data generation, Monte-Carlo simulation techniques, generation of spreading sequences for spread spectrum communications, and cryptography [1]. Pseudo-random spreading sequences used in spread spectrum communications must be repeatable, while for most simulations using random numbers this is not necessary. In cryptographic applications, security depends on the randomness of the source and the unpredictability of the used random bits [1].

Chaotic circuits represent an efficient alternative to classical TRBG [2]. Studies in nonlinear dynamics show that many of the seemingly complex systems in nature are described by relatively mathematical equations [3]. Although chaotic systems appear to be highly irregular, they are also deterministic in the sense that it is possible to reproduce them with certainty. These promising features of chaotic systems attracted many researchers to try chaos as a possible medium for secure communication.

The nonlinear phenomenon of chaos poses a promising alternative for pseudo-random number generation due to its unpredictable behaviour.

The chaotic system generates "unpredictable" pseudo random orbits which can be used to generate RNGs (Random Number Generators). Many different chaotic systems have been used to generate RNGs such as Logistic map [4], and its generalized version [5], Chebyshev map, [1] piecewise linear chaotic maps [6] and piecewise nonlinear chaotic maps [7]. Chaotic systems are characterized by a "sensitivity dependence on initial conditions", and with such initial uncertainties, the system behaviour leads to large uncertainty after some time.

The aim of this paper is to show how to use a second order zero crossing digital phase locked loop (ZCDPLL) operating in a chaotic mode as True Random Binary Generator (TRBG). Digital Phase locked Loops (DPLLs) were introduced to minimize some of the problems associated with the analogue loops such as sensitivity to DC drift and the need for periodic adjustments [8,9]. The most commonly used DPLL is the Zero Crossing Digital Phase Locked Loop (ZCDPLL). The ZCDPLL operation is based on non uniform sampling techniques. The loop is simple to implement and easy to model. The ZCDPLL consists of a sampler that acts as phase detector, a digital filter, and a Digital Controlled Oscillator (DCO) [8].

The global dynamics of the second order ZCDPLL shows chaos operation for certain values of filter gains [10]. The non-linear behaviour of ZCDPLL shows period doubling or bifurcation instabilities to its route to chaos. The chaotic behaviour has been confirmed through the use of phase error spectrum, bifurcation diagram, and Lyapunov exponent [3,10]. The proposed TRBG pass the statistical tests described by AIS 31 documents [11] However, one should notice that the statistical tests prove that the generator is an ideal random bit generator (the tests are in fact necessary but not sufficient) [12]. The proposed TRBG is implemented on a Texas Instruments TMS320C6416 DSP development platform [13].

The remainder of the paper is organized as follows. In Section 2, the ZCDPLL model is presented. Random bit sequence generation using ZCDPLL is presented in Section 3. Simulation results are discussed in Section 4. Section 5 draws the conclusion.

2. Second Order ZCDPLL

The structure of second order ZCDPLL is shown in Figure 1. As soon as the filter finishes its operation, the stored data are transferred to the register II. The input signal to the loop is taken as $x(t) = s(t) + n(t)$, where $s(t) = A\sin(\omega_0 t + \theta(t))$, and $n(t)$ is additive white Gaussian Noise (AWGN); $\theta(t) = \theta_0 + \Omega_0 t$ by which the signal dynamics are modelled; θ_0 is the initial phase which we will assume to be zero; Ω_0 is the frequency offset from the nominal value ω_0. The input signal is sampled at time instances t_k determined by the Digital Controlled Oscillator (DCO). The DCO period control algorithm is given by [14] is

$$T_k = T_0 - c_{k-1} = t_k - t_{k-1} \quad \textbf{(1)}$$

where $T_0=(2\pi/\omega_0)$ is the nominal period, c_{k-1} is the loop digital filter. The sample value of the incoming signal x(t) at t_k is

$$x(t_k)=s(t_k)+n(t_k) \quad \textbf{(2)}$$

Or simply

$$x_k=s_k+n_k \quad \textbf{(3)}$$

where $s_k = A\sin(\omega_0 t_k + \theta(t_k))$. The sequence x_k is passed through a digital filter whose transfer function is $D(z)$s whose output ck is used to control the period of the DCO. For noise free analysis, then

$$x_k=A\sin[\omega_0(kT_0-\sum_{i=0}^{k-1}c_i+\theta_k] \quad \textbf{(4)}$$

The phase error is defined to be

$$\phi_k=\theta_k-\omega_0\sum_{i=0}^{k-1}c_i \quad \textbf{(5)}$$

Then

$$\phi_k-\phi_{k-1}=\theta_k-\theta_{k-1}-\omega_0 c_{k-1} \quad \textbf{(6)}$$

Using z-operator, equation (6) can be written as

$$(1-z^{-1})\phi_k=(1-z^{-1})\theta_k-\omega_0 z^{-1}c_k \quad \textbf{(7)}$$

The control signal c_k is the output of the digital filter and is formed by

$$c_k = D(z)x_k = D(z)\sin(\phi_k) \quad \textbf{(8)}$$

Substituting (8) into (7) yields

$$\phi_k=\theta_k-\frac{\omega_0 z^{-1}D(z)}{1-z^{-1}}A\sin(\phi_k) \quad \textbf{(9)}$$

In the second order ZCDPLL, the digital filter $D(z)=G_1+\frac{G_2}{1-z^{-1}}$, then (6) becomes

$$\phi_k=2\phi_{k-1}-\phi_{k-2}+K_1\sin(\phi_{k-2})-rK_1\sin(\phi_{k-1})=f(\phi_k) \quad \textbf{(10)}$$

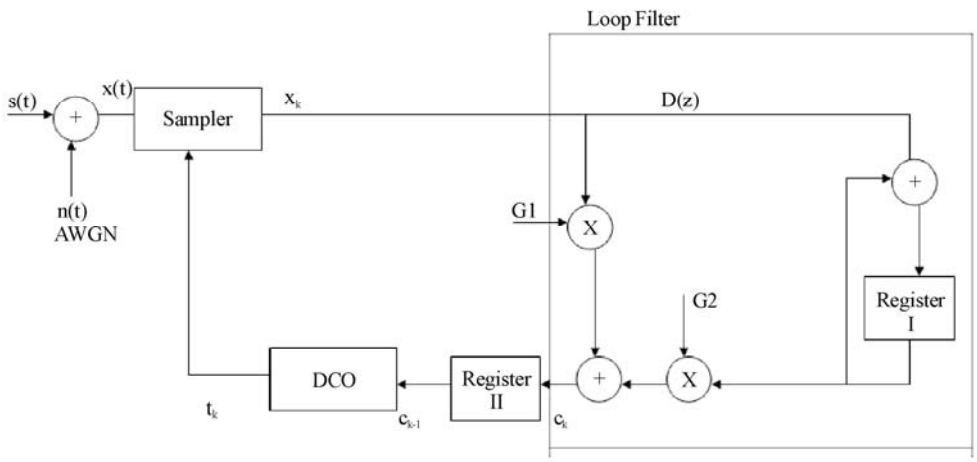

Figure 1. Block diagram of the second order ZCDPLL.

where $K_1 = AG_1\omega_0$ and $r = 1 + \frac{G_2}{G_1}$ Let $x_x=\phi_k$, $y_x=\phi_{k-1}$, $\mathbf{X} = (x, y)^T$ then (1) can be rewritten as

$$\begin{pmatrix} x_{k+1} \\ y_{k+1} \end{pmatrix} = \begin{pmatrix} 2x_k - y_k + K_1 \sin(y_k) - rK_1 \sin(x_k) \\ x_k \end{pmatrix}$$
$$\vdots \quad = \begin{pmatrix} g(\mathbf{X}_k) \\ g(\mathbf{X}_k \end{pmatrix} = G(x_k) \tag{11}$$

If the above system equation is linearized around the equilibrium points $\mathbf{X}^*_k=0$, so that $\sin(x^*_k)\approx x^*_k$ and $\sin(y^*_k) \approx y^*_k$. Then (11) becomes

$$\begin{pmatrix} x_{k+1} \\ y_{k+1} \end{pmatrix} = \begin{pmatrix} (2 - rK_1)x_k + (K_1 - 1)y_k \\ x_k \end{pmatrix}$$
$$= \begin{Bmatrix} (2 - rK_1) & (K_1 - 1) \\ 0 & 1 \end{Bmatrix} \begin{pmatrix} x_k \\ y_k \end{pmatrix} \tag{12}$$

Consequently the Jacobian $\mathbf{G'}(x)=\partial g_i/\partial x$ is given by

$$G'(x^*) = \begin{Bmatrix} (2 - rK_1) & (K_1 - 1) \\ 0 & 1 \end{Bmatrix} \tag{13}$$

The loop will converge if the eigen values $\mathbf{G'}(x^*)$ are be less than one. Following [14] the operational regions of the second order ZCDPLL are given by (as shown in Figure 2): region (I), the loop converges locally to $\mathbf{x}^*=0$, $2n\pi$, region (II), the loop phase error ϕ oscillates between two values, region (III), the loop phase error ϕ oscillates between n values or diverges, while in region (IV), the loop phase error ϕ diverges.

Fundamental to most definitions of chaos is the concept that two trajectories of the system, no matter how closely they start to one another, will eventually diverge. This divergence is of exponential order. The Lyapunov exponent is used to measure the average rate of divergence of nearby trajectories. It is defined as [3,10]:

$$\lambda = \lim_{N\to\infty} \frac{1}{N} \sum_{n=0}^{N} \ln \left| f'(\phi_n) \right| \tag{14}$$

A positive Lyapunov exponent indicates chaos. The largest Lyapunov exponent for the two dimensional a dynamical ZCDPLL system is defined as [3]

$$\lambda = \lim_{N\to\infty} \frac{1}{2N} \sum_{n=0}^{N} \ln \left| \frac{(a + bY_n^{'})^2 + (c + dY_n^{'})^2}{1 + Y_n^{'2}} \right| \tag{15}$$

where Y' is the tangent of the direction of maximum growth which evolves according to

$$Y_{n+1}^{'} = \frac{c + dY_n^{;'}}{a + bY^{;'}} \tag{16}$$

where $a = \partial g_1 / \partial x_k, b = \partial g_1 / \partial y_k, c = \partial g_2 / \partial x_k, a = \partial g2 / \partial y_k$, are members of Jacobian matrix of (13).

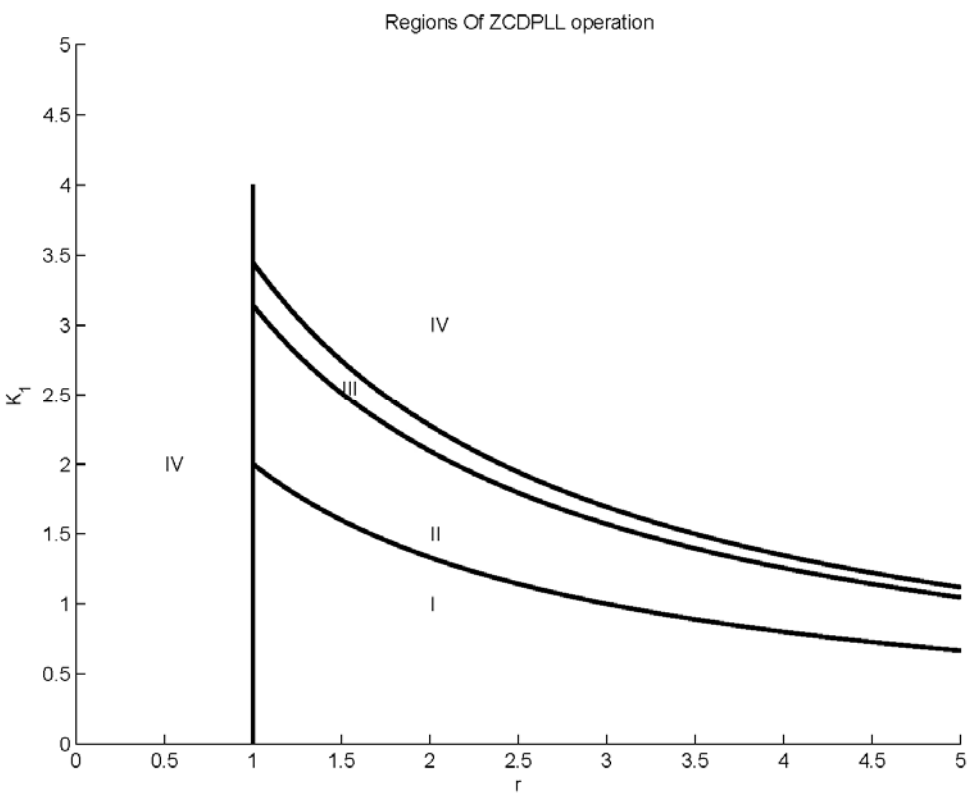

Figure 2. Loop behaviour as a function of K_1 and r for second-order ZCDPLL.

3. True Random Binary Generation-TRBG

Security algorithms and protocols rely on the unpredictability of the random bits they use, True Random Binary Generators (TRBGs) play an important role in cryptographic applications [15] Classical TRBG uses some random physical phenomenon. The most frequently used phenomenon in embedded TRBGs is a jitter noise of digital clock signals [16].

Chaotic circuits represent an efficient alternative to the classical TRBGs [16,17]. Contrary to traditionally used sources of randomness they use a well-defined analog deterministic circuit that exhibits chaos. Many random number generators based on analog and deterministic chaotic phenomena have been proposed, see [16,17].

To obtain random bits from ZCDPLL, the output of the sampler is monitored and assigned bit values of zero and one based on whether the output of the sampler is positive or negative as it can be seen in Figure 3. Hence, $\varphi \in [0,\pi)$ corresponds to a "1" and $\varphi \in [\pi, 2\pi)$ corresponds to a "0".

A natural source of random bits may not give unbiased bits as direct output. Many applications, especially in cryptography, rely on sequences of unbiased bits. There are various techniques to extract unbiased bits from a defective generator with unknown bias. These are called de-skewing techniques [18]. These techniques also eliminate the correlation in the output of the natural sources of random bits. Von Neumann [19] proposed a digital post-processing technique that balances the distribution of bits. Post-processing converts non-overlapping pairs of bits into output bits by converting the bit pair [0,1] into an output 0, input pair [1,0] into an output 1, input pairs [1,1] and [0,0] are discarded [18].

A large number of statistical test suits have been proposed to assess the statistical properties of random number generators. A finite set of statistical tests may only detect defects in statistical properties. Furthermore, the tests cannot verify the unpredictability of the random sequence which is demanded in cryptographic applications. In this section, the proposed random bit generator is evaluated with statistical tests proposed by BSI as Applications Notes and Interpretation of the Scheme (AIS) [11]. The statistical tests are applied to a bit sequence obtained after the de-skewing. A better result of the statistical test can be obtained, if a strong de-skewing technique is used such as a cryptographic hash function, but these create a long delay [18].

Although random numbers play an important role in numerous cryptographic applications, Information Technology Security Evaluation Criteria (ITSEC) [20] nor Common Criteria [21] (CC) specify any uniform evaluation criteria for random numbers. For this purpose the AIS 31 Document Standard describes some evaluation criteria for true (physical) random number generators. AIS has been effective in Germany since 2001 [11]. The monobit, poker, runs, long runs, and entropy tests have been used in this paper as defined by AIS 31 document in order to test the randomness of the chaotic bits sequence generated by the ZCDPLL.

4. System Performance

The TRBG using ZCDPLL has been verified by simulation. A modulation free input signal $x(t)= \sin(\omega_1 t)$ is considered, where ω_1 is the input frequency, and the center frequency of the DCO is assumed to be $\omega_0 =1$ rad/sec.

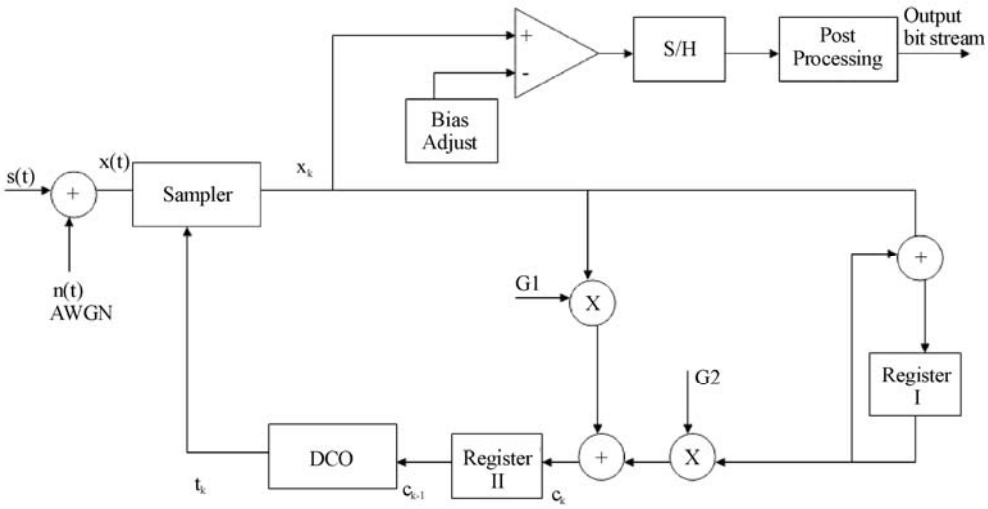

Figure 3. Block diagram of the TRBG using second order ZCDPLL.

In order to see where the loop has chaotic behavior, Lyapunov exponent has been calculated for all possible values of the loop parameters (K_1 and r) and has been given black dot when they have values greater than 1 (positive Lyapunov represents chaotic operation). The distribution of these black dots is shown in Figure 4. In order to produce chaotic sequence of phase error, one should work in black regions.

The chaotic phase φ_k distribution generated by the second order ZCDPLL distribution is shown in Figure 5 where K_1 =2.5, and r =2.5. Sample 2 is shown in Figure 6 for K_1 =3.0, and r =2.5. The two phase sequences are random. The one million bits extracted from the phase sequence of ZCDPLL have been collected ($\varphi \in [0,\pi)$ corresponds to a "1" and $\varphi \in [\pi, 2\pi)$ corresponds to a "0". The autocorrelation properties of the outputs are shown in Figure 7. Chaotic sequence have very low cross correlation as shown in Figure 8 for the two binary streams generated using two different loop parameters. This is an important issue with regard to the security, because the receiver can not be determined from a few points in the sequence.

The chaotic bit stream generated by the second order ZCDPLL of length 20000 bits is subject to each of the tests. The Monobit test is projected as evidence if the number of 1's and 0's in the sequence are nearly equal. The AIS standard specified the value of the number of 1's in the bit stream to be somewhere between 9654 and 10346. The Pocker Test requires the division of the initial sequence into 4 bit contiguous segments, the counting and the storing of each of the 16 possible 4 bit values. Denoting as f (k) the number of each value, $0 \le k \le 15$, the X statistic is computed by means of (The test will pass if $1.03 \le X \le 57.4$):

$$X = \frac{16}{5000}\left(\sum (f(k))^2 - 5000\right) \quad \textbf{(16)}$$

The third test used is runs test. If we describe a run as the maximal sequence of consecutive bits of the same kind then the incidence of runs for both consecutive zeros and consecutive ones of all lengths of what between 1 and 6 in the sample stream should be in the corresponding interval as specified in Table 1.

It is worth noticing the fact that the sequences longer than 6 are considered of length 6 when counting them. The test is passed if for the generated sequence the number of consecutive bits of each length is between the limits given in the Table 2. The long run test is passed if there are no runs of length 34 or more.

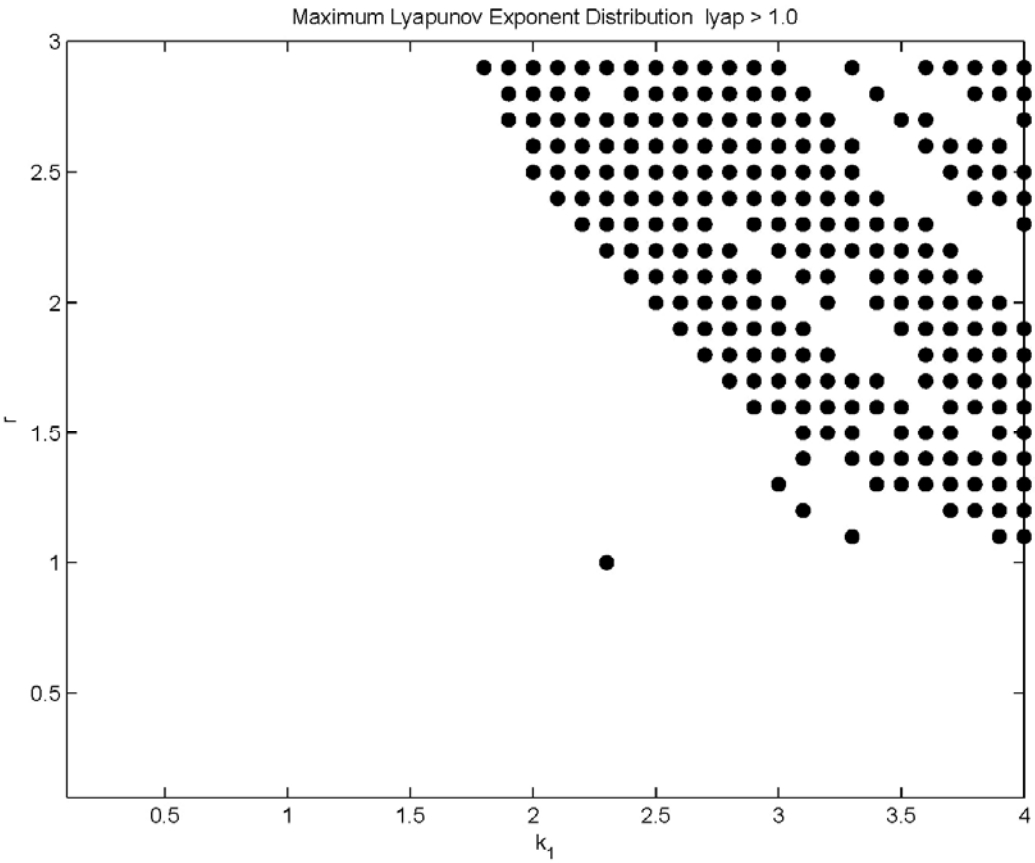

Figure 4. Largest Lyapunov Exponent of ZCDPLL - dot when it is greater than 1.0.

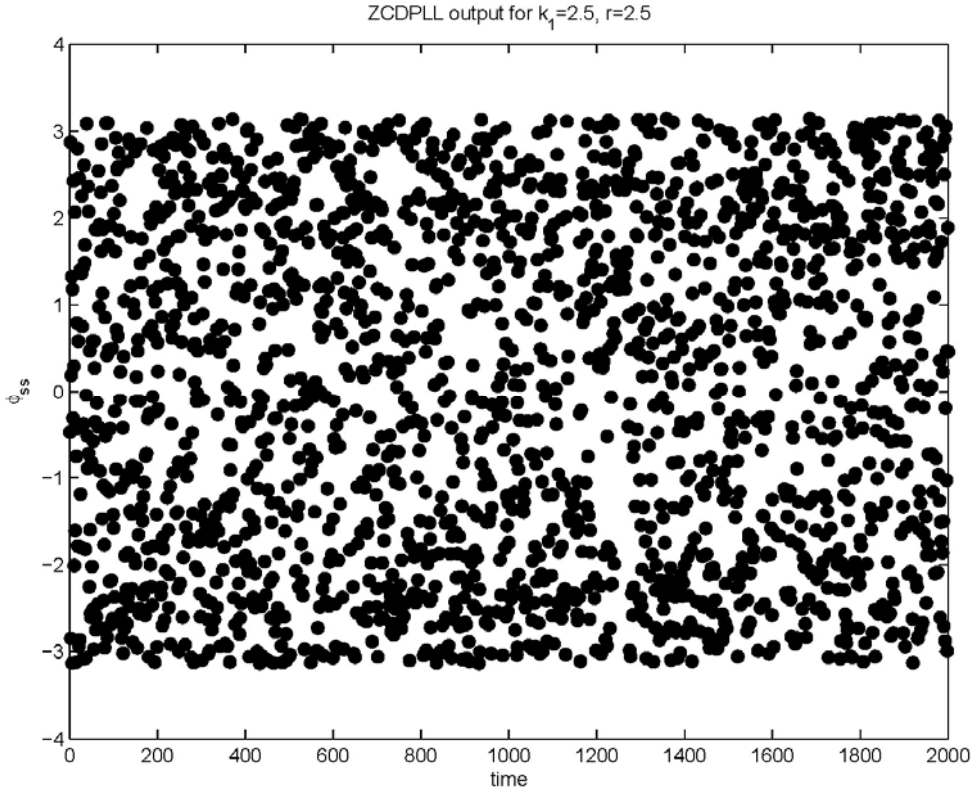

Figure 5. Distribution of ZCDPLL output (Sample 1) for a set of filter gain.

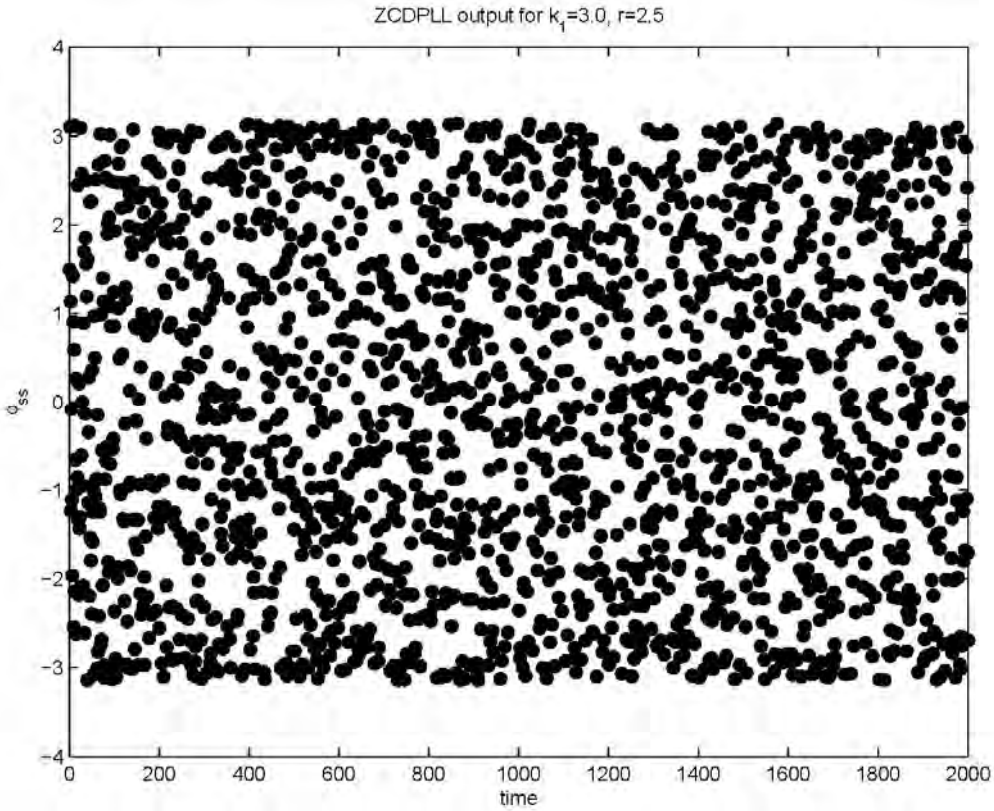

Figure 6. Distribution of ZCDPLL output (Sample 2) for other set of filter gain.

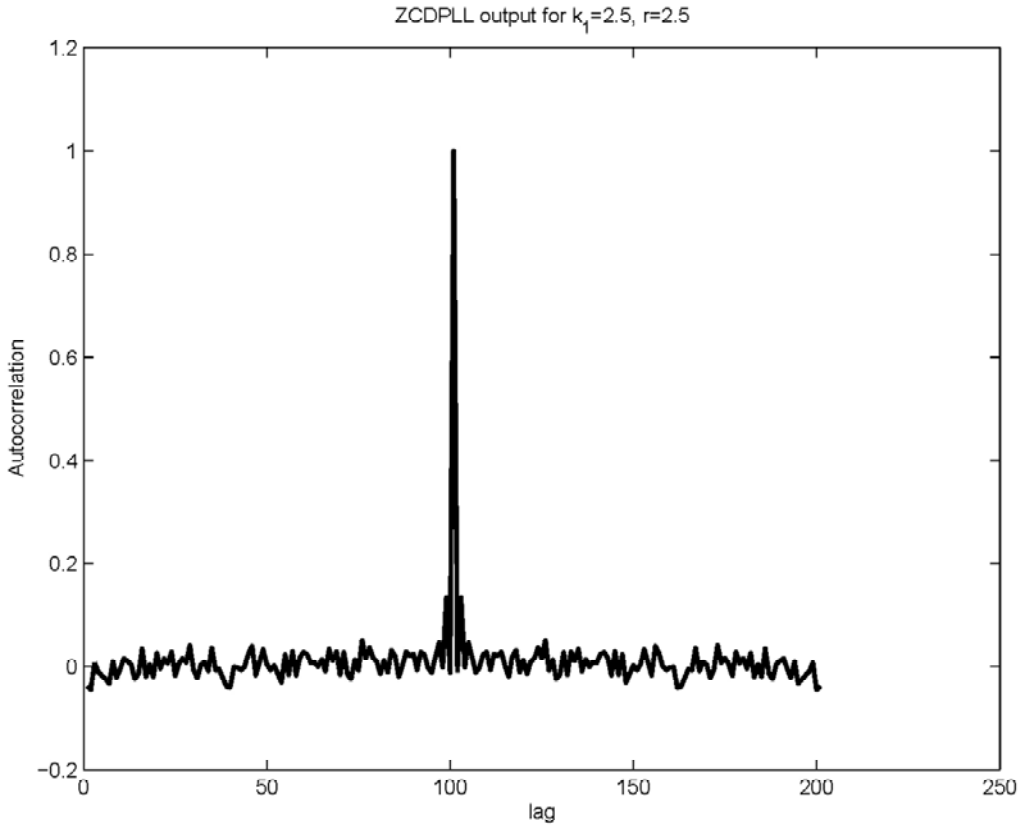

Figure 7. Autocorrelation of ZCDPLL mm output (Sample 1).

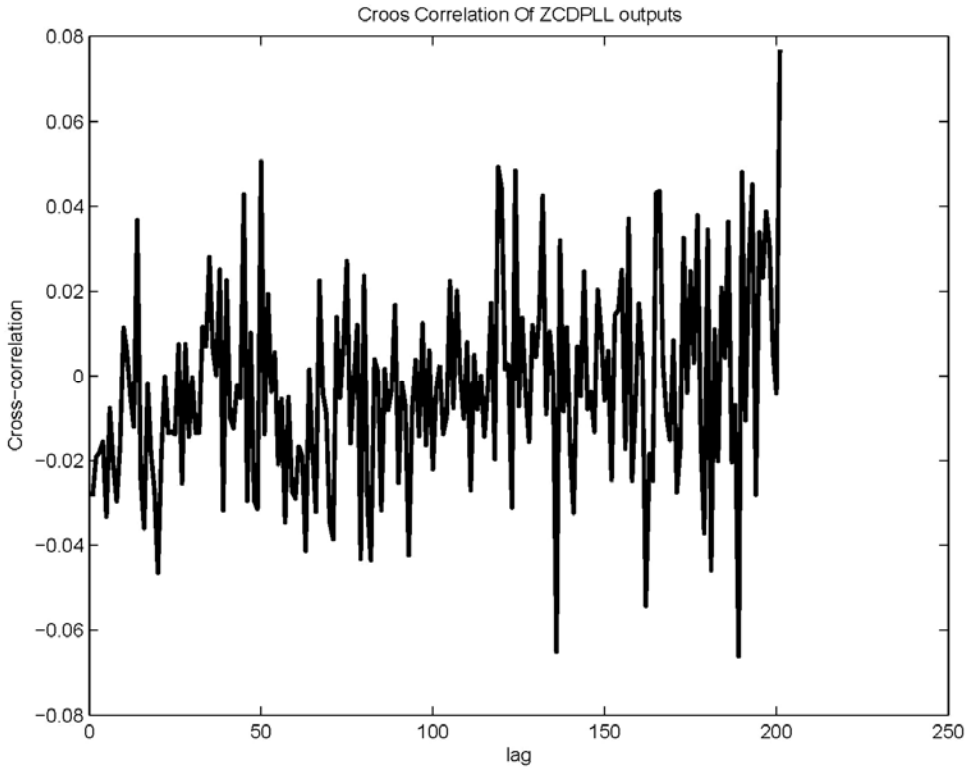

Figure 8. Cross Correlation of two ZCDPLL outputs (Sample 1 and Sample 2).

Table 1. Number of occurrences versus length.

Length	1	2	3	4	5	6+
Number Of occurrences	2267/2733	1079/1421	502/748	223/402	90/223	90/223

Table 2. Simulation test results.

AIS 31 Statistical Test	Result	Limits
Test 1 (Monobit Test)	Monobit = 9986	9645 < Monobit < 10346
Test 2 (Poker Test)	X = 44.498	1.03 < X < 57.4
Test 3 (Runs Test)	All Passed	
Test 4 (Long Run Test)	Long Run = 16	Long Run = 34

The proposed true random bit generator successfully passes all four statistical tests for every run. Table 2 shows the results of AIS 31 Standard Statistical Tests ran over 1 million random bits generated by ZCDPLL with K_1=2.5, r=2.5. As can be seen, all results are within the accepted range of the tests.

5. TMS320C6416 Implementation

The TRBG using ZCDPLL has been implemented in the software code targeted at a Texas Instruments TMS 320C6416 DSP. The generated bits are collected by the host PC. The key issue in the realization of the TRBG using ZCDPLL is the implementation of variable sample rate signal processing. In the realization based of DSP, variable sampling rate can be efficiently implemented using the DSP chip timer. At the beginning of the software program, the DSP timer (e.g Timer1) is set to be equal to maximum value of the sampling period. While the timer counts towards zero, an input (error) sample is read from the Analogue to Digital converter (ADC). On the basis of the error sample, the controller output and the actual value of the sampling period T are computed. Then the computed value of the sampling period is used to set the timer period. The DSP processor will enter an idle state till the timer expired, then the processed will be interrupted and the Interrupt Service Routine (ISR) will be called and the program loop repeats (see Figure 9).

Real-Time Data Exchange (RTDX) is used to provide real time, continuous visibility into the way TRBG software application operates in TMS320C6416. RTDX allows transfer the random bits generated in the DSP to a host PC for testing. On the host platform, an RTDX host library operates in conjunction with Code Composer Studio. In RTDX an output channel should be configured within ZCDPLL software. The generated data from ZCDPLL is written to the output channel. This data is immediately recorded into a C6416 DSP buffer defined in the RTDX C6416 library. The data from this buffer is then sent to the host PC through the JTAG interface. The RTDX host library receives this data from the JTAG interface and records it into either a memory buffer for testing purposes.

One million bits have been collected by the host PC. The same AIS 31 test suit has been used to check the truly randomness of the generated bits by the DSP kit. The results of these tests are shown in Table 3. It can be seen that the bits passed all the three proposed tests.

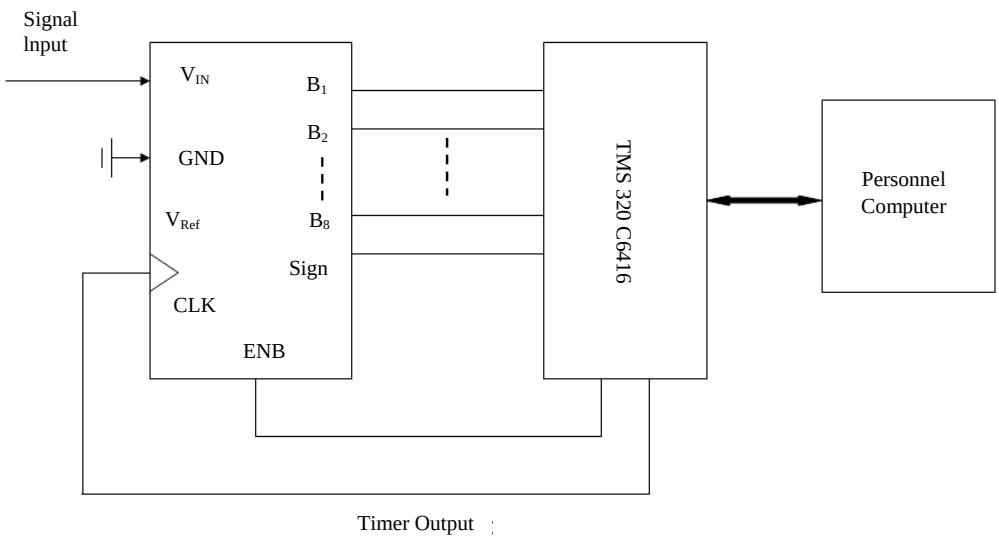

Figure 9. TMS320C6416 based TRBG.

Table 3. DSP card based test results.

AIS 31 Statistical Test	Result	Limits
Test 1 (Monobit Test)	Monobit = 10122	9645 < Monobit < 10346
Test 2 (Poker Test)	X = 51.32	1.03 < X < 57.4
Test 3 (Runs Test)	All Passed	
Test 4 (Long Run Test)	Long Run = 28	Long Run = 34

6. Conclusions

In this paper, True Random Binary Generator (TRBG) using second order ZCDPLL has been described and evaluated. The chaotic phase error produced by the ZCDPLL has been used to generate TRB. The proposed TRBG is subjected to statistical test suit AIS 31. The proposed TRBG successfully passed the tests described by AIS31 document. Another essential result of this paper is that the proposed TRBG based on ZCDPLL is implemented fully by software based on TMS320C6416 DSP kit. TRBG synchronization is still a challenging task which will be dealt within future work. Post processing is used to improve the statistical properties of the bit sequences generated by the ZCDPLL.

7. References

[1] T. Kohda and A. Tsuneda., "Chaotic bit sequences for stream cipher cryptography and their correlation functions," Proceedings of SPIE's International Symposium on Information, Communications and Computer Technology, Applications and Systems, Vol. 2612, pp. 86−97, 1995.

[2] M. Drutarovsk and P. Galajda, "Chaos based true random number generator embedded in a mixed-signal reconfigurable hardware," Journal of Electrical Engineering, Vol. 57, pp. 218−225, April 2006.

[3] J. C. Sprott, "Chaos and time-series analysis," Oxford University Press, 2003.

[4] N. Sajeeth, K. Philip, and J. Babu, "Chaos for stream cipher," http://uk.arxiv:org/PScache/cs/pdf/0102012v1.pdf.

[5] R. Matthews, "On the derivation of a chaotic encryption," Vol. 8, pp. 29−49, January 1989.

[6] N. Masuda and K. Aihara, "Cryptosystems with discretized chaotic maps,". IEEE Transactions on Circuits and Systems, Vol. 49, pp. 28−40, January 1999.

[7] S. Tao, W. Ruili, and Y. Yixun, "The theoretical design for a class of new chaotic feedback stream ciphers," Acta Eletronica Sinica, Vol. 27, pp. 47−50, July 1999.

[8] W. Lindsay and C. M Chie, "A survey of digital phase locked loops," IEEE Proceedings, Vol. 69, pp. 410−431, April 1981.

[9] G. Hsieh and C. Hung, "Phase locked loops–A survey," IEEE Transactions on Industrial Electronics, Vol. 43, pp. 609−615, December 1996.

[10] Q. Nasir, "Chaotic behavior of first order zero crossing digital phase locked loop," 2004 IEEE Asia-Pacific Conference on Circuits and Systems, pp. 977−980, 2004.

[11] AIS 31, "Functionality classes and evaluation methodology for true (physical) random number generators ver 3.1," Bundesmat fur Sicherheir in der Information technik (BSI), Bon, Germany, September 2001.

[12] M. E. Yalcin, J. K. Suykens, and J. Vandewalle, "True random bit generation from a double scroll attractor," IEEE Transactions on Circuits and Systems I: Fundamental Theory and Applications, Vol. 51, pp. 1395−1404, July 2004.

[13] Texas Instrument, TMS320C6416 DSP Starter Kit (DSK), http://focus.ti.com/docs/prod/folders/print/tms320c6416.html.

[14] H. C. Osborne, "Stability analysis of an nth power digital phase-locked loop–Part I: First-order DPLL," IEEE Transactions on Communications, Vol. 28, No. 8, pp. 1343−1354, 1980.

[15] D. Croker and J. Schiller, "Randomness recommendations for security," Request for Comments 1750, 1994. http://www.ietf.org/rfc/rfc1750.txt.

[16] M. Bucci, L. Germani, R. Luzzi, A. Trifiletti, and M. aranouovo, "A high-speed oscillator-based truly random number source for cryptographic applications on a smart card IC," IEEE Transactions on Computers, Vol. 52, pp. 403−409, April 2003.

[17] M. D. Restituto and A. R. V'azques, "Chaos-based random number generators–Part II: Practical realization," IEEE Proceedings, Vol. 90, pp. 747−767, May 2002.

[18] A. J. Menezes, P. C. van Oorschot, and S. A. Vanstone, "Handbook of applied cryptography," CRC Press, 1997. http://www.cacr.math.uwaterloo.ca/hac/.

[19] J. Von Neumann, "Various techniques used in connection with random digits," Applied Math Series, Notes by G. E. Forsythe, in National Bureau of Standards, Vol. 12, pp. 36−38, 1951.

[20] Standards, Information Technology Security Evaluation Criteria (ITSEC), Provisional Harmonized Criteria, Version 1.2, 1991.

[21] CEM-99/045, Common Methodology for Information Technology Security Evaluation (CEM) version 1.0,. 1999.

Int. J. Communications, Network and System Sciences, 2009, 4, 249-324
doi:10.4236/ijcns.2009.24029 Published Online July 2009 (http://www.SciRP.org/journal/ijcns/).

Investigations into the Effect of Spatial Correlation on Channel Estimation and Capacity of Multiple Input Multiple Output System

Xia LIU[1], Marek E. BIALKOWSKI[2], Feng WANG[1]
[1]*Student Member IEEE, School of ITEE, The University of Queensland, Brisbane, Australia*
[2]*Fellow IEEE, School of ITEE, The University of Queensland, Brisbane, Australia*
Email: {xialiu, meb, fwang}@itee.uq.edu.au
Received December 17, 2008*; revised March* 28, 2009*; accepted May* 25, 2009

ABSTRACT

The paper reports on investigations into the effect of spatial correlation on channel estimation and capacity of a multiple input multiple output (MIMO) wireless communication system. Least square (LS), scaled least square (SLS) and minimum mean square error (MMSE) methods are considered for estimating channel properties of a MIMO system using training sequences. The undertaken mathematical analysis reveals that the accuracy of the scaled least square (SLS) and minimum mean square error (MMSE) channel estimation methods are determined by the sum of eigenvalues of the channel correlation matrix. It is shown that for a fixed transmitted power to noise ratio (TPNR) assumed in the training mode, a higher spatial correlation has a positive effect on the performance of SLS and MMSE estimation methods. The effect of accuracy of the estimated Channel State Information (CSI) on MIMO system capacity is illustrated by computer simulations for an uplink case in which only the mobile station (MS) transmitter is surrounded by scattering objects.

Keywords: MIMO, Channel Estimation, Channel Capacity, Spatial Correlation, Channel Modelling

1. Introduction

In recent years, there has been a growing interest in multiple input multiple output (MIMO) techniques in relation to wireless communication systems as they can significantly increase data throughput (capacity) without the need for extra operational frequency bandwidth. In order to make use of the advantages of MIMO, precise channel state information (CSI) is required at the receiver. The reason is that without CSI decoding of the received signal is impossible [1–5]. In turn, an inaccurate CSI leads to an increased bit error rate (BER) that translates into a degraded capacity of the system [6–8].

Obtaining accurate CSI can be accomplished using suitable channel estimation methods. The methods based on the use of training sequences, known as the training-based channel estimation methods, are the most popular. In [9,10], several training-based methods including least square (LS) method, scaled least square (SLS) method and minimum mean square error (MMSE) method have been investigated. It has been shown that the accuracy of the investigated training-based estimation methods is influenced by the transmitted power to noise ratio (TPNR) in the training mode, and a number of antenna elements at the transmitter and receiver. In particular, it has been pointed out that when TPNR and a number of antenna elements are fixed, the SLS and MMSE methods offer better performance than the LS method. This is due to the fact that SLS and MMSE methods utilize the channel correlation in the estimator cost function while the LS estimator does not take the channel properties into account.

It is worthwhile to note that the channel properties are governed by a signal propagation environment and spatial correlation (SC) that is dependent on an antenna configuration and a distribution of scattering objects that are present in the path between the transmitter and receiver. The works in [9,10] have demonstrated superiority of SLS and MMSE estimation methods, which make use of channel correlation, over the LS method neglecting channel properties. However, no specific relationship

between spatial correlation and channel estimation accuracy has been shown. The works presented in [11,12] have reported on the relationship between spatial correlation and estimation accuracy of MMSE method. However, only simulation results, giving trends without any further mathematical insight have been presented.

In this paper, we try to fill the existing void by presenting the mathematical analysis explaining the effects of channel properties on SLS and MMSE channel estimation methods. It is shown that for a fixed TPNR, the accuracy of SLS and MMSE methods is determined by the sum of eigenvalues of channel correlation matrix, which in turn characterizes the signal propagation conditions. In addition, we report on the effect of spatial correlation on both the channel estimation and capacity of MIMO system. In the work presented in [13–16], it has been shown that the existence of spatial correlation leads to the reduced MIMO channel capacity. However, these conclusions rely on the assumption of perfect CSI available to the receiver. In practical situations, obtaining perfect CSI can not be achieved. Therefore, in this paper we take imperfect knowledge of CSI into account while evaluating MIMO capacity.

The rest of the paper is organized as follows. In Section 2, a MIMO system model is introduced. In Section 3, LS, SLS and MMSE channel estimation methods are described and the channel estimation accuracy analysis is given. Section 4 shows derivations for the lower bound of MIMO channel capacity when the channel estimation errors are included. Section 5 describes computer simulation results. Section 6 concludes the paper.

2. System Description & Channel Model

We consider a flat block-fading narrow-band MIMO system with M_t antenna elements at the transmitter and M_r antenna elements at the receiver. The relationship between the received and transmitted signals is given by (1):

$$Y_s = HS + V \tag{1}$$

where Y_s is the $M_r \times N$ complex matrix representing the received signals; S is the $M_t \times N$ complex matrix representing transmitted signals; H is the $M_r \times M_t$ complex channel matrix and V is the $M_r \times N$ complex zero-mean white noise matrix. N is the length of transmitted signal. The channel matrix H describes the channel properties which depend on a signal propagation environment. Here, the signal propagation is modeled as a sum of the line of sight (LOS) and non-line of sight (NLOS) components. As a result, the channel matrix is represented by two terms and given as [17,18],

$$H = \sqrt{\frac{1}{1+K}} H_{NLOS} + \sqrt{\frac{K}{1+K}} H_{LOS} \tag{2}$$

where H_{LOS} denotes the LOS part as and H_{NLOS} denotes NLOS part. K is the Rician factor defined as the ratio of power in LOS and the mean power in NLOS signal component [17]. The elements of H_{LOS} matrix can be written as [18]

$$H_{LOS}^{rt} = \exp(-j\frac{2\pi}{\lambda} D_{rt}) \tag{3}$$

where D_{rt} is the distance between t-th transmit antenna and r-th receive antenna. Assuming that the components of NLOS are jointly Gaussian, H_{NLOS} can be written as [19,20],

$$H_{NLOS} = R_R^{1/2} H_g R_T^{1/2} \tag{4}$$

where H_g is a matrix with i.i.d Gaussian entries.

Here, the Jakes fading model [21,22] is used to describe the spatial correlation matrices R_R at the receiver and R_T at the transmitter. An uplink case between a base station (BS) and a mobile station (MS) is assumed, as shown in Figure 1.

The BS antennas are assumed to be located at a large height above the ground where the influence of scatterers close to the receiver is negligible. In turn, MS is assumed to be surrounded by many scatterers distributed within a "circle of influence". For this case, the signal correlation coefficients at the receiver BS and transmitter MS, ρ_R^{BS} and ρ_T^{MS}, can be obtained from [22] and are given as:

$$\rho_T^{MS}(\delta_{mn}^T) = J_0[2\pi\delta_{mn}^T / \lambda] \tag{5}$$

$$\rho_R^{BS}(\delta_{mn}^R) = J_0[\frac{2\pi}{\lambda}\delta_{mn}^R \gamma_{\max}\cos(\theta)]\exp(-j\frac{2\pi}{\lambda}\delta_{mn}^R \sin(\theta)) \tag{6}$$

where, δ_{mn}^T and δ_{mn}^R are the antenna spacing distances between m-th and n-th antennas at transmitter and receiver, respectively; λ is the wavelength of the carrier; γ_{max} is the maximum angular spread (AS); θ is the AoA of LOS and J_0 is the Bessel function of 0-th order. Using $\rho_R^{BS}(\delta_{mn}^T)$ and $\rho_T^{MS}(\delta_{mn}^R)$, the correlation matrices R_R^{BS} and R_T^{MS} for BS and MS links can be generated as

$$R_R^{BS} = \begin{bmatrix} \rho_R^{BS}(\delta_{11}^{BS}) & \cdots & \rho_R^{BS}(\delta_{1M_r}^{BS}) \\ \vdots & \ddots & \vdots \\ \rho_R^{BS}(\delta_{M_r1}^{BS}) & \cdots & \rho_R^{BS}(\delta_{M_rM_r}^{BS}) \end{bmatrix} \tag{7}$$

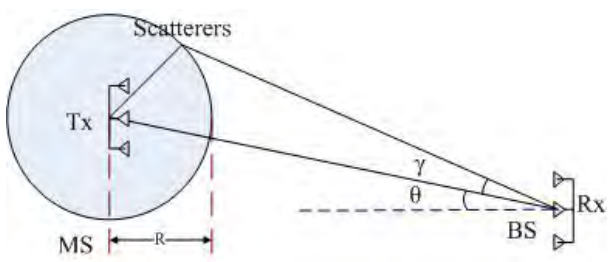

Figure 1. Jakes model for the considered MIMO channel.

$$R_T^{MS} = \begin{bmatrix} \rho_T^{MS}(\delta_{11}^{MS}) & \cdots & \rho_T^{MS}(\delta_{1M_t}^{MS}) \\ \vdots & \ddots & \vdots \\ \rho_T^{MS}(\delta_{M_t1}^{MS}) & \cdots & \rho_T^{MS}(\delta_{M_tM_t}^{MS}) \end{bmatrix} \quad \textbf{(8)}$$

3. Training-Based Channel Estimation

For a training based channel estimation method, the relationship between the received signals and the training sequences is given by Equation (1) as

$$Y = HP + V \quad \textbf{(9)}$$

Here the transmitted signal S in (1) is replaced by P, which represents the $M_t \times L$ complex training matrix (sequence). L is the length of the training sequence. The goal is to estimate the complex channel matrix H from the knowledge of Y and P.

Here the transmitted signal S in (1) is replaced by P, which represents the $M_t \times L$ complex training matrix (sequence). L is the length of the training sequence. The goal is to estimate the complex channel matrix H from the knowledge of Y and P.

The transmitted power in the training mode is assumed to be constrained by $\|P\|_F^2 = \mathrm{P}$ where P is a constant and $\|.\|_F^2$ stands for the Frobenius norm. According to [9,10], the estimation using LS, SLS or MMSE method requires orthogonality of the training matrix P. In the undertaken analysis, the training matrix P is assumed to satisfy this condition.

3.1. LS Method

In the LS method, the estimated channel can be written as [23],

$$\hat{H}_{LS} = YP^{\dagger} \quad \textbf{(10)}$$

where $\{.\}^{\dagger}$ stands for the pseudo-inverse operation.

The mean square error (MSE) of LS method is given as

$$MSE_{LS} = E\{\left\|H - \hat{H}_{LS}\right\|_F^2\} \quad \textbf{(11)}$$

in which $E\{.\}$ denotes a statistical expectation. According to [9,10], the minimum value of MSE for the LS method is given as

$$MSE_{\min}^{LS} = \frac{M_t^2 M_r}{\rho} \quad \textbf{(12)}$$

in which ρ stands for transmitted power to noise ratio (TPNR) in training mode. Equation (12) indicates that the optimal performance of the LS estimator is not influenced by channel matrix H.

3.2. SLS Method

The SLS method reduces the estimation error of the LS method. The improvement is given by the scaling factor γ which can be written as

$$\gamma = \frac{tr\{R_H\}}{MSE_{LS} + tr\{R_H\}} \quad \textbf{(13)}$$

The estimated channel matrix is given as [9], [10]

$$\hat{H}_{SLS} = \frac{tr\{R_H\}}{\sigma_n^2 M_r + tr\{(PP^H)^{-1}\} + tr\{R_H\}} YP^{\dagger} \quad \textbf{(14)}$$

Here, σ_n^2 is the noise power; R_H is the channel correlation matrix defined as $R_H = E\{H^H H\}$ and $tr\{.\}$ implies the trace operation. The SLS estimation MSE is given as [9,10]

$$\begin{aligned} MSE_{SLS} &= E\{\left\|H - \gamma \hat{H}_{LS}\right\|_F^2\} \\ &= (1-\gamma)^2 tr\{R_H\} + \gamma^2 MSE_{LS} \end{aligned} \quad \textbf{(15)}$$

The minimized MSE of MMSE method can be written as [9,10]

$$MSE_{\min}^{SLS} = \frac{MSE_{LS} tr\{R_H\}}{MSE_{LS} + tr\{R_H\}} \quad \textbf{(16)}$$

By taking into account expression (12), the minimized MSE of the SLS method (16) can rewritten as

$$\begin{aligned} MSE_{SLS} &= [(tr\{R_H\})^{-1} + \frac{\rho}{M_t^2 M_r}]^{-1} \\ &= [(tr\{\Lambda\})^{-1} + \frac{\rho}{M_t^2 M_r}]^{-1} \\ &= [(\sum_i^n \lambda_i)^{-1} + \frac{\rho}{M_t^2 M_r}]^{-1} \end{aligned} \quad \textbf{(17)}$$

where $n = min(M_r, M_t)$ and is λ_i the i-th eignvalue of the channel correlation R_H.

If TPNR is fixed then the following equality can be derived

$$MSE_{SLS} = [(\sum_i^n \lambda_i)^{-1} + \frac{\rho}{M_t^2 M_r}]^{-1} < \sum_i^n \lambda_i \quad \textbf{(18)}$$

As observed from (18), MSE decreases when the sum of eignvalues of R_H decreases. This shows that in order to minimize MSE, the sum of eigenvalues of R_H has to be reduced.

3.3. MMSE Method

In the MMSE method, the estimated channel matrix is given as (19) [9,10,23],

$$\hat{H}_{MMSE} = Y(P^H R_H P + \sigma_n^2 M_r I)^{-1} P^H R_H \quad \textbf{(19)}$$

The MSE of MMSE estimation is given as

$$MSE_{MMSE} = E\{\left\| H - \hat{H}_{MMSE} \right\|_F^2\} = tr\{R_E\} \quad \textbf{(20)}$$

in which R_E is an estimation error correlation written as

$$\begin{aligned} R_E &= E\{(H - \hat{H}_{MMSE})(H - \hat{H}_{MMSE})^H\} \\ &= (R_H^{-1} + \sigma_n^{-2} M_r^{-1} P P^H)^{-1} \end{aligned} \quad \textbf{(21)}$$

The minimized MSE is given as (22) [2,3,11]

$$MSE_{MMSE} = tr\{(\Lambda^{-1} + \sigma_n^{-2} M_r^{-1} Q^H P P^H Q)^{-1}\} \quad \textbf{(22)}$$

In (22), Q is the unitary eigenvector matrix of R_H and Λ is the diagonal matrix with eigenvalues of R_H. The minimized MSE for the MMSE method, given by Equation (22), can be rewritten using the orthogonality properties of the training sequence P and the unitary matrix Q, as shown by

$$\begin{aligned} MSE_{MMSE} &= tr\{(\Lambda^{-1} + \rho M_r^{-1} I)^{-1}\} \\ &= tr\{\begin{bmatrix} (\lambda_1^{-1} + \rho M_r^{-1})^{-1} & 0 & \cdots & 0 \\ 0 & (\lambda_2^{-1} + \rho M_r^{-1})^{-1} & \ddots & \vdots \\ \vdots & \ddots & \ddots & 0 \\ 0 & 0 & \cdots & (\lambda_2^{-1} + \rho M_r^{-1})^{-1} \end{bmatrix}\} \\ &= \sum_i^n (\lambda_i^{-1} + \rho M_r^{-1})^{-1} \end{aligned} \quad \textbf{(23)}$$

Assuming that TPNR in expression (13) is fixed, the bound for MSE is given by

$$MSE_{MMSE} = \sum_i^n (\lambda_i^{-1} + \rho M_r^{-1})^{-1} < \sum_i^n \lambda_i \quad \textbf{(24)}$$

The expression (24) shows that, similarly as in the SLS method, a smaller sum of eigenvalues of the channel correlation R_H leads to a smaller estimation error for the MMSE method. In other words, a smaller sum of eigenvalues of the channel correlation leads to the more accurate channel estimation.

From the above mathematical analysis it becomes apparent that when the value of TPNR is fixed the accuracy of a training-based MIMO channel estimation is governed by the sum of eigenvalues of the channel correlation matrix R_H. In turn, the properties of R_H and its eigenvalues are determined by the channel properties which are influenced by a signal propagation environment and an array antenna elements and configuration.

It is worthwhile to note that the spatial correlation (for example due to the presence of LOS component) is responsible for the channel rank reduction. In this case, the sum of eigenvalues of R_H has a smaller value. Thus from the derived expressions, it is apparent that the spatial correlation (due to an increased LOS component) contributes in a positive manner to improving the training-based MIMO channel estimation accuracy.

4. MIMO Channel Capacity Taking into Account Channel Estimation Errors

The achievement of high channel capacity in a MIMO system depends on two factors. One is a rank of channel matrix or effectiveness of freedom (EDOF). The other one is the availability of CSI at the receiver. In [26,27,29] it has been shown that higher accuracy of CSI leads to higher channel capacity. However, the undertaken investigations have not considered the channel properties.

If CSI is perfectly known at the receiver (but unknown at the transmitter), the capacity of a MIMO system with M_r receive antennas and M_t transmit antennas can be expressed as [1,24,25],

$$C = E(\log_2\{\det[I_{M_R} + \frac{\rho_{SNR}}{M_t}(HH^H)]\}) \quad \textbf{(25)}$$

In Equation (25), ρ_{SNR} is a signal to noise ratio (SNR). The channel matrix H is assumed to be perfectly known at the receiver.

In practical cases, H has to be replaced by the estimated channel matrix, which carries an estimation error. By assuming that the channel estimation error is defined as e and the estimated channel matrix as $\hat{H}$

$$\hat{H} = H + e \quad \textbf{(26)}$$

The received signal can accordingly be written as,

$$Y = \hat{H}S + eS + V \quad \textbf{(27)}$$

Correlation of e is given as

$$R_E = E\{(H - \hat{H})(H - \hat{H})^H\} = \sigma_e^2 I \quad \textbf{(28)}$$

in which σ_e^2 is the error variance. In [26,27], the definition of error variance is slightly different. Using Equation (20), we have

$$\sigma_e^2 = \frac{MSE}{M_r} \quad \textbf{(29)}$$

The channel capacity of MIMO system with an imperfectly known H at the receiver is defined as the maximum mutual information between Y and S and is given as

$$C = \max_{tr\{Q\} \le P} \{I(S; Y, \hat{H})\} \quad \textbf{(30)}$$

If the transmitter does not have any knowledge of the estimated channel, the mutual information in Equation (30) can be written as [26–29],

$$I(S; Y, \hat{H}) = I(S; Y \mid \hat{H}) = h(S \mid \hat{H}) - h(S \mid Y, \hat{H}) \quad \textbf{(31)}$$

Because adding any dependent term on Y does not change the entropy [28], then

$$h(S \mid Y, \hat{H}) = h(S - uY \mid Y, \hat{H}) \quad \textbf{(32)}$$

in which u is the MMSE estimator given as

$$u = \frac{E\{SY^H \mid \hat{H}\}}{E\{YY^H \mid \hat{H}\}} \quad \textbf{(33)}$$

Combining this with Equation (27), we have

$$u = \frac{E\{S(\hat{H}S + eS + V)^H \mid \hat{H}\}}{E\{(\hat{H}S + eS + V)(\hat{H}S + eS + V)^H \mid \hat{H}\}} = \frac{Q\hat{H}^H}{\hat{H}Q\hat{H}^H + E\{eQe^H\} + \sigma_n^2 I_{M_r}} \quad \textbf{(34)}$$

where $Q=E\{SS^H\}$ is a M_t by M_t correlation matrix of transmitted signal S defining the signal transmission scheme. The autocorrelation matrix holds the property that *trace*(Q) equal to the total transmitted signal power P_s ($\rho_{SNR}=P_s/\sigma_n^2$). If we assume the special case of M_t equal to M_r and the transmitted signal power being equally allocated to transmitting antennas, (34) becomes

$$u = \frac{Q\hat{H}^H}{\hat{H}Q\hat{H}^H + Q\sigma_e^2 I_{M_r} + \sigma_n^2 I_{M_r}} = \frac{p\hat{H}^H}{p\hat{H}\hat{H}^H + p\sigma_e^2 I_{M_r} + \sigma_n^2 I_{M_r}} \quad \textbf{(35)}$$

in which $p=P_s/M_t$ is the power allocated to the signal transmitted through each transmit antenna. Because conditioning decreases the entropy therefore

$$h(S - uY \mid \hat{H}) = h(S - uY \mid Y, \hat{H}) \quad \textbf{(36)}$$

Then we have

$$h(S - uY \mid \hat{H}) = h(S - uY \mid Y, \hat{H}) \quad \textbf{(37)}$$

In this case,

$$I(S;Y \mid \hat{H}) = h(S \mid \hat{H}) - h(S - uY \mid Y, \hat{H}) \quad \textbf{(38)}$$

For the case of $S \mid \hat{H}$ and $(S - uY \mid Y, \hat{H})$ having a Gaussian distribution, (38) can be expressed as [26,27,29],

$$\begin{aligned} I(S;Y \mid \hat{H}) &\geq E\{\log_2[\det(\pi e Q)]\} - \\ &\quad E\{\log_2[\det(\pi e E\{(S - uY)(S - uY)^H \mid \hat{H}\})]\} \\ &\geq E\{\log_2[\det(I_{M_r} + \frac{p\hat{H}\hat{H}^H}{I_{M_r}(p\sigma_e^2 + \sigma_n^2)})]\} \end{aligned} \quad \textbf{(39)}$$

The lower bound of the ergodic channel capacity can be shown to be given as

$$\begin{aligned} C &= E\{\log_2[\det(I_{M_r} + \frac{p\hat{H}\hat{H}^H}{p\sigma_e^2 + \sigma_n^2})]\} \\ &= E\{\log_2[\det(I_{M_r} + \frac{\frac{P_s}{M_t}\hat{H}\hat{H}^H}{\sigma_n^2}\frac{1}{1 + \frac{P_s}{M_t}\frac{\sigma_e^2}{\sigma_n^2}})]\} \\ &= E\{\log_2[\det(I_{M_r} + \frac{\rho_{SNR}\hat{H}\hat{H}^H}{M_t}\frac{1}{1 + \frac{\rho_{SNR}}{M_t}\frac{MSE}{M_r}})]\} \end{aligned} \quad \textbf{(40)}$$

Equation (40) indicates that for a fixed value of SNR, the capacity is a function of the estimated channel matrix $\hat{H}$ and the channel estimation error σ_e^2. As a result, the channel properties and the quality of channel estimation influence the MIMO capacity.

5. Simulation Results

Here we present computer simulation results which demonstrate the influence of channel properties on the training-based channel estimation. A 4×4 MIMO system including 4-element linear array antennas both at the transmitter and receiver is considered. The Jakes model presented in Section 2 is used to describe the propagation environment between BS and MS. The distance between transmitter and receiver is assumed to be 100λ. The Angle of Arrival (AoA) of LOS is set to 0°. The training sequence length L is assumed to be 4. The default antenna element spacing at both BS and MS is set to 0.5λ (wavelength).

Figure 2 shows a relationship between MSE and the sum of eigenvalues of the channel correlation matrix for both MMSE and SLS methods. The results include an effect of maximum angle spread (AS), antenna spacing and Rician factor K, which are related to the sum of eigenvalues of R_H. The obtained results are given in four sub-figures A, B, C and D.

Sub-figure A supports the theory presented in Section 3 that for MMSE and SLS methods channel estimation errors are smaller for smaller sums of eigenvalues of R_H. When the sum of eignvalues increases, the channel estimation accuracy becomes worse.

The relationship between the sum of eignvalues of R_H and the maximum AS is shown in sub-figure B. The sum of eigenvalues increases when AS increases. Larger values of AS correspond to a lower level correlation while smaller values of AS correspond to a higher level correlation. Higher values of spatial correlation lead to a smaller sum of eigenvalues of R_H. This condition helps to

improve the accuracy of the training based MIMO channel estimation.

Sub-figure C presents the relationship between the sum of eigenvalues and the MS transmitter antenna spacing. One can see that the sum of eigenvalues becomes smaller when the spacing distance is less than 0.2λ.

Sub-figure D gives the relationship between the sum of eigenvalues and the Rician factor K. The sum of eigenvalues is smaller at higher values of K (when the LOS component is strongest). This means that a stronger LOS component reduces the sum of eigenvalues and thus improves the channel estimation accuracy.

Figure 3 is plotted in three dimensions (3D) to provide a further support for the results of Figure 2. In this figure, the relationship between MSE, TPNR ρ and K for MMSE method is presented at three different values of maximum AS (indicating three special correlation levels). One can see that when TPNR is increased to 30dB the estimation error decreases almost to zero. When the value of Rician factor K is increased, indicating a stronger LOS component in comparison with NLOS components, the MSE decreases. This is consistent with the trend observed in Figure 2 that a stronger LOS component results in better estimation accuracy.

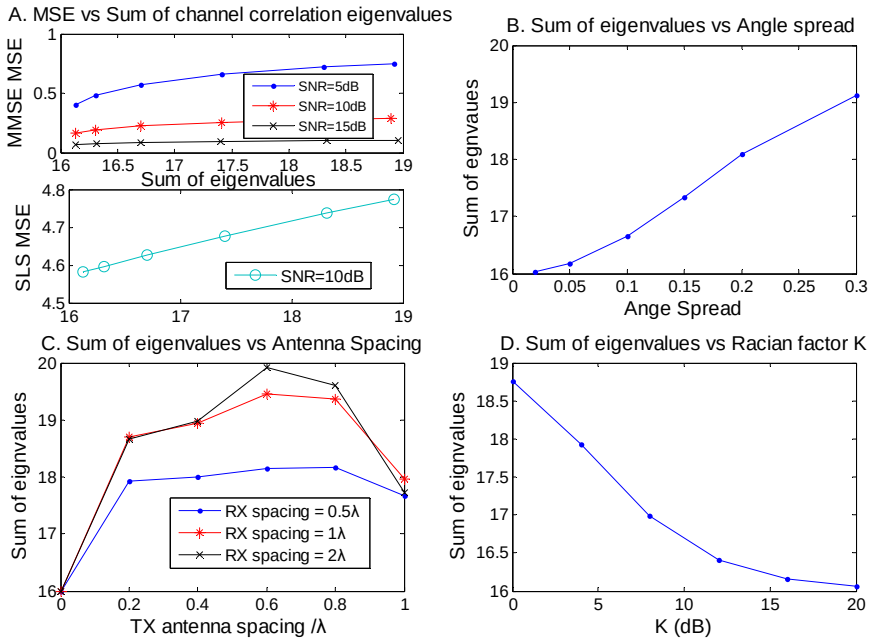

Figure 2. Relationship between MSE vs Sum of eigenvalues of R_H showing an impact of antenna spacing and the Rician factor K.

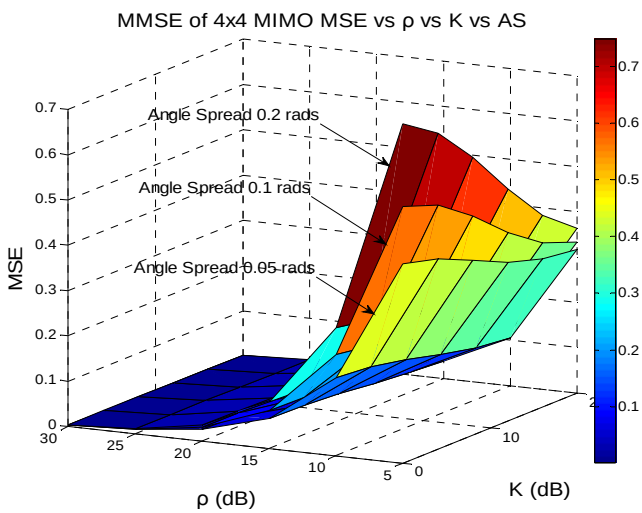

Figure 3. 3D plot of MSE vs TPNR and K for different values of AS for MMSE method.

The presented results also show that for MMSE method MSE is reduced for the smallest AS, which corresponds to the highest level of spatial correlation.

In the next step, we simulate the MIMO channel capacity under the condition of channel estimation error. Simulations are run for the cases of 2×2 MIMO and 4x4 MIMO systems. The simulation settings including the distance between the transmitter and receiver, training sequence length, AoA, AS and antenna element spacing are same as in the earlier undertaken simulations. The minimum mean square error (MMSE) channel estimation method is applied for the Jakes model representing the channel between the BS and MS. The channel capacity is determined using Equation (40). For simulation purposes, R_H is obtained using the actual channel matrix H and TPNR is assumed to be equal to SNR. 100000 channel realizations are used to obtain the value of capacity. Figure 4 shows the results for the 2×2 MIMO system.

Simulation results are plotted in two-dimensions (2D) and include two sub-figures. Sub-figure A presents the relationship between MSE and angle spread (AS). There are three groups of lines drawn for three different values of SNR. In each group, the lines correspond to three different values of K factor. The relationship between channel capacity and the angle spread is given in sub-figure B.

From Figure 4, one can see that the mean square error increases as the angle spread becomes larger. For all three groups, at K factor of 20dB, MSE shows the best performance while the worst accuracy occurs at the K factor of 0dB. In sub-figure B, the relationship trends are different from the ones observed in sub-figure A. As the angle spread increases, the channel capacity is enhanced. In all three groups of lines at three SNR values, the highest capacity occurs at K equal to 0dB while at 20dB the capacity is decreased. These two sub-figures indicate that the channel capacity is increased when the channel estimation accuracy is reduced. This finding is opposite to the one shown in [26,27,29]. This could be due to the fact that in [26,27,29] the influence of spatial correlation or K factor on the channel capacity was not considered. The presented simulation results strengthen the notion that the higher spatial correlation (due to a stronger LOS component) helps to improve the channel estimation accuracy. At the same time it decreases the rank and EDOF of the channel matrix.

Similar findings are obtained for the 4×4 MIMO system, as illustrated in Figure 5. The results are shown for SNR of 5, 10 and 15dB and the Rician factor K of 0 and 10dB.

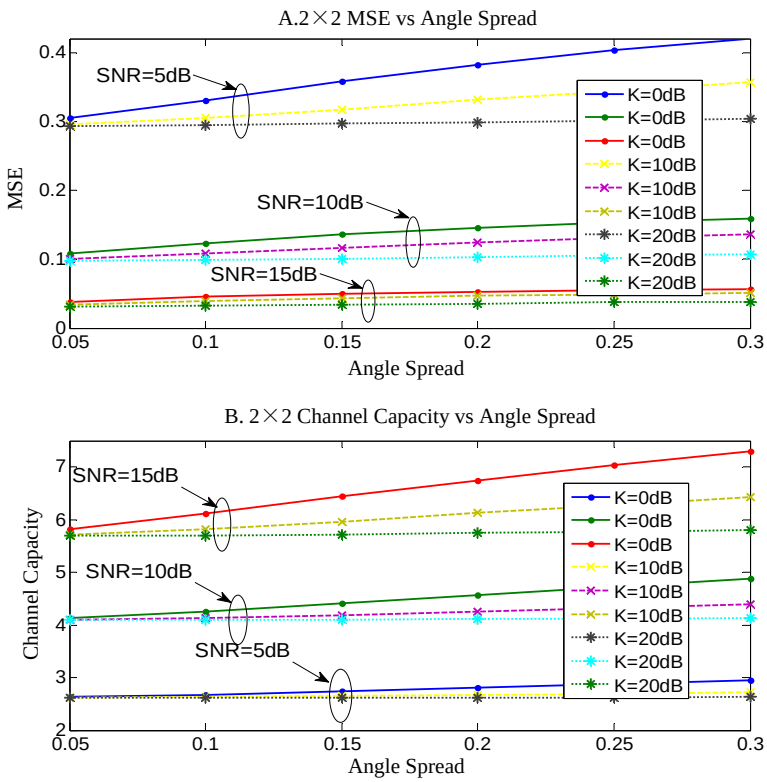

Figure 4. MSE vs Angle Spread and Channel estimation vs Angle Spread of a 2×2 MIMO under 3 different SNR and 3 different K factor.

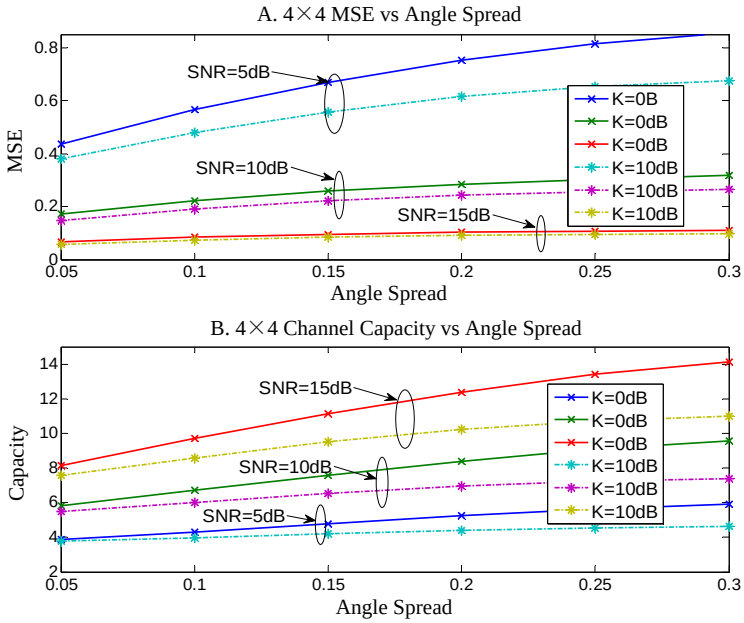

Figure 5. MSE vs Angle Spread and Channel estimation vs Angle Spread of a 4×4 MIMO under 3 different SNR and 3 different K factor.

At K factor of 10dB, MSE shows the best performance while the worst accuracy occurs at the K factor of 0dB. As the angle spread increases, the channel capacity increased. The highest capacity occurs at K equal to 0dB while at 10dB the capacity is decreased.

6. Conclusions

In this paper, the effect of spatial correlation on MIMO channel estimation accuracy and the resulting channel capacity has been investigated. The mathematical analysis and simulation results have shown that the accuracy of the training based MIMO channel estimation is governed by the sum of eigenvalues of the channel correlation matrix when the transmitted power to noise ratio (TPNR) in the training mode is fixed. Specifically, a smaller sum of eigenvalues leads to a more accurate channel estimation. A higher level of spatial correlation (that is due to a stronger LOS component and smaller angle spread) leads to a reduced value of the sum of channel correlation eigenvalues and hence has a positive influence on the channel estimation accuracy. However, this improvement in channel estimation does not necessarily lead to improving the channel capacity. This is because the channel matrix rank becomes reduced. The undertaken computer simulations undertaken for the uplink case, in which a mobile station (MS) transmitter is surrounded by scattering objects, have shown that higher spatial correlation levels due to a stronger LOS component decrease MIMO channel capacity despite the fact that channel estimation accuracy is improved.

7. References

[1] E. Telatar, "Capacity of multi-antenna Gaussian channels," European Transactions on Telecommunications, Vol. 10, No. 6, pp. 585− 596, November 1999.

[2] T. L. Marzetta and B. M. Hochwald, "Capacity of a mobile multiple-antenna communication link in Rayleigh flat fading," IEEE Transactions on Information Theory, Vol. 45, No. 1, pp. 139−157, January 1999.

[3] A. Narula, M. J. Lopez, M. D. Trott, and G. W. Wornell, "Efficient use of side information in multiple-antenna data transmission over fading channels," IEEE Journal on Selected Areas in Communications, Vol. 16, No. 8, pp. 1423−1436, October 1998.

[4] C. Budianu and L. Tong, "Channel estimation for space-time orthogonal block codes," IEEE Transactions on Signal Processing, Vol. 50, pp. 2515−2528, October 2002.

[5] A. Grant, "Joint decoding and channel estimation for linear MIMO channels," Proceedings of IEEE Wireless Communications Networking Conference, Vol. 3, pp. 1009−1012, Chicago, IL, September 2000.

[6] A. S. Kyung, R. W. Heath, and B. K. Heung, "Shannon capacity and symbol error rate of space-time block codes in MIMO Rayleigh channels with channel estimation error," IEEE Transactions on Wireless Communication, Vol. 7, No. 1, pp. 324−333, January 2008.

[7] X. Zhang and B. Ottersten, "Performance analysis of V-BLAST structure with channel estimation errors," IEEE 4th Workshop on Signal Processing Advances in Wireless Communications SPAWC, pp. 487−491, June 2003.

[8] P. Layec, P. Piantanida, R. Visoz and A. O. Berthet, "Capacity bounds for MIMO multiple access channel with imperfect channel state information," IEEE Information Theory Workshop ITW08, pp. 21−25, May 2008.

[9] M. Biguesh and A. B. Gershman, "MIMO channel estimation: Optimal training and tradeoffs between estimation techniques," Proceedings of International Conference on Communications, ICC'04, Paris, France, Vol. 5, pp. 2658−2662, June 2004.

[10] M. Biguesh and A. B. Gershman, "Training-based MIMO channel estimation: A study of estimator tradeoffs and optimal training signals," IEEE Transactions on Signal Processing, Vol. 54, No. 3, pp. 884−893, March 2006.

[11] X. Liu, S. Lu, M. E. Bialkowski and H. T. Hui, "MMSE Channel estimation for MIMO system with receiver equipped with a circular array antenna," Proceedings of IEEE Microwave Conference APMC2007, pp. 1−4, December 2007.

[12] X. Liu, M. E. Bialkowski, and S. Lu, "Investigation into training-based MIMO channel estimation for spatial correlation channels," Proceedings of IEEE International Antennas Propagation Symposium (APS-2007), pp. 51−55, August 2007.

[13] P. B. Rapajic and D. Popescu, "Information capacity of a random signature multiple-input multiple-output channel," IEEE Transactions on Communications, Vol. 48, pp. 1245−1248, August 2000.

[14] P. J. Smith and M. Shafi, "On a Gaussian approximation to the capacity of wireless MIMO systems," Proceedings of International Conference on Communications, ICC'02, pp. 406−410, 2002.

[15] P. F. Driessen and G. J. Foschini, "On the capacity formula for multiple-input multiple-output wireless channels: A geometric interpretation," IEEE Transactions on Communications, Vol. 47, pp. 173−176, February 1999.

[16] D. Shiu, G. J. Foschini, M. J. Gans, and J. M. Kahn, "Fading correlation and its effect on the capacity of multielement antenna systems," IEEE Transactions on Communications, Vol. 48, No. 3, pp. 502−513, March 2000.

[17] V. Erceg, "Indoor MIMO WLAN channel models," IEEE 802.11-03/161r2, September 2003.

[18] P. Uthansakul, M. E. Bialkowski, S. Durrani, K. Bialkowski, and A. Postula, "Effect of line of sight propagation on capacity of an indoor MIMO system," Proceedings of IEEE International Antennas Propagation Symposium (APS-2005), Washington, DC, pp. 707−710, 2005.

[19] E. G. Larsson and P. Stoica, "Space-time block coding for wireless communication," Cambridge University Press, 2003.

[20] C. N. Chuah, D. N. C. Tse, and J. M. Kahn, "Capacity scaling in MIMO wireless systems under correlated fading," IEEE Transactions on Information Theory, Vol. 48, pp. 637−650, March 2002.

[21] W. C. Jakes, "Microwave mobile communications," New York: John Wiley & Sons, 1974.

[22] T. L. Fulghum, K. J. Molnar and A. Duel-Hallen, "The Jakes fading model for antenna arrays incorporating azimuth spread," IEEE Transactions on Vehicular Technology, Vol. 51, No. 5, pp. 968−977, September 2002.

[23] S. M. Kay, "Fundamentals of statistic signal processing: Estimation theory", Prentice-Hall, Inc., 1993.

[24] G. J. Foschini and M. J. Gans, "On the limits of wireless communications in fading environment when using multiple antennas," Wireless Personal Communications, Vol. 6, pp. 311−335, 1998.

[25] B. M. Hochwald and T. L. Marzetta, "Capacity of a mobile multiple antenna communication link in Rayleigh flat fading," IEEE Transactions on Information Theory, Vol. 45, No. 1, pp. 139−157, January 1999.

[26] T. Yoo and A. Goldsmith, "Capacity and power allocation for fading MIMO channels with channel estimation error," IEEE Transactions on Information Theory, Vol. 52, No. 5, pp. 2203−2214, May 2006.

[27] T. Yoo and A. Goldsmith, "Capacity of fading MIMO channels with channel estimation error," IEEE International Conference on Communications, Vol. 2, pp. 808−813, June 2004.

[28] M. Medard, "The effect upon channel capacity in wireless communications of perfect and imperfect knowledge of the channel," IEEE Transactions on Information Theory, Vol. 46, pp. 933−946, May 2000.

[29] M. Torabi, M. R. Soleymani, and S. Aissa, "On the performance of MIMO-OFDM systems with imperfect channel information," International Conference on Wireless Networks, Communications and Mobile Computing, Vol. 1, pp. 600−605, June 2005.

Int. J. Communications, Network and System Sciences, 2009, 4, 249-324
doi:10.4236/ijcns.2009.24030 Published Online July 2009 (http://www.SciRP.org/journal/ijcns/).

BER Performance of Space-Time Coded MMSE DFE for Wideband Code Division Multiple Access (WCDMA)

Sanjay Kumar SHARMA[1], S. Naseem AHMAD[2]
[1]*Dept. of Electronics and Communication Engg., Krishna Institute of Engg. and Technology, Ghaziabad, India*
[2]*Dept. of Electronics and Communication Engg, Jamia Millia Islamia, Delhi, India*
Email: *sanjaysharma*1515*@yahoo.co.in*
Received January 20, 2009; *revised March* 1, 2009; *accepted April* 27, 2009

ABSTRACT

In recent times, there has been growing interests in integration of voice, data and video traffic in wireless communication networks. With these growing interests, WCDMA has immerged as an attractive access technique. The performance of WCDMA system is deteriorated in presence of multipath fading environment. The paper presents space-time coded minimum mean square error (MMSE) Decision Feedback Equalizer (DFE) for wideband code division multiple access (WCDMA) in a frequency selective channel. The filter coefficients in MMSE DFE are optimized to suppress noise, intersymbol interference (ISI), and multiple access interference (MAI) with reasonable system complexity. For the above structure, we have presented the estimation of BER for a MMSE DFE using computer simulation experiments. The simulation includes the effects of additive white Gaussian noise, multipath fading and multiple access interference (MAI). Furthermore, the performance is compared with standard linear equalizer (LE) and RAKE receiver. Numerical and simulation results show that the MMSE DFE exhibits significant performance improvement over the standard linear equalizer (LE) and RAKE receiver.

Keywords: Decision Feedback Equalizer, Multiple Access Interference (MAI), RAKE Receiver, Transmit Diversity, Wideband Code-Division Multiple-Access (WCDMA), Bit Error Rate (BER)

1. Introduction

During the period of last one decade, the large demands for wireless services and high data speeds have driven the wireless cellular networks to a tremendous growth. These large demands require some advanced techniques like WCDMA that can support more users and higher data rates. WCDMA has been accepted as standard access method for the third and fourth generation wireless systems. The WCDMA system assigns each user a specific signature sequence from the signature set. One limiting factor in the capacity (i.e. the number of users) of the WCDMA systems is the multiple access interference (MAI). In fact, in WCDMA system, multiple access interference (MAI) and intersymbol interference (ISI) are caused by multipath dispersion and are major problems. These problems cannot be efficiently suppressed by conventional RAKE receivers. The MAI caused by one user is usually small, but as the number of interferers or their power increases, effect of MAI becomes noticeable. To alleviate the effect of MAI, a number of multiple user detection methods have been proposed in literature in recent years [1]. Usually, the multiuser receiver can perform much better than the conventional correlator based receiver, but at the cost of increased system complexity. For uplink channel, the increased complexity is not a big issue since the base station may be equipped with some powerful computing processors. Whereas, a mobile terminal is limited by cost and size. Therefore, it will be very difficult to use the multiuser receiver for the downlink channel. But, irrespective of this problem, there is a strong emphasis to improve the performance of the downlink channel in WCDMA.

Another limiting factor in the cellular systems is fading. An usual technique for combating fading is spatial

diversity. In WCDMA systems, two methods of spatial diversity and interference cancellation can be combined to increase the system performance and capacity. The combination of MUD and receive diversity techniques has been proposed in [2,3]. In third generation WCDMA systems, the processing transmit gain may be very small. This makes the use of diversity quite effective. Transmit diversity can be used to alleviate fading efficiently. There are several forms of transmit diversity. In open-loop scenarios, where the transmitter does not have the channel state information, space-time transmit diversity (STTD) is generally used. When channel state information is available, closed-loop transmit diversity such as beam forming can be used. Over the period of last decade, various transmit diversity schemes have been proposed in modern wireless communications to combat fading. Among various proposed techniques, Alamouti's space-time block code [4], called as space- time transmit diversity (STTD), is one of the most effective solutions for two transmit antennas. Because of its effectiveness, Alamouti's space-time block code has been adopted for third generation WCDMA systems in indoor applications for high data rate.

WCDMA downlink has two interesting features. One is that all transmissions are synchronized and the other is that the spreading codes can be orthogonal. By taking advantages of these features, the chip-level equalization has been proposed to mitigate MAI with a despreader [5, 6]. A despreader can mitigate the MAI after chip-level equalization to restore the orthogonality. In [7], it has been shown that a receiver with a chip-level equalizer can be easily implemented with adaptive algorithms. Unfortunately, the performance of the receiver with a chip-level linear equalizer (LE) is not significantly better than the rake receiver, unless the receiver of the mobile station is equipped with multiple receiving antennas or uses over sampling. Because the LE cannot perfectly suppress the miltiptah interference with a single receive antenna and chip rate sampling, a residual multipath interference exists. Thus, the MAI cannot be completely removed by the correlator or despreder. To avoid this, multiple receive antennas or a higher sampling rate can be used for the chip level minimum mean square error linear equalizer (MMSE-LE) [10]. Decision feedback equalization is a powerful equalization technique that provides postcursor ISI cancellation with reduced noise enhancement and is widely used to offer better steady-state performance than a linear equalizer (LE). Recent research has been devoted to the receiver design using zero forcing [11], minimum MSE (MMSE) [12] methods.

The zero forcing receivers can completely suppress the ISI and multi-user interference under certain conditions. However, explicit knowledge of all the signature waveforms is required and the noise may be enhanced. Hence, the receiver designed by using the MMSE criterion seems to be better than zero-forcing receivers in terms of their bit error rate (BER) performance. In this paper, we investigate and analyze a minimum mean-square error (MMSE) decision feedback equalizer (DFE) for space-time coded WCDMA downlink channel to achieve better performance than the chip level LE and a RAKE receiver in a frequency selective channel.

The rest of the paper is organized as follows. The signals and system models have been introduced in section 2.In subsection 2.1 we have discussed the basic space-time encoder in WCDMA. In subsection 2.2,we have presented the structure of a traditional decision feedback equalizer (DFE). The space-time coded decision feedback equalizer (DFE) has been formulated in subsection 2.3. Subsection 2.4 presents the mathematical analysis. In section 3, we have formulated the simulation environments. Computer simulation results are presented in section 4 to see the performance and we conclude the paper with some remarks in section 5.

2. Signal and System Models

2.1. Basic Space-Time Encoder in WCDMA

Figure 1 shows the basic space-time transmit diversity (STTD) encoder in WCDMA. We consider two symbols periods, 0 and 1, over which two symbols are sent. During symbol period 0, symbol c_0 is sent on transmit antenna A and c_1^* is sent on antenna B.

During symbol period 1, c_1 is sent on transmit antenna A and c_0^* is sent on antenna B. It is assumed that the same channelization code is used to send these STTD encoded symbols. But, the pseudo-random scrambling codes are different for different symbol periods. Let $h_{ji}(t)$ denote the continuous-time impulse response of the multipath channel from transmitter antenna i to the receive antenna j. A time-variant multipath signal propagation through the mobile cellular radio channel can be modeled as:

$$h_{ji}(t)=\sum_{q=0}^{Q-1}\alpha_{ji,q}(t)e^{j\theta_{ji,q}(t)}\,\delta(t-\tau_{ji,q}(t)) \qquad \textbf{(1)}$$

where Q is the number of channel multipath, $\delta(\cdot)$ is

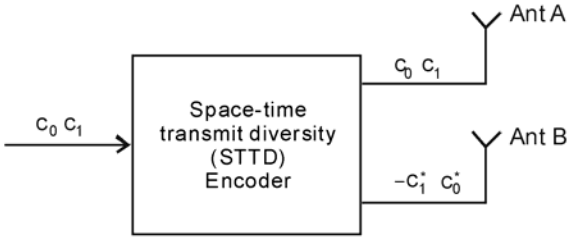

Figure 1. Space-time encoder in WCDMA.

the Dirac-delta function, and $_{ji,q}(t)$, $_{ji,q}(t)$ and $_{ji,q}(t)$ are the time-variant attenuation, phase distortion and propagation delay of the qth path from transmit antenna *i* to receive antenna *j*, respectively.

2.2. Traditional Decision Feedback Equalizer

We first describe a traditional decision feedback equalizer (DFE) receiver, upon which a two dimensional DFE for WCDMA system builds. Figure 2 shows a discrete-time complex base band model for the conventional DFE. The DFE consists of a feed forward filter $f(n)$ and a feedback filter $b(n)$, where n is the symbol index. Since the feedback filter sits in a feedback loop, it must be strictly causal. The signal propagates through a discrete time-variant frequency selective fading channel $h(n)$.

Also, r(n) → received signal, d(n) → transmitted symbols information, $\hat{d}(n)$ → output of DFE.

2.3. Space-Time Coded Decision Feedback Equalizer (DFE)

We concentrate on WCDMA downlink channel with transmit diversity. The system employs two transmit antennas at the transmitter side and one receive antenna at the receiver side. We assume that there are K active users in the cell under consideration and that the inter-cell interference is negligibly small in cellular scenario. Also, there are M transmit antennas and V receive antennas in the system.

Now, the transmitted signal of user k from antenna m, represented by $x_k^{(m)}(t)$, is given by

$$x_k^{(m)}(t) = \sum_{n=0}^{N-1} A_k\, c_k^{(m)}(n)\, w_{k,n}(t - nT_s) \qquad \textbf{(2)}$$

where, $c_k^{(m)}(n)$, $n = 0, \ldots, N\text{-}1$, is the kth user's space-time coded data sequence to be transmitted from antenna m within a specific time-frame

A_k is the average amplitude of the kth user

T_s is the symbol duration

$w_{k,n}(t)$ is the signature waveform of user k at the nth symbol period

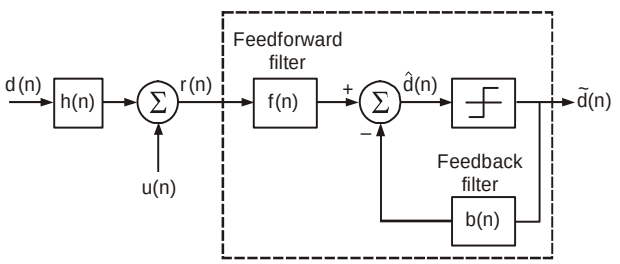

Figure 2. The traditional DFE structure.

The signature waveform $w_{k,n}(t)$ is represented as

$$w_{k,n}(t) = \frac{1}{\sqrt{G}} \sum_{i=0}^{G-1} s_{k,n}(i)\, p(t - iT_c) \qquad \textbf{(3)}$$

where G is the processing gain,

T_c is the chip duration,

$p(t)$ is the chip pulse shape signal

$s_{k,n}(i)$ is the kth user's signature sequence

The spread signal is transmitted over the frequency and time selective channels. The channels from the two base station antennas to the receiver are modeled as Rayleigh multipath fading channels. Then, according to basic equation (1), the impulse response of the channels between the base station transmitter and the mobile station receiver is

$$h^{(m)}(t) = \sum_{q=0}^{Q-1} h_q^{(m)}\, \delta(t - t_q), \quad m = 1, 2 \qquad \textbf{(4)}$$

where Q is the number of paths,

$h_q(m)$ is a complex coefficient which is used to model the qth path

t_q is the delay related to the qth path.

We assume that the number of paths and their delay times are equal for the two channels. Finally, the received signal from all K users at a mobile base station after demodulation is given by

$$r(t) = \sum_{m=1}^{2} \sum_{q=0}^{Q-1} \sum_{k=0}^{K-1} h_q^{(m)}\, x_k^{(m)}(t - t_q) + u(t) \qquad \textbf{(5)}$$

where $u(t)$ is the additive white Gaussian noise (AWGN) with noise variance of σ^2.

It may be more convenient to consider a discrete-time signal model. Accordingly, the received signal sequence is written as

$$r(n) = \sum_{m=1}^{2} \sum_{q=0}^{Q-1} \sum_{k=0}^{K-1} h_q^{(m)}\, x_{k-q}^{(m)} + u_k \qquad \textbf{(6)}$$

where $r(n)$ is the received signal sequence, and u_k is the white noise sequence.

2.4. Mathematical Analysis

To achieve transmit diversity; we use Alamouti's space-time block code for two transmit and one receive antennas [4]. In a space-time block-level encoding scheme, each block of 2N information symbols $d_k(n)$, $n = 0, \ldots, 2N\text{-}1$, is split into two blocks of odd and even symbols, each having length N. Further, these two blocks are space-time encoded and transmitted during two subsequent periods, each having a duration of NT_s. This means that for the first and second period, we have

$$\left.\begin{aligned} c_k^{(1)}(n) &= d_k(2n) \\ c_k^{(2)}(n) &= d_k(2n+1) \\ c_k^{(1)}(n+N) &= -d_k^*(2n+1) \\ c_k^{(2)}(n+N) &= d_k^*(2n) \end{aligned}\right\} \quad \textbf{(7)}$$

where $n = 0, \ldots\ldots, N-1$.

If we place a guard-time t_g between two transmission periods, the received signal $r(t)$ consist of two non- interfering signals. Now, let $d_o(2n)$ and $d_o(2n + 1)$ be the desired symbols to be detected at the receiver. According to Figure 2, $r(t)$ is first allowed to pass through the two matched filters which are matched to the corresponding spreading waveforms of the user and then sampled at times t_v, $v = 0, \ldots, i-1$. Then, we have

$$r_1 = \int_0^{T_s} w_{0,n}^*(\tau)\, r(\tau + nT_s + t_v)\, d\tau \quad \textbf{(8)}$$

$$r_2 = \left[\int_0^{T_s} w_{0,n+N}^*(\tau)\, r(\tau + (n+N)T_s + t_v + t_g)\, d\tau\right]^* \quad \textbf{(9)}$$

For ideal correlation properties of signature waveforms, there shall be no ISI and MAI in above samples. Thus, in ideal scenario, a RAKE receiver and a linear equalizer (LE) can work as optimum receiver [8]. But, in practice, because of non-zero auto and cross-correlations of the shifted signature waveforms, ISI and MAI occur and hence the performance of a RAKE receiver deteriorates in highly interference environments. Thus, to achieve the performance improvement, we use a space-time coded DFE structure with two transmit and one receive antenna as shown in Figure 3. Now, the input to the first decision part, to detect $d_0(2n)$, is written as

$$d_e = \sum_{q=0}^{L_f-1} [f_{11}(L_f - 1 - q) r_{1,q} + f_{21}(L_f - 1 - q) r_{2,q}] + \sum_{m=1}^{L_b} [b_{11}(L_b - m)\hat{d}_o(2n-2m) + b_{21}(L_b - m)\hat{d}_o(2n-2m+1)] \quad \textbf{(10)}$$

The expression in equation (10) may be written in matrix form as under:

$$\mathbf{d_e} = \mathbf{F^H}\ \mathbf{Y} \quad \textbf{(11)}$$

Here,

$$\mathbf{F^H} = [f_{11}(L_f - 1), \ldots, f_{11}(0), f_{21}(L_f - 1), \ldots, f_{21}(0), b_{11}(L_b - 1), \ldots, b_{11}(0), b_{21}(L_b - 1), \ldots, b_{21}(0)] \quad \textbf{(12)}$$

And

$$Y = [r_{1,0}, \ldots, r_1, L_f - 1, r_{2,0}, \ldots, r_2, L_f - 1, d_o(2n-2) \ldots, d_o(2n - 2L_b), d_0(2n-1), \ldots, d_o(2n - 2L_b + 1)]^J \quad \textbf{(13)}$$

The mean square error (MSE) is given by

$$\boldsymbol{\varepsilon} = E\{|d - d_o(2n)|^2\}$$

Now, to achieve the performance improvement, we have to minimize the mean square error (MSE). For that purpose, we must decide appropriate value of weight vector. The solution to the MMSE problem is given by

$$\mathbf{F^H} = \mathbf{A^{-1}}\ \mathbf{G} \quad \textbf{(14)}$$

where $\mathbf{A} = E.\{\mathbf{Y}\ \mathbf{Y}^H\}$ **(15)**

and $\mathbf{G} = E\{\mathbf{Y}\ \mathbf{Y}\ \boldsymbol{d}_o^*(2n)\}$ **(16)**

To determine matrix **A** and vector **G**, we must know the channel model and also we assume that the interfering user's signature codes and all the information symbols are independent random sequences. Now, the minimum mean-square error for the system can be written as

$$\boldsymbol{\varepsilon}_{\min} = 1 - \mathbf{G}^{\mathrm{H}}\,\mathbf{S}^{-1}\,\mathbf{G} \quad \textbf{(17)}$$

We can estimate the overall signal-to-noise ratio per symbol, using the Gaussian approximation, from the MMSE as [9]

$$\mathrm{SNR} = (1 - \boldsymbol{\varepsilon}_{\min}) / \boldsymbol{\varepsilon}_{\min} \quad \textbf{(18)}$$

Hence, the bit error rate (BER) can be approximated as under:

$$\mathrm{P_e} = Q(\sqrt{SNR})$$

$$\mathrm{P_e} = Q\left(\sqrt{(1 - \boldsymbol{G}^H \boldsymbol{A}^{-1}\boldsymbol{G}) / \boldsymbol{G}^H \boldsymbol{A}^{-1}\boldsymbol{G}}\right)$$

From above expression, it is obvious that P_e depends upon the coefficients of the channel and signature waveform of the desired user.

3. Simulation Environments

We study the performance of a chip-rate DFE in a WCDMA downlink channel using QPSK modulation scheme and a spreading factor of 32. We have assumed Rayleigh fading channels and channel coefficients as complex Gaussian random variables. The system transmits the data at 480 kbps, and the frame structure of 10ms duration includes 15 slots. Each slot consists of 160 QPSK symbols that are spread by the Walsh-Hadmard code with period 32. As a whole, a chip rate of 3.84 Mc/s is used. The channel taps are each subject to the Rayleigh fading around their mean value. Throughout the simulation work, the estimation is performed at S/N = 10 dB. We assume 16 active users within the same cell/frequency. However, the actual number of users may be more depending upon the service.

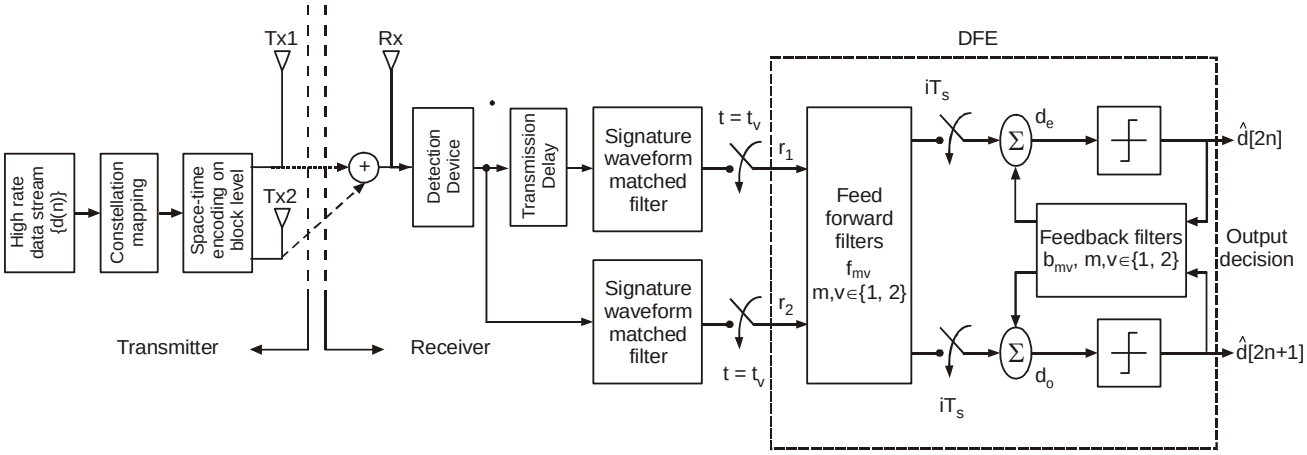

Figure 3. System model.

For two transmit antenna structure shown in figure 3, the feed forward filters are represented by $f_{mv}(n)$, $m, v \in \{1, 2\}$, each having L_f taps and sampling is performed at i times the chip rate. Also, the feedback filters are represented by $b_{mv}(n)$, $m, v \in \{1, 2\}$, each having L_b taps and operating at the symbol rate. Throughout the simulation work, the Rayleigh fading channel uses $Q = 3$ paths and the number of DFE feed-forward taps, L_f is equal to four. Because of shorter length of channel memory than the period of symbols, it is evident that ISI is produced only by the adjacent symbols. Thus, the DFE feedback filters each requires only single tap. This means that we take $L_b = 1$. Further, simulation has been performed on over 4000 blocks each consisting of 800 space-time coded symbols and also channel is assumed constant during each frame.

Table 1. List of parameters for simulation.

S. No.	Simulation Parameter	Value
1	Carrier frequency	2 GHz
2	Modulation technique	QPSK
3	Data Rate	480 kbps
4	Processing gain	32
5	Signature or Spreading code	Walsh-Hadamard Code
6	Number of multipaths	3
7	Number of feed forward taps	4
8	Number of feedback filter taps	1
9	Chip rate	3.84 Mc/s
10	No. of transmit antenna	2
11	No. of receive antennas	1
12	Performance parameter	BER
13	Channel Model	Rayleigh multipath fading channel

4. Simulation Results

In Figure 4, the bit error rate (BER) has been plotted as a function of average signal to noise per bit (E_b/N_o) for Rake receiver, adaptive linear equalizer (LE) and DFE with two transmit antennas (two dimensional DFE) and one receive antenna. In this case, we have assumed 3-paths channels and 16 active users within the cell of interest. Also, the number of feed-forward taps, L_f for two-dimensional DFE has been taken equal to 4. Simulation has been performed on over 4000 blocks each consisting of 800 space-time coded symbols. From Figure 4, it may be observed that as E_b/N_o increases, BER of DFE fall faster than RAKE and linear equalizer. At higher values of E_b/N_o, the MAI dominates and the performance curve of RAKE receiver approaches a saturation level. At this point, significant performance improvement is achieved by DFE. In Figure 5, the bit error rate (BER) has been plotted as a function of number of active users for Rake receiver, adaptive linear equalizer (LE) and DFE with two transmit antennas (two dimensional DFE) and one receive antenna at E_b/N_o = 20dB. In this case also, we have assumed 3-paths channels and the number of feed-forward taps, L_f for two-dimensional DFE has been taken equal to 5. It can be observed as the number of users increases, MMSE DFE offers better performance than Rake receiver, adaptive linear equalizer (LE). Figure 6 reveals that as the speed of the mobile becomes higher, it is more difficult for the equalizer to manage successfully the variation of channel. It results in the increase of MAI in the receivers. Consequently, the performance of the DFE deteriorates as the speed of the mobile becomes higher. Also, the variation of the channel does not affect the performance of the rake receiver since the performance degradation is only due to the channel estimation error.

5. Conclusions

In the paper, we have investigated the receiver using MMSE DFE for WCDMA downlink with space-time transmit diversity in a frequency selective channel. Bit error rate (BER) of various systems has been calculated using Gaussian approximation. In simulation curves, we have shown the BER performances with respect to the number of users, E_b/N_o and mobile speed. It is observed that with the increase in number of transmissions, the performance of all the receivers, *i.e.*, adaptive LE, the Rake and the DFE, becomes worse because of increase in intersymbol interference (ISI) and multiple access interference (MAI). According to simulation curves, a MMSE DFE outperforms an adaptive LE and a RAKE receiver for the large number of users and also when BER is compared with respect to the E_b/N_o values. This happens because a MMSE DFE suppresses interference

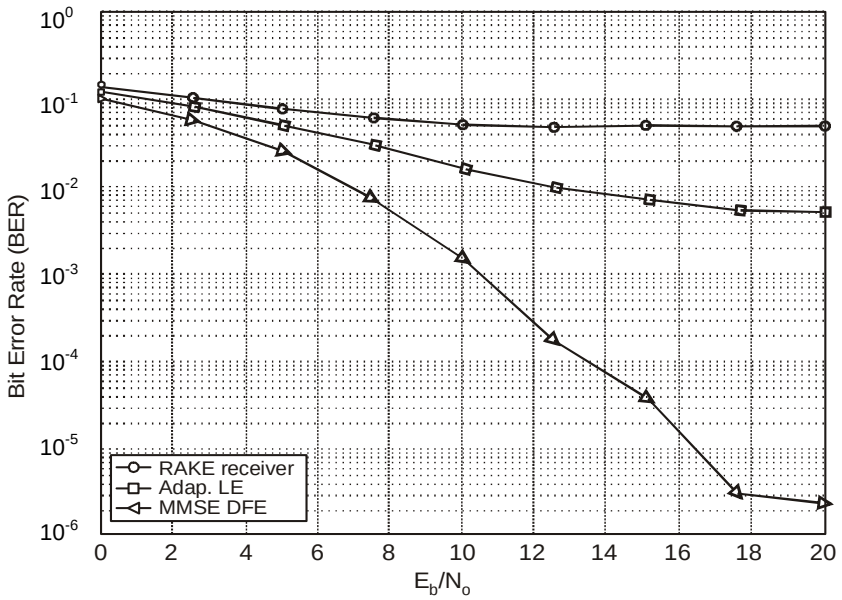

Figure 4. BER versus E_b/N_o.

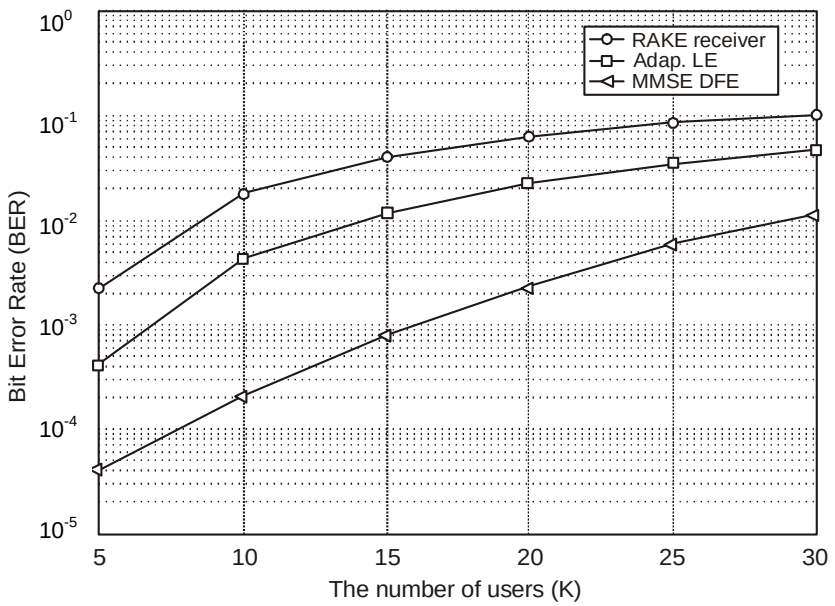

Figure 5. BER versus the number of active users.

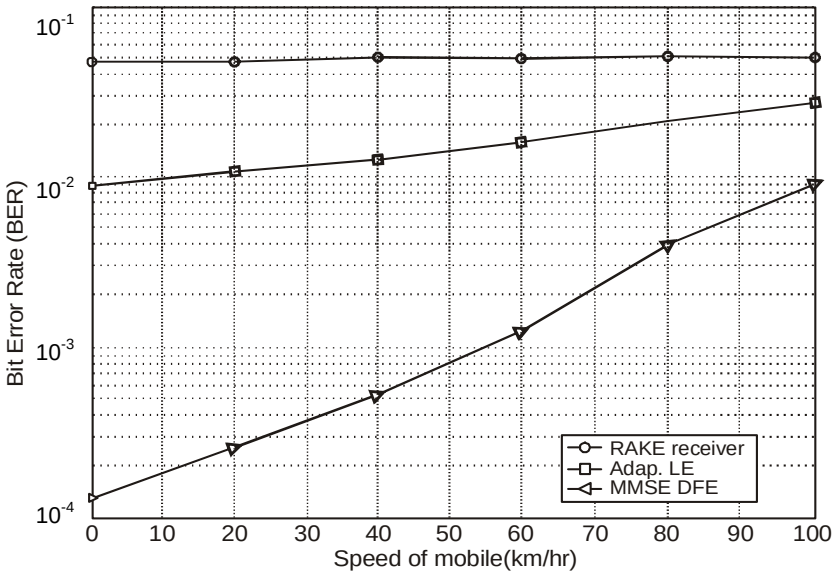

Figure 6. BER performance with respect to the speed of the mobile.

more efficiently compared to an adaptive LE and a RAKE receiver. It is also concluded that the structure of space-time coded MMSF DFE, when compared to other schemes of similar complexity, provides a reasonable balance between noise, ISI and MAI. Thus, this scheme works well when any of these three problems dominates. However, at very high interference levels, the use of transmit diversity does not improve the performance, unless the interference is suppressed by more sophisticated methods such as multi-user detection. As a whole, it is concluded that, in a wireless system, equalization, diversity, and STBC coding can be used together to boost the received signal quality and link performance. Although the system with only two transmit antennas is investigated here, it can be straightforwardly extended to a system with more transmit antennas. All these elegant results can be used for evaluating the system capacity, designing power control algorithms and appropriate channel coding techniques for WCDMA.

7. References

[1] S. Verdu, "Multiuser detection," Cambridge University Press, New York, 1998.

[2] S. M. Razavizadeh, V. T. T. Vakili, and P. Azmi, "Comparison of several multiple antenna multiuser detectors in wireless CDMA system," in Proceedings of the 5th IFIP TC6 Conference on Mobile and Wireless Networks (MWCN2003), 2003.

[3] Z. Zvonar, "Combined multiuser detection and diversity reception for wireless CDMA system," IEEE Transactions on Vehicular Technology, Vol. 45, pp. 205−211, February 1996.

[4] S. M. Alamouti, "A simple transmit diversity technique for wireless communication," IEEE Journal on Selected Areas in Communications, Vol.16, No. 8, pp. 1451−1458, October 1998.

[5] C. D. Frank and E. Visotsky, "Adaptive interference suppression for direct-sequence CDMA systems with long spreading codes," presented at the 36th Allerton Conference, 1998.

[6] A. Klein, "Data detection algorithms specially designed for the downlink of CDMA mobile radio system," in Proceedings of IEEE VTC-1997, pp. 203−207, 1997.

[7] F. Petre, M. Moonen, M. Engels, B. Gyselincky, and H. D. Man, "Pilot-aided adaptive chip equalizer receiver for interference suppression in DS-CDMA forward link," in Proceedings of IEEE VTC-Fall 2000, pp. 303−308, 2000.

[8] J. Wang and K. Yao, "Space-time coded wideband CDMA system," in Proceedings of VTC 2002, Vol. 1, pp. 260−264, Spring 2002.

[9] M. Abdulrahman, A. U. H. Sheikh, and D. D. Falconer, "Decision feedback equalization for CDMA in indoors wireless communication," IEEE Journal on Selected Areas in Communications, Vol. 12, No. 4, pp. 698−706, May 1994.

[10] T. Udomsripariboon, C. Mingukwan, C. Benjangkaprasert, O. Sangaroon, and K. Janchitrapongvej, "Soft output decision feedback equalizer using variable step-size algorithm for turbo codes DS/CDMA systems," in Proceedings of IEEE ISPACS, pp. 505−508, December 2005.

[11] S. Haykin and M. Moher, "Modern wireless communications," Prentice-Hall, 2005.

[12] K. Takeda, K. Ishihara, and F. Adachi, "Downlink DS-CDMA transmission with joint MMSE equalization and ICI cancellation," Proceedings of IEEE VTC 2006-spring, Melbourne, Australia, Vol. 4, pp. 1762−1766, May 7−10, 2006.

Int. J. Communications, Network and System Sciences, 2009, 4, 249-324
doi:10.4236/ijcns.2009.24031 Published Online July 2009 (http://www.SciRP.org/journal/ijcns/).

Optimal Positions of Relay Stations for Cluster-Based Two-Hop Cellular Network

Hrishikesh VENKATARAMAN[1,2], Pradeep Kumar JAINI[2], Segu REVANTH[2]
[1]*Performance Engineering Laboratory (PEL), School of Electronic Engineering, Dublin City University, Ireland*
[2]*Next Generation Wireless Systems, Dhirubhai Ambani Institute of Information and Communication Technology (DAIICT), Gandhinagar, India*
Email: *hrishikesh@ieee.org*
Received December 22, 2008; *revised February* 27, 2009; *accepted April* 1, 2009

ABSTRACT

Multihop cellular networks is an exciting and a fledgling area of wireless communication which offers huge potential in terms of coverage enhancement, data-rates, power reduction, and various other quality of service improvements. However, resource allocation in MCN is an NP-hard problem. Hence, significant research needs to be done in this field in order to efficiently design the radio network. In this paper, optimal position of relay stations in a hierarchical cluster-based two-hop cellular network is investigated. Vector algebra has been used to derive general equation for carrier-to-interference ratio (C/I) of a mobile station. It has been observed that when the transmit power of base station (BS) and the gateway (GTW)/relay station (RS) are same, the RSs should be located close to mid-point of BS and the edge of the cell. However, significantly, when the transmit power of the BS is greater than that of the GTW, then the RSs should be placed closer to the edge of the cell, in order to maximize the minimum C/I at any point in the cell. This in turn results in higher modulation technique at the physical layer, and hence, a higher data-rate to all the users in the system.

Keywords: Cluster-Based Design, Power Control, Relay Stations, Two-Hop Cellular

1. Introduction

The next generation cellular networks need to provide very high data-rates to the end users in order to support the ever growing demand of high quality multimedia services while on the move. An increase in the data-rate is possible either by increasing the bandwidth or reducing the interference. The data-rate can also be increased by increasing the transmit power or by reducing the distance between the source and destination node. Since mobile stations (MSs) are energy constrained devices, the transmit power of the MSs cannot be increased indiscriminately, and hence, traditional single-hop cellular networks cannot provide high data-rate communication. Importantly, a high quality of service (QoS) cannot be provided to the wireless devices due to the large transmission distance between the base station (BS) and MSs. Reducing the cell coverage area by increasing the number of BSs is not a feasible solution due to the enormous cost of installing a BS. An efficient alternate solution to increase the data-rate is to employ relay stations (RSs), alternatively known as gateways (GTWs), whereby, the BSs would communicate with the far off and otherwise unreachable MSs in multiple hops through GTWs [1]. Figure 1 shows a single cell scenario for next generation multihop cellular networks (MCN). Combining cellular and multihop communication models in a wireless network results in better relaying and avoids traffic congestion [2]. It is shown in [3] that connectivity of the network is increased drastically in an infrastructure-based multihop network as compared to a traditional single-hop cellular or a distributed *ad hoc* network. Usage of relays can clearly help in improving the performance of the users especially at the edge of the cells, and thereby solves the coverage problems for high data-rates in macrocells [4].

A relay based multihop hybrid cellular network was proposed in [5] in order to balance the traffic load among highly loaded cells and lightly loaded cells. Several architectures and mechanisms have been proposed in the

recent past [6,7] in order to efficiently design a MCN. In addition, a time division duplexing (TDD)-based MCN offers the potential to integrate various overlapping wireless technologies such as UMTS or CDMA 2000 (3G networks), WiMAX and WiFi [8]. Hence, by having simultaneous transmission by both BSs and relays, capacity gains can also be achieved in the cellular network. At the same time, integrating multihop component into cellular networks requires additional radio resources and increased overhead signals to transmit data in different hops and that too over a heterogeneous network [9]. In addition, interference is created due to a larger number of simultaneous transmissions in the network. Hence, the actual benefit of multihop relaying becomes unclear [10]. In fact, it is shown in [9,11] that if the MSs are close to the BS, then relaying and multihop need not be always beneficial. Hence, an efficient and an adaptive resource allocation scheme is needed in order to maximize the system capacity. However, resource allocation is a very challenging issue and is proved to be an NP-hard problem [12]. Hence, researchers across the world have mainly focused on two-hop cellular networks. Several algorithms have been recently proposed for two-hop cellular networks [13–15]. Though effective, these algorithms only provide a marginal benefit. Recently, a novel hierarchical cluster-based architecture for two-hop cellular network has been proposed in [16,17]. The cluster-based design is found to be superior in terms of the attainable system capacity than the benchmark algorithms available in the literature [17]. In this architecture, the cells are divided into two regions, the inner and outer region. The MSs in the inner region communicate with the BS directly, like in a traditional single-hop cellular network. Significantly, the MSs in the outer region are grouped into several clusters, and these MSs communicate with the BS in two hops through the cluster-head nodes, which act as RSs/GTWs.

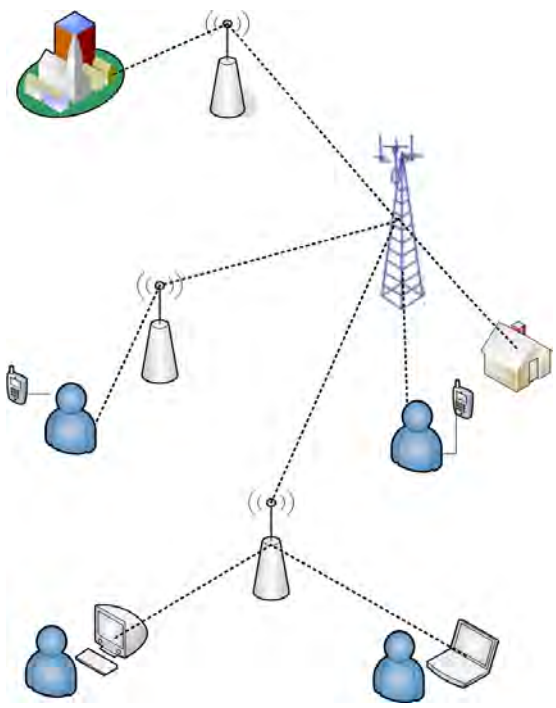

Figure 1. Example of a multihop cellular network.

In this paper, the optimum position of the GTWs in the cluster-based architecture is investigated for different transmit power ratios between the BS and GTW. An uncoded system is considered in the baseband design, and a minimum uncoded bit error rate (BER) of 10^{-2} is taken as the prerequisite for any link to communicate (an equivalent BER of approximately 10^{-6} in a coded system). A carrier to interference ratio (*C/I*) threshold is defined according to the BER so that the *C/I* at any position in the cell does not fall below the threshold. Vector algebra is used to compute the optimum GTW position in the cell that would minimize the transmit power required at both the BS and the GTW.

The organization of the paper is as follows: Section 2 describes the hierarchical cluster-based two-hop cellular architecture. Section 3 provides a mathematical analysis for calculating the *C/I* at any position in the outer region of the cell, and also derives the relation between the GTW position, and the transmit power ratio between the BS and the GTW node. Section 4 explains the numerical results and its implication, and finally, conclusions are provided in Section 5.

2. System Model

A multi-cellular network is considered with a center cell surrounded by six cells in the 1st tier. Each cell has a BS at the center, and has an edge of length, r. Each cell is divided into two regions: an inner region and an outer region. The inner region is a circle and has a radius, τr, where $0 \le \tau \le 1$. The MSs in the inner region communicate with the BS directly. The outer region is divided into several elliptical sectors, also called as clusters. It has been shown mathematically in [18] that a maximum system capacity is achieved when the number of clusters in a cell is *six*. Hence, in the cluster-based design, the MSs in the outer region are clubbed into six clusters per cell, as shown in Figure 2. Each MS in any of the clusters communicates with the BS in two hops, through the GTWs, that act as cluster-heads. A time division multiple access (TDMA) scheme is considered so that the relays can receive and transmit the signal at the same frequency. Being a two-hop network, the MSs in the outer region require two different radio resources (two time instants in a TDMA system) to communicate to the BS. Hence, every pair of the two-hop network would communicate over only half the TS period, as compared to an equiva

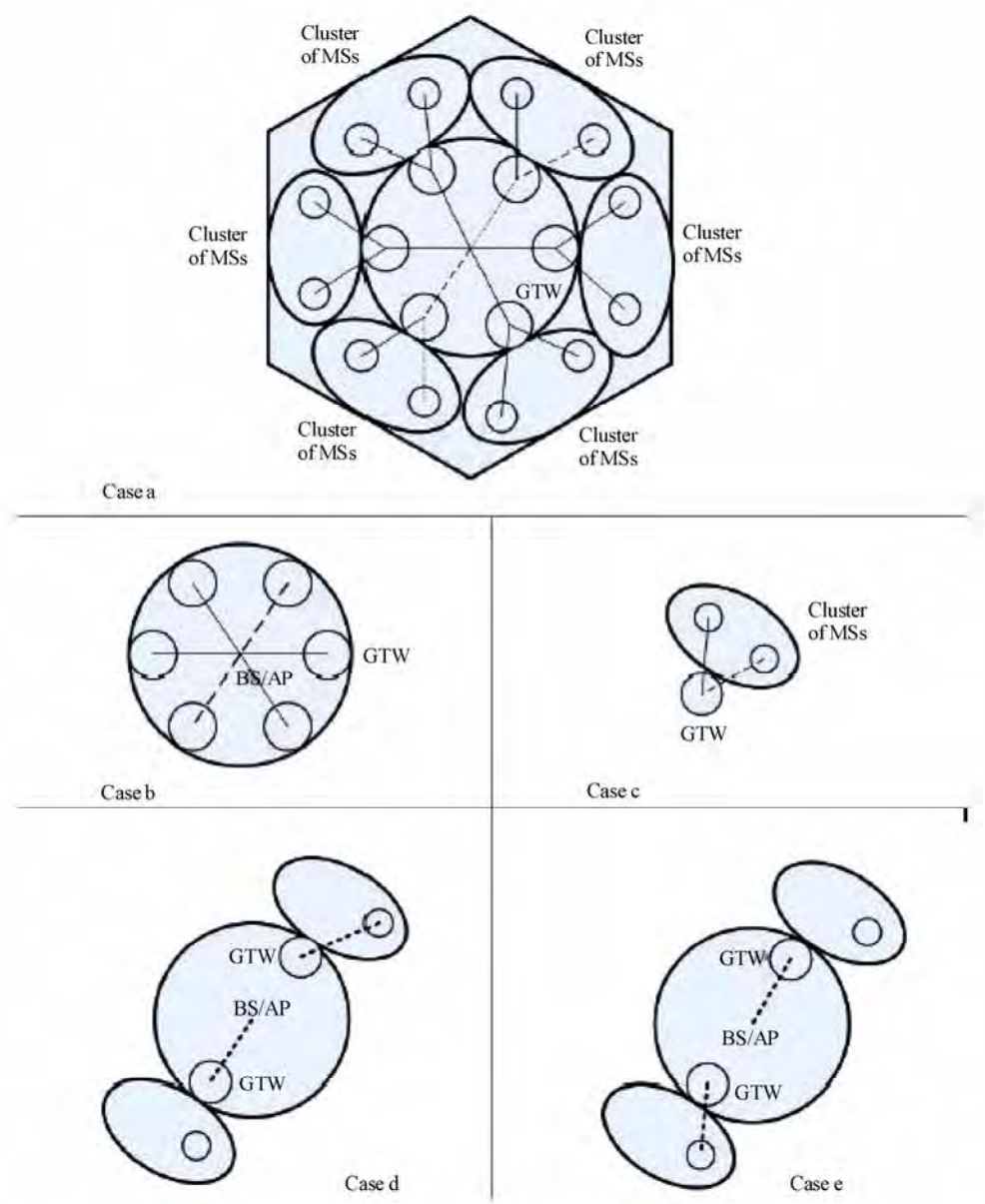

Figure 2. Multi-cellular architecture with all GTWs in cell located at equidistant distance from the BS.

lent single-hop network. Since the transmission distance of every communicating pair is reduced in the cluster-based two-hop design, as compared to a single-hop network, the same radio resource could be potentially reused twice in every cell, and also in every adjacent cell in the seven-cell scenario. Thereby, a frequency reuse ratio of *one* is achieved. However, this also results in an increase in the interference across every communicating receiver. A *Protocol Model* is considered in the system design in order to reduce the interference [19]. As per this model, if d_c is the transmission distance between a transmitter and receiver, then a circular region of radius $(1 + \Delta)d_c$ is defined around every communicating receiver so that, within this region, there is no other transmitter apart from the desired transmitter. The term, Δ, is known as the spatial protection margin, or as the exclusion range ratio. It should be noted that increasing Δ decreases the interference that the receiver might experience, but at the same time, it also decreases the number of pairs in the network that can communicate using the same radio resource [20].

It has been shown in [21] that in order to optimally trade-off between the amount of interference experienced by each user and the number of simultaneously communicating users, the value of Δ should be close to *unity*. Hence, a Δ of 1.0 is considered in the hierarchical clus-

ter-based two-hop cellular design. In Figure 2, the BS →GTW1 pair communicates simultaneously with the GTW2 → MS pair that is located diametrically opposite with respect to the BS. A perfect synchronization is thereby maintained in the cluster-based design with regard to the selection of concurrent communicating pairs within the cell. Two sets of concurrently communicating pairs are shown in Figure 2(d) and Figure 2(e). In case of downlink transmission, for example, the transmission distance of BS → GTW communicating pair is $r/2$, and the interfering transmitter GTW is located at a distance of r from the intended receiver. Similarly, the transmission distance of GTW → MS in the outer layer is less than or equal to $r/2$. Irrespective of the transmission distance of GTW → MS pair, the desired receiver in this case (MSs located in the outer layer) is at least twice the distance from the interfering transmitter (BS in this case). Hence, it can be observed that the intended receiver is separated from all the interfering transmitters by a minimum distance of *twice* the transmission distance, i.e., $\Delta = 1.0$. In the next section, a general equation for *C/I* of the MS at any position in the outer layer of center cell is derived. During the complete analysis carried out in this paper, the center cell in the seven-cell scenario is the cell of interest (CoI).

3. Mathematical Analysis

The CoI is surrounded by six cells in the 1st tier. In each of the six cells, there is a BS at the center, given by BS_1, BS_2, ..., BS_6. A constant traffic pattern between uplink and downlink is considered in both the CoI and also in all the adjacent cells (it could be symmetric or an asymmetric traffic). For the mathematical analysis, a downlink communication is being considered. Hence, as per the cluster-based design, the BS in each adjacent cell would communicate with a GTW node, and at the same time, another GTW node located diametrically opposite to the receiver GTW node would communicate with the MS in its cluster. Let the transmitting GTWs in the adjacent cells be GTW_{TX1}, GTW_{TX2},..., GTW_{TX6}. In the cluster-based design, each cluster is represented by an ellipse, as shown in Figure 2(a). Also, as can be seen from Figure 2(a), there is a small area between two elliptical clusters. The MSs in these areas are assigned to one of the clusters, and hence, these MSs would communicate with the BS through the corresponding cluster-head GTWs. However, in order to simplify the mathematical analysis, the cluster is still approximated by an ellipse. As can be seen from Figure 3, every point in the cluster region is given by the vector: $\beta(a\cos(\theta_0)\,\hat{\imath} + b\sin(\theta_0)\hat{\jmath})$, where $0 \le \theta_0 \le 2\pi$ is the angle measured from the center of the ellipse to the position of the MS. By varying the value of β from 0 to 1, the whole area of the ellipse is spanned, with b and a being the semi-major axis and semi-minor axis of the ellipse, respectively.

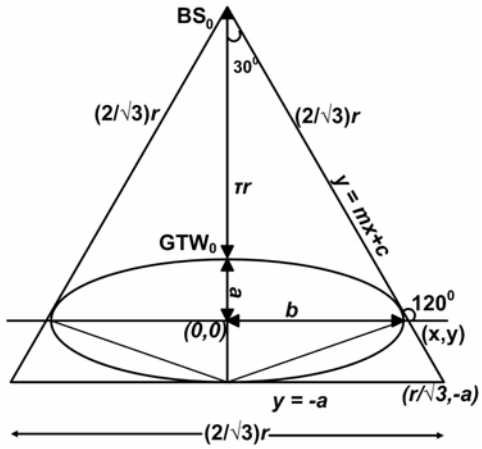

Figure 3. One sector of a hexagonal cell.

3.1. Calculation of a & b

Consider a sector of the cell as shown in Figure 3. For the ease of mathematical analysis, the two edges of the sector are expanded to form an equilateral triangle. Hence, the edge length of the equilateral triangle is $2r/\sqrt{3}$. The height of the triangle is of length, r. The radius of the inner layer circle is τr. As the value of τ changes, the value of 'a' and 'b' also changes. The center of the ellipse (in the desired cluster in CoI) is taken as the origin. Figure 3 shows the elliptical cluster and the distance of the BS from the reference point. The radius of the inner region and the edge of the cell are related by the semi-minor axis of the ellipse by the expression: $\tau r + 2a = r$. Therefore, $a = r/2\,(1 - \tau)$. From Figure 3, it can be figured out that the slope of the tangent to the ellipse is $-\sqrt{3}$. Hence, by equating the tangent slope of the ellipse to $-\sqrt{3}$, we get:

$$\left(\frac{a^2}{b^2}\right)\left(\frac{x}{y}\right) = -\sqrt{3} \tag{1}$$

Substituting for x in the above equation, we get:

$$y = \frac{a^2}{\sqrt{3b^2 + a^2}} \tag{2}$$

and

$$x = \frac{\sqrt{3}b^2}{\sqrt{3b^2 + a^2}} \tag{3}$$

Substituting x, y and m in the tangent equation, $y = mx + c$, the value for c is obtained as:

$c^2 = a^2 + 3b^2$. Also, $(r/\sqrt{3}, -a)$ passes through the tangent equation. Therefore, substituting it, one gets:

$$b = \frac{r\sqrt{\tau}}{\sqrt{3}} \tag{4}$$

3.2. Calculation of GTW Power with Respect to BS Power

For a transceiver pair separated by a distance, d and transmit power, P_T the receiver power is given by [22]:

$$P_R = P_T - (k_1 + 10\alpha \log_{10}(d) + \gamma_c)\text{dB} \quad \textbf{(5)}$$

where k_1 is the propagation constant, α is the pathloss exponent and γ_c is the shadowing factor. In case of a cluster-based two-hop cellular network, the transmission distance is small, and hence, shadowing is much less than compared to an equivalent single-hop network. Hence, the shadowing factor is taken as $\gamma_c = 0$, in the mathematical analysis in this paper. However, the effect of shadowing is considered in the simulations, as can be observed in Section 4.

The minimum receiver sensitivity (minimum carrier power) for any MS in the cell in order to correctly decode the data is taken as X dB (i.e., x Watts). Hence, the farthest point both in the inner region and in the outer region should have this sensitivity level. In the inner region, the farthest point is at a distance τr from BS. Therefore,

$$P_{T_{BS}} = \text{x}(\tau r)^{\alpha} \quad \textbf{(6)}$$

In the outer region, the farthest point from the cluster-head GTW is at $\theta_o = \pi/3$. Therefore, the distance of farthest point in the outer region from GW, $d_{\max}$ is given by

$$d_{\max} = \frac{r}{2}\sqrt{4\tau^2 - 6\tau + 3} \quad \textbf{(7)}$$

Therefore,

$$P_{T_{GTW}} = \text{x}(d_{\max})^{\alpha} \quad \textbf{(8)}$$

and the transmit power ratio between BS and GTW is given by:

$$\frac{P_{T_{BS}}}{P_{T_{GTW}}} = \left(\frac{2\tau}{4\tau^2 - 6\tau + 3}\right)^{\alpha} \quad \textbf{(9)}$$

3.3. Calculation of Position Vector for All Transmitters

The position vector of an MS from its cluster-head GTW_1 is given by:

$$\vec{d} = a\hat{i} + \beta\left(\alpha\cos(\theta_0)\hat{i} + b\sin(\theta_0)\hat{j}\right) \quad \textbf{(10)}$$

On similar lines, the position vector of the MS from its own BS is given by,

$$\vec{p} = (\tau r)\hat{i} + \vec{d} \quad \textbf{(11)}$$

The position vector of the BSs in the adjacent cells, with respect to the BS in the central cell, is given by:

$$\vec{b}_i = \sqrt{3r}\,(\cos(\phi_l)\hat{i} + \sin(\phi_l)\hat{j}) \quad \textbf{(12)}$$

where

$$\phi_l = (l-1)\frac{\pi}{3} - \frac{\pi}{6}$$

and l is an integer which varies from 1 to 6. Similarly, if θ_1, ..., θ_6 are the angles measured between the BS_1, BS_2, ..., BS_6 and the transmitting GTWs of the adjacent cells, GTW_{TX1}, GTW_{TX2}, ..., GTW_{TX6}, then the position vectors of these gateways from their corresponding BSs would be given by:

$$\vec{g}_k = \tau r\left(\cos(\theta_k)\hat{i} + \sin(\theta_k)\hat{j}\right) \quad \textbf{(13)}$$

where $0 \le \theta_k \le 2\pi$ and k is an integer which varies from 1 to 6.

3.4. Calculation of C/I

The MS in the center cell (CoI) would experience intra-cell interference from its own BS, BS_0. In addition, it would experience significant interference from all simultaneous transmitters from the 1st tier of cells. As shown in Figure 4, the MS would experience inter-cell interference from BS_1, ..., BS_6 and GTW_1, ..., GTW_6. Let the interference powers of these twelve inter-cell interferers be denoted by P_{I1}, ..., P_{I12}. Similarly, let d_0 be the distance of the intended receiver from the intra-cell interferer and d_1, d_2, ..., d_{12} be the distances between the MS and BS_1, ..., BS_6, GTW_1, ..., GTW_6. Hence, the distance of the intra-cell interferer (BS_0) and the twelve inter-cell interferers would be given by:

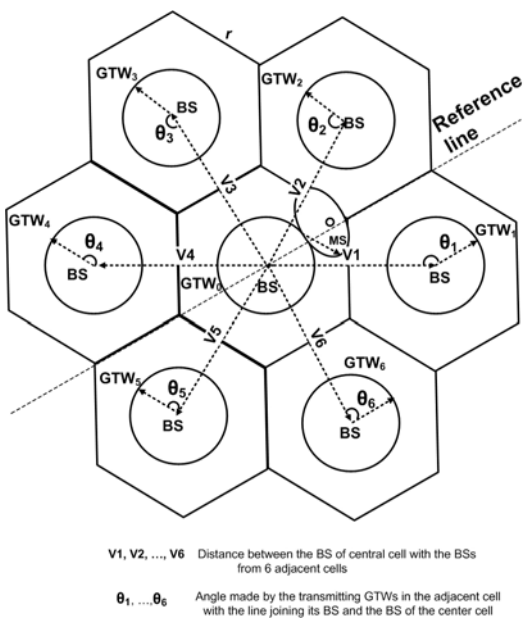

Figure 4. 7-cell scenario for location of transmitting BSs and GTWs.

$$d_0 = |\vec{p}|$$
$$d_l = |\vec{p} - \vec{b}_l|$$
$$d_{k+6} = |\vec{p} - \vec{b}_k - \vec{g}_k|$$

where l and k are integers which vary from 1 to 6. The distance of the interfering transmitters from the desired receiver, d_0, d_l and d_{k+6} are given as:

$$\begin{aligned}|d_0|^2 &= a^2(1+2\beta\cos(\theta_0)) \\ &+ r\tau(r\tau + 2\alpha\beta\cos(\theta_0) + 2\alpha) \\ &+ \beta^2(a^2\cos^2(\theta_0) + b^2\sin^2(\theta_0))\end{aligned} \quad \textbf{(14)}$$

$$\begin{aligned}|d_l|^2 &= r^2\left(\tau^2 + 3 - 2\sqrt{3}\tau\cos(\phi_l)\right) \\ &+ 2\beta r(\tau\alpha\cos(\theta_0) - \sqrt{3}a\cos(\theta_0)\cos(\phi_l) \\ &- \sqrt{3}b\sin(\theta_0)\sin(\phi_l)) + 2ra(\tau - \sqrt{3}\cos(\phi_l)) \\ &+ a^2(1+2\beta\cos(\theta_0)) + \beta^2(a^2 - \cos^2(\theta_0) + b^2\sin^2(\theta_0))\end{aligned} \quad \textbf{(15)}$$

$$\begin{aligned}|d_{k+6}|^2 &= r^2[3 + 2\tau^2 - 2\sqrt{3}\tau\cos(\phi_k) \\ &- 2\tau^2\cos(\theta_k) + 2\sqrt{3}\tau\cos(\phi_k)\cos(\theta_k) \\ &+ 2\sqrt{3}\tau\sin(\theta_k)\sin(\phi_k)] + 2\beta r[\tau a\cos(\theta_0) \\ &- \sqrt{3}a\cos(\theta_0)\cos(\phi_k) - a\tau\cos(\theta_0)\cos(\theta_k) \\ &- \sqrt{3}b\sin(\theta_0)\sin(\phi_k) - b\tau\sin(\theta_0)\sin(\theta_k)] \\ &+ 2ra[\tau - \sqrt{3}\cos(\phi_k) - \tau\cos(\theta_k)] \\ &+ a^2[1+2\beta\cos(\theta_0)] \\ &+ \beta^2[a^2\cos^2(\theta_0) + b^2\sin^2(\theta_0)]\end{aligned} \quad \textbf{(16)}$$

Therefore, using the above distance magnitudes, the interference power received at the MS is given by the following equations:

The power from the intra-cell interferer is:

$$P_{I0} = P_{T_{BS}}(|d_0|)^{-\alpha} \quad \textbf{(17)}$$

The power received from the interfering BS transmitters, $P_{I1}, \ldots, P_{I6}$ are given by:

$$P_{I1} = P_{T_{BS}}(|d_l|)^{-\alpha} \quad \textbf{(18)}$$

Similarly, the received power, $P_{I7}, \ldots, P_{I12}$ from the interfering GTWs of the adjacent cells are given by:

$$P_{I(k+6)} = P_{T_{GTW}}(|d_k|)^{-\alpha} \quad \textbf{(19)}$$

If C is the carrier power of the desired transmitter, then:

$$C = P_{T_{BS}}(|d|)^{-\alpha}$$

where

$$\begin{aligned}|d|^2 &= a^2(1+2\beta\cos(\theta_0)) \\ &+ \beta^2(a^2\cos^2(\theta_0) + b^2\sin^2(\theta_0))\end{aligned} \quad \textbf{(20)}$$

The *C/I* experienced at the MS in the outer layer is therefore given by:

$$\frac{C}{I} = \frac{C}{\sum_{i=0}^{12} P_{Ii}} \quad \textbf{(21)}$$

4. Performance Evaluation

A seven-cell scenario with a center cell and six cells in the 1st tier is considered in the system design. The edge length of each of the hexagonal cells is taken as 1 km. The BS is located at the center of the cell. All the GTWs are equidistant from the BS and also equidistant from each other. However, the exact location of the GTWs with respect to the BS would vary with τ. A downlink transmission scenario is considered in the analysis. Hence, in the cluster-based design, the BS and the GTWs in the adjacent cells would be the interfering transmitters for the receivers in the CoI. The MSs in the center cell are distributed uniformly. However, the position of the MS in the outer layer of CoI does not play any significant role in our analysis. This is because; the main focus of the analysis is in determining the exact location in the CoI where the *C/I* would be minimum and how this minimum *C/I* could be maximized by varying the GTW position and the transmitter power. The equations derived in Section 3 in the mathematical analysis are used to calculate *C/I* for all possible positions of GTW nodes in all the six adjacent cells. The position of the transmitting GTW in each adjacent cell is varied across 360 degrees with every 1 degree variation. This results in huge number of possible combinations (360^6 = 2.1768*e*15). Hence, the computations were done using Matlab. It should however be noted that these are not simulation results but theoretical results obtained from the different position of GTWs in the adjacent cells in the cluster-based two-hop design. In order to assess the performance of varying the location of τ, the value of τ is varied from 0.1 to 1 in steps of 0.01. The performance is evaluated for different values of path-loss exponent, α.

For high data-rate transmissions in B3G (beyond 3G) and 4G networks, a coded BER of 10^{-6} to 10^{-7} is required. In a corresponding uncoded network design, as in our system, a BER of 10^{-2} would however be sufficient [22]. When a combination of convolutional coding and Reed Solomon coding techniques is considered, a BER of 10^{-2} would translate into a BER of 10^{-6} or beyond, in a coded system. Table 1 shows the minimum required *C/I* for different modulation schemes for an uncoded system at a BER of 10^{-2}. The higher the modulation technique, the higher is the achievable link data-rate. Hence, in this paper, the optimum GTW positions are analyzed for different *C/I* values. A minimum *C/I* of 4.6 dB is required at the receiver of a communicating pair in order to transmit

Table 1. Minimum required *C/I* for different modulation schemes for an uncoded system with a BER of 10^{-2}.

Type of Modulation	*C/I* (dB)	No. of bits/symbol
BPSK	4.6	1
QPSK	7.1	2
8PSK	11.3	3
16QAM	14.2	4
32QAM	17.4	5
64QAM	19.6	6
128QAM	22.4	7
256QAM	25.2	8
512QAM	28.4	9

signal using BPSK modulation technique. Similarly, a minimum *C/I* of 7.1 dB is required for data transmission using QPSK modulation technique. Hence, if the received *C/I* is between 4.6 dB and 7.1 dB, only BPSK scheme could be used. Table 2 shows the minimum transmit power required at the GTW and at the BS for different power ratios, for three different *C/I* values: 4.6 dB, 6 dB and 7.1 dB. It can be observed that in order to achieve a minimum *C/I* of 4.6 dB at any point in the cell, if the BS and the GTW transmit powers are same, then both BS and GTW should transmit with a minimum power of 0.47 W. Also, for this point, all the GTWs in the cell should be located at a distance of 0.48*r* from the BS. The transmit power of the GTW can be reduced by increasing the BS to GTW transmit power ratio. When the transmit power ratio between the BS and GTW is 2:1, the minimum transmit power of the GTW reduces to 0.441 W. Similarly, if the transmit power ratio is further increased to 4:1, then the minimum transmit power at the GTW reduces to 0.334 W, in order to achieve the same minimum *C/I* of 4.6 dB at any point in the cell. It should be noted that for this particular transmit power ratio, the GTWs should be placed at a distance of 0.54*r* from the BS.

In order to transmit data with higher rate, a higher modulation technique should be used. As shown in Table 1, this requires a higher *C/I* at the receiver of a communicating pair. Table 3 shows the transmit power requirement at the BS and at the GTW for different power ratios for higher *C/I* values (9 dB and higher). It can be observed from Figure 5 that as the *C/I* threshold increases, the GTWs should be placed away from the BS in order to meet the *C/I* threshold. Also, it can be observed that this is true for all different transmit power ratios. This is a very significant result. It implies that for high data-rate communication in the cellular network, the GTW should be placed to wards the edge of the cell rather than close to the BS. Similarly, it can be observed from Figure 6 that as the minimum *C/I* threshold increases, the GTW transmit

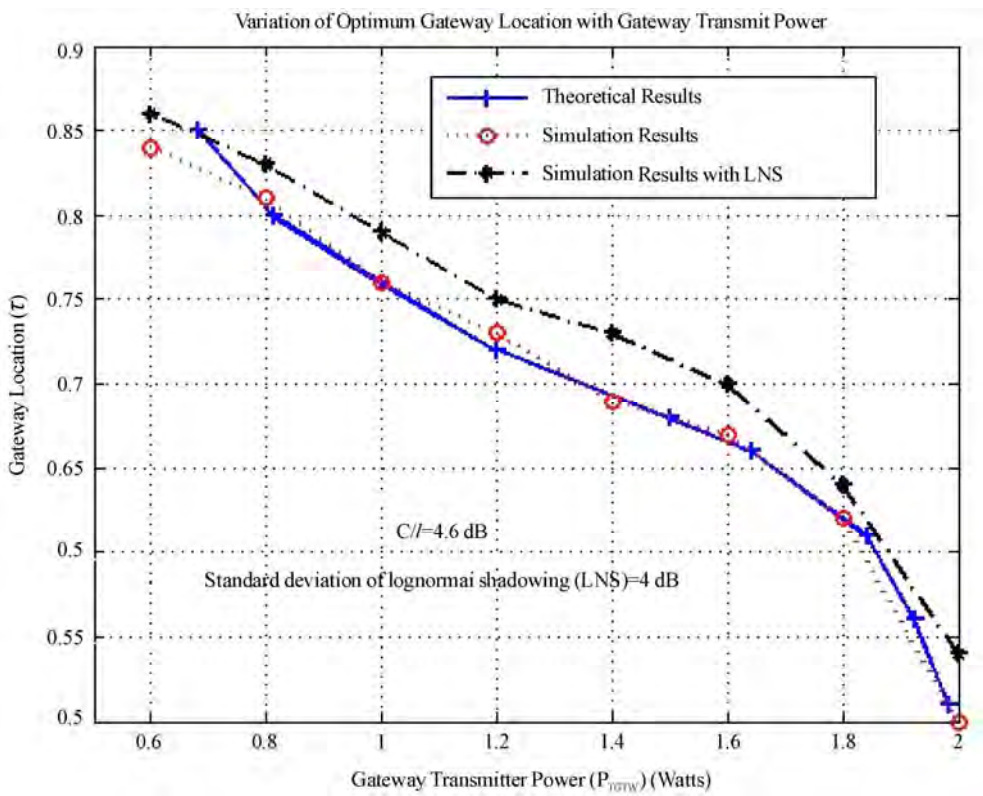

Figure 5. Variation of GTW location (*τ*) with gateway transmit power for *α* = 4.

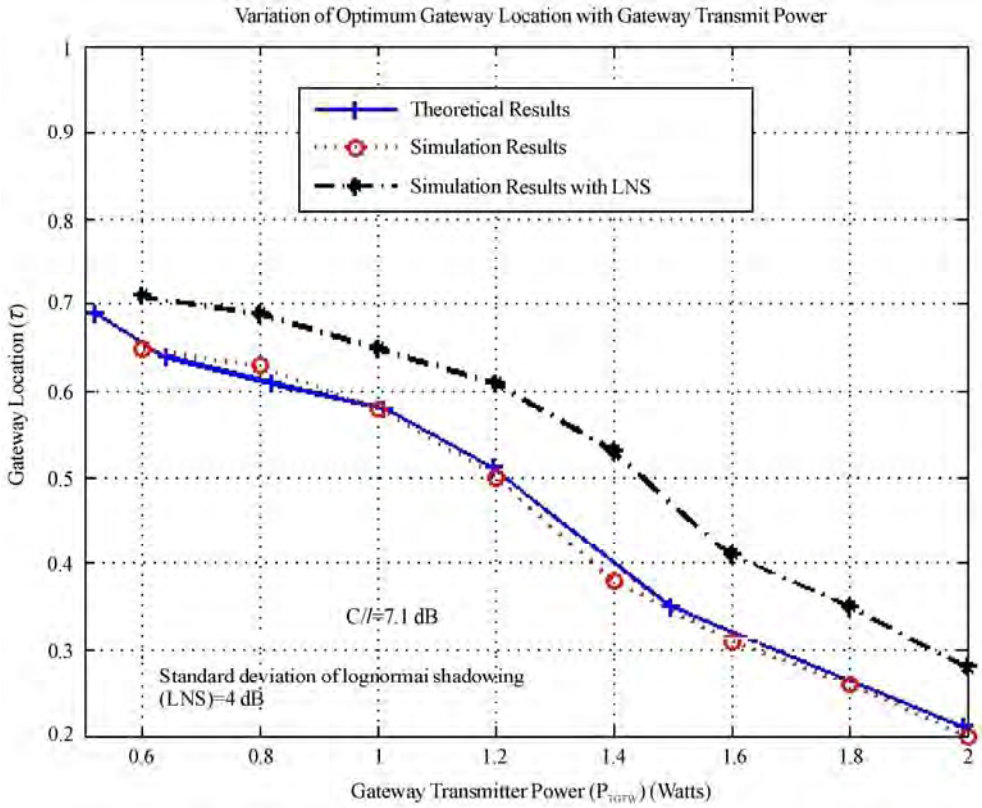

Figure 6. Variation of GTW location (τ) with gateway transmit power for α = 4.

Table 2. Minimum transmission power at GTW for a C/I of 9 dB, 11.3 dB and 14.2 dB at the receiver and the corresponding optimum location for GTW when base station transmit power is 2W.

α =	3.5	3.5	4.0	4.0	4.5	4.5
C/I (dB)	$P_{T\,GTW}$	τ	$P_{T\,GTW}$	τ	$P_{T\,GTW}$	τ
4.6	*1.967*	*0.49*	*1.983*	*0.51*	*1.995*	*0.53*
4.6	1.902	0.53	1.924	0.56	1.945	0.59
4.6	1.812	0.58	1.842	0.61	1.865	0.64
4.6	0.624	0.63	1.643	0.66	1.652	0.69
4.6	1.471	0.66	1.5	0.68	1.532	0.71
4.6	1.182	0.7	1.2	0.72	1.23	0.75
4.6	**0.976**	**0.74**	**0.998**	**0.76**	**1.012**	**0.77**
4.6	0.795	0.79	0.812	0.8	0.834	0.82
4.6	0.654	0.83	0.683	0.85	0.696	0.88
4.6	**0.502**	**0.83**	**0.512**	**0.85**	**0.523**	**0.88**
6	1.984	0.32	1.997	0.34	2.018	0.35
6	*1.345*	*0.51*	*1.382*	*0.53*	*1.412*	*0.55*
6	**0.977**	**0.56**	**0.998**	**0.58**	**1.006**	**0.61**
6	0.754	0.62	0.765	0.64	0.786	0.67
6	0.64	0.69	0.65	0.71	0.67	0.72
6	**0.51**	**0.74**	**0.53**	**0.76**	**0.57**	**0.79**
7.1	1.987	0.19	1.995	0.21	2.014	0.24
7.1	1.485	0.34	1.497	0.35	1.506	0.37
7.1	*1.134*	*0.49*	*1.198*	*0.51*	*1.232*	*0.54*
7.1	**0.98**	**0.56**	**1.01**	**0.58**	**1.04**	**0.61**
7.1	0.79	0.59	0.82	0.61	0.84	0.63
7.1	*0.61*	*0.62*	*0.64*	*0.64*	*0.67*	*0.66*
7.1	**0.5**	**0.67**	**0.52**	**0.69**	**0.54**	**0.71**

Table 3. Minimum transmission power at GTW for a *C/I* of 9 dB, 11.3 dB and 14.2 dB at the receiver and the corresponding optimum location for GTW when base station transmit power is 2W.

α= *C/I* (dB)	3.5 $P_{T\,GTW}$	3.5 *τ*	4.0 $P_{T\,GTW}$	4.0 *τ*	4.5 $P_{T\,GTW}$	4.5 *τ*
9	2	-	2	-	2	-
9	1.488	0.27	1.496	0.29	1.504	0.3
9	1.002	0.41	1.012	0.43	1.134	0.48
9	0.895	0.44	0.912	0.47	0.934	0.51
9	0.721	0.49	0.754	0.52	0.767	0.55
9	0.643	0.53	0.675	0.56	0.692	0.59
9	0.543	0.57	0.586	0.6	0.613	0.62
9	0.484	0.61	0.497	0.65	0.512	0.68
11.3	2	-	2	-	2	-
11.3	1.5	-	1.5	-	1.5	-
11.3	**0.981**	**0.19**	**0.993**	**0.22**	**1.002**	**0.24**
11.3	0.75	0.34	0.78	0.36	0.81	0.37
11.3	**0.501**	**0.44**	**0.512**	**0.46**	**0.522**	**0.47**
11.3	*0.452*	*0.49*	*0.474*	*0.51*	*0.492*	*0.54*
11.3	0.362	0.55	0.378	0.57	0.391	0.59
14.2	2	-	2	-	2	-
14.2	1.5	-	1.5	-	1.5	-
14.2	**0.978**	**0.14**	**0.985**	**0.16**	**0.998**	**0.18**
14.2	**0.5**	**0.34**	**0.506**	**0.35**	**0.52**	**0.37**
14.2	0.382	0.41	0.396	0.42	0.401	0.43
14.2	*0.312*	*0.5*	*0.334*	*0.52*	*0.345*	*0.53*

power should also increase for high data-rate communication, even though the GTW would be close to the edge of the cell. The bold entries in Table 2 and Table 3 indicate the *P*GTW and *τ* values (optimum GTW position) when the *P*GTW is near 1W and 0.5 W. It can be observed from both the tables that with a decrease in the GTW transmit power (with respect to the BS transmit power), the optimum location of the GTW that would maximize the minimum *C/I* moves to wards the cell edge. Significantly, this is true irrespective of the *C/I* values.

Figure 5 and Figure 6 also show the results in the presence of lognormal shadowing. A standard deviation of 4 dB is selected, based on the realistic values for a suburban or a semi-outdoor environment [23]. It can be observed from both the figures that the behavior of the graph remains the same as compared to the case where there is no shadowing. However, for the particular gateway location, the absolute value of the required gateway transmit power increases marginally in the presence of shadowing. This shows that lognormal shadowing does affect the system performance. But, the results of the analysis on the GTW location remains still valid.

5. Conclusions

The cluster-based two-hop cellular network has been analyzed in this work for different BS and GTW transmit powers and for different possible data-rates in the system. The mathematical and numerical results indicate that for minimum data-rate transmission at the physical layer, with equal transmit power at both BS and GTW, the GTW should be located close to the center of the line joining the BS and the edge of the cell. However, for high data-rate communication, not only the minimum transmit power of both BS and GTW should be increased, but also the GTW should be moved to wards the edges of the cell. This is a significant result and indicates that the GTW location and its transmit power plays a crucial role in determining the data-rate of the two-hop cellular network. The next generation cellular networks would not only be required to support both voice and data but also multimedia transmission, which requires high and flexible data-rate between different communicating links. Hence, a further research in this direction is to modify the cluster-based design for three-hop cellular networks and to investigate the relation between minimum transmit power of BSs and GTWs and the GTW location in the cell in order to further increase the data-rate of the communication links in the cellular network.

6. Acknowledgement

The authors would like to thank Dr. Sinan Sinanovi´c and Prof. Harald Haas from the University of Edinburgh, Scotland, UK and Dr. Gabriel-Miro Muntean from Dublin

City University, Ireland for their useful comments and suggestions during the initial stage of this research work.

7. References

[1] R. Ananthapadmanabha, B. Manoj, and C. Murthy, "Multihop cellular networks: The architecture and routing protocol," in Proceedings of IEEE International Symposium on Personal Indoor Mobile Radio Communications (PIMRC'01), San Diego, USA, Vol. 2, pp. 78−82, September 30− October 3, 2001.

[2] A. Agarwal and P. Kumar, "Capacity bounds for ad hoc and hybrid wireless networks," ACM Special Interest Group on Data Communications (SIGCOMM), Vol. 34, No. 3, pp. 71−81, July 2004.

[3] O. Dousse, P. Thiran, and M. Hasler, "Connectivity in ad hoc and hybrid networks," in Proceedings of IEEE International Conference on Computer Communications (INFOCOM), Vol. 2, pp. 1079−1088, June 23−27, 2002.

[4] H. Vishwanathan and S. Mukherjee, "Performance of cellular networks with relays and centralized scheduling," in Proceedings of IEEE Vehicular Technology Conference (VTC Fall'03), Orlando, Florida, USA, Vol. 3, pp. 1923−1928, October 6−9, 2003.

[5] H. Wu, C. Qao, S. De, and O. Tonguz, "Integrated cellular and ad hoc relaying systems," IEEE Journal on Selected Areas in Communication, Vol. 19, No. 10, pp. 2105−2115, October 2001.

[6] A. Zahran and B. Liang, "A generic framework for mobility modeling and performance analysis in next generation heterogeneous wireless networks," IEEE Communication Magazine, Vol. 45, No. 9, pp. 92−100, September 2007.

[7] K. G. J. He, K. Yang, and H. Chen, "Application of IEEE 802.16 mesh networks as the backhaul of multihop cellular networks," IEEE Communication Magazine, Vol. 45, No. 9, pp. 82−91, September 2007.

[8] H. Haas and S. McLaughlin, "Next generation mobile access technologies: Implementing TDD," Cambridge University Press, ISBN: 13: 9780521826228, pp. 420, January 2008.

[9] T. Rouse, S. McLaughlin, and I. Band, "Congestion-based routing strategies in multihop TDD-CDMA networks," IEEE Journal on Selected Areas in Communication, Vol. 23, No. 3, pp. 668−681, March 2005.

[10] L. Le and E. Hossain, "Multihop cellular networks: Potential gains, research challenges, and a resource allocation framework," IEEE Communications Magazine, Vol. 45, No. 9, pp. 66−73, September 2007.

[11] J. Cho and Z. Haas, "On the throughput enhancement of the downstream channel in cellular radio networks through multihop relaying," IEEE Journal on Selected Areas in Communications, Vol. 2, No. 7, pp. 1206−1219, September 2004.

[12] Y. Liu, R. Hoshyar, X. Yang, and R. Tafazolli, "Integrated radio resource allocation for multihop cellular networks with fixed relay stations," IEEE Journal on Selected Areas in Communications, Vol. 24, No. 11, pp. 2137−2146, November 2006.

[13] H. Vishwanathan and S. Mukherjee, "Performance of cellular networks with relays and centralized scheduling," IEEE Transactions on Wireless Communications, Vol. 4, pp. 2318−2328, September 2005.

[14] M. Grossglauser and D. Tse, "Mobility increases the capacity of ad hoc wireless networks," IEEE/ACM Transactions on Networking, Vol. 10, No. 4, pp. 477−486, August 2002.

[15] Z. Dawy, S. Davidovic and I. Oikonomidis, "Coverage and capacity enhancement of cdma cellular systems via multihop transmission," in Proceedings of IEEE Global Communication Conference (GLOBECOM), San Francisco, USA, pp. 1147−1151, December 1−5, 2003.

[16] K. S. Hassan, H. Haas, S. Yun, Y. Lee, and S. McLaughlin, "Hybrid wireless communication system and communication method using the same," Patent No: 200701121531. http://www.freepatentsonline.com/2007 0121531.html.

[17] H. Venkataraman, S. Sinanovic, and H. Haas, "Cluster-based design for two-hop cellular networks," International Journal for Communications, Networks and Systems (IJCNS), Vol. 1, No. 4, pp. 369−384, December 2008.

[18] H. Venkataraman, S. Nainwal, and P. Shrivastava, "Optimum number of gateways in cluster-based two-hop cellular networks," AEU Journal of Electronics and Communications, Elsevier, Accepted for Publication, 2008. http: //nextgenwireless.daiict.ac.in/Sub Papers/AEU May 2008 Hrishikesh Venkataraman.pdf.

[19] P. Gupta and P. Kumar, "The capacity of wireless networks," IEEE Transactions on Information Theory, Vol. 46, No. 2, pp. 388−404, February 2000.

[20] H. Venkataraman, H. Haas, S. Yun, Y. Lee, and S. McLaughlin, "Performance analysis of hybrid wireless networks," in Proceedings of IEEE International Symposium on Personal Indoor and Mobile Radio Communications (PIMRC'05), Berlin, Germany, Vol. 3, pp. 1742−1746, September 11−14, 2005.

[21] H. Venkataraman, A. Mudesir, S. Sinanovic, and H. Haas, "Time slot partitioning and random data hopping for multihop wireless networks," in Proceedings of IEEE Vehicular Technology Conference (VTC Spring'07), Dublin, Ireland, April 22−24, 2007.

[22] S. Sampei and H. Harada, "System design issues and performance evaluations for adaptive modulation in new wireless access systems," Proceedings of IEEE, Vol. 95, No. 12, pp. 2456−2467, December 2007.

[23] 3rd Generation Partnership Project (3GPP), Technical Specification Group Radio Access Network, "Selection procedures for the choice of radio transmission technologies of UMTS," 3GPP TR 30.03U, May 1998. Retrieved November 30, 2008, from http://www.3gpp.org/ftp/Specs/html-info/3003U.htm.

Int. J. Communications, Network and System Sciences, 2009, 4, 249-324
doi:10.4236/ijcns.2009.24032 Published Online July 2009 (http://www.SciRP.org/journal/ijcns/).

The Study on the Hierarchy of Internet Router-Level Topology

Jun ZHANG, Hai ZHAO, Chao LI, Xin GE
College of Information Science and Engineering, Northeastern University, Shenyang, China
Email: *zhangjun1@ise.neu.edu.cn; zhangjun*1967*@sina.com*
Received April 9, 2009; *revised November* 5, 2008; *accepted February* 2, 2009

ABSTRACT

Being a huge system, Internet topology structure is very complex. It can't be treated as a plane simply, and its hierarchy must be analyzed. We used the k-core decomposition to disentangle the hierarchical structure of Internet Router-level topology. By analyzing the router-lever Internet topology measuring data from CAIDA (The Cooperative Association for Internet Data Analysis) ,we studied the characteristics of the nodes in the inner hierarchy and outer hierarchy respectively. The frequency-degree power law of the nodes which coreness is lower and the regionally distribution of the nodes which coreness is higher were concluded. At last, the topology of every hierarchy was described by giving their figures. These descriptions can provide a valuable reference for modeling on the Internet topology.

Keywords: Complex Network, Hierarchy, Coreness, Power Law, Regionally, Internet

1. Introduction

Being a classical instance of complex network, the research and modeling on Internet topology has become a hot topic at present [1–10]. It is significant for network application, development and the building of the next generation.

Although Internet is constructed by people, no one can describe what Internet looks like and how it works. The study on Internet topology is to find out some laws that exist in it but have not been known by us [11]. The research on the evolvement of the Internet macroscopic topology and its inherent mechanism is the foundation for developing and utilizing Internet.

The complexity of Internet results directly the complexity of its topology, especially for the router-level topology. Facing the millions of Internet routers, the first difficulty faced by us is how to measure them from Internet.

The Embed Laboratory of Northeastern University was authorized by CAIDA in 2005, and has been taking part in the research on the characteristics of Internet topology actively after the first node of CAIDA in China (neu node) was founded [12]. The Embed Laboratory of Northeastern University can not only get the topology measuring data from CAIDA in the world, but can also analyze the first topology information of neu node timely and dynamically. It can provide us abundant data resources and convenient conditions for researching the characteristics of Internet router-level topology. Under such background, the study on hierarchy of Internet router-level topology is carried out.

Internet has not only got LAN/WAN or AS/Router level hierarchy in traditional meaning, but also exhibits a spontaneous and multi hierarchical characteristics [13]. Based on coreness, analyzing the hierarchy of Internet, and then finding the laws among the hierarchies can not only describe the characteristics of Internet topology in detail, but can also provide a feasible thought for modeling on Internet topology.

2. The Hierarchical Measurement of Node Coreness

The node coreness that is an important measurement factor for analyzing the Internet topology is defined as follows:

Let us consider a graph G = (V, E) of |V| = n vertices and |E| = e edges; a k-core is defined as follows[14]:

Definition1 A subgraph H = (C, E|C) induced by the set $C \subseteq V$ is a k-core or a core of order k iff $\forall v \in C$: degree H(v) $\geqslant$ k, and H is the maximum subgraph with this property [14].

A k-core of G can therefore be obtained by recursively removing all the vertices of degree less than k, until all vertices in the remaining graph have at least degree k.

Definition2 A vertex i has coreness c if it belongs to the c-core but not to (c+1)-core. We denote by ci the coreness of vertex i [14].

It is worth remarking that the coreness of a node is not equivalent to the degree of it. Indeed, a star-like subgraph formed by a vertex with a high degree that connects many vertices with degree one, and connected only with a single edge to the rest of the graph, has only got coreness one no matter how high is the degree of the vertex.

The k-core of the network and the characteristics related with it can therefore describe the network topology hierarchy. It decomposes the networks layer by layer, revealing the structure of the different hierarchies from the outmost one to the most internal one.

3. Data Access

The data used in the paper is from the router-lever Internet topology measuring data of CAIDA in May 2007. We have got the Internet topology measuring results from 15 CAIDA monitors around the world, and resolved IP aliases of them by using CAIDA iffinder IP Alias Resolution. The results show in Table 1.

In order to resolve the sampling bias, we combined the measurement results from 15 monitors in Table 1. At last, we got a graph with 360652 nodes and 925769 edges. The biggest degree of it is 1206 and the highest coreness of it is 25.

4. The Study on the Characteristics of the Nodes' Distribution in Every Hierarchy

According to the definition of coreness, Internet topology can be divided into different hierarchies. From higher coreness to lower coreness, the corresponding hierarchy is from inner to outer. We analyzed the router-level Internet topology measuring data from CAIDA in May 2007. The results showed that the distribution of node coreness was similar to that of node degree. That is the coreness of most nodes is lower, and only a few nodes have got higher coreness. The distribution on coreness of the router-level nodes satisfies power law [15]. In the following section, we will study on the distribution of the nodes' degree and network addresses in every hierarchy respectively.

4.1. The Power Law Distribution on Degree of the Nodes in Outer Hierarchies

During our research, we first computed the degree of the nodes in every hierarchy and analyzed their distribution according to the topology measuring data from CAIDA. We found that the distribution on degree of the nodes satisfied power law in outer hierarchies. The fitness

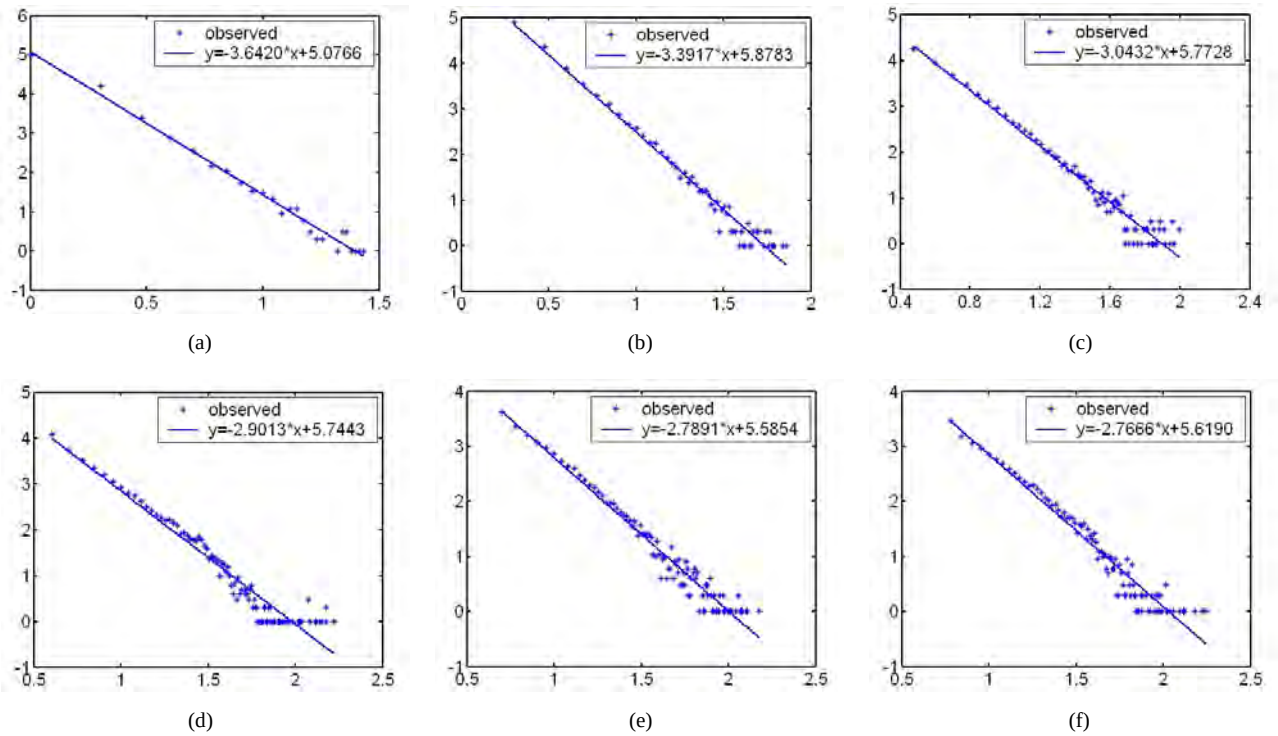

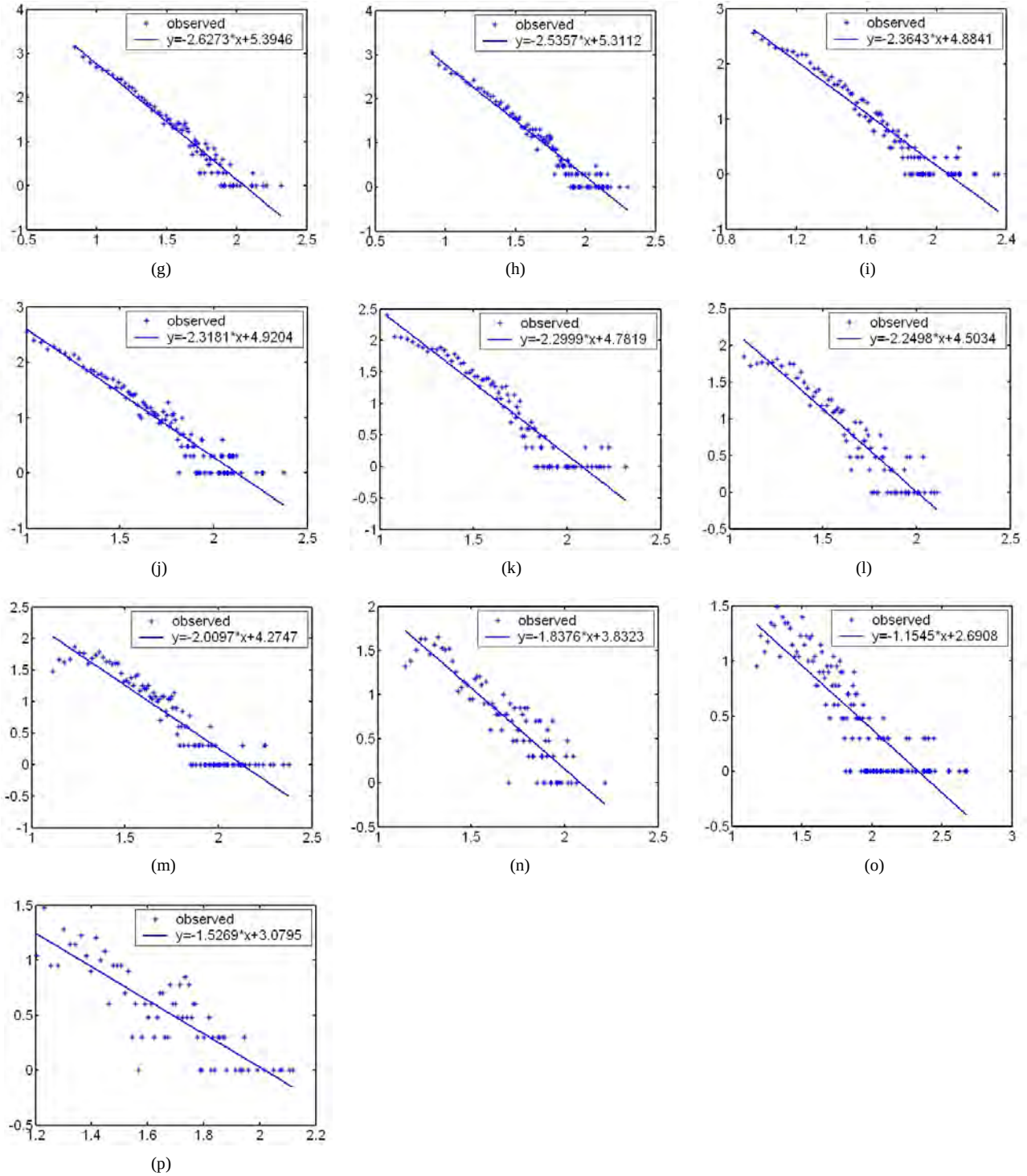

Sub-figures (a)~(p) are corresponding to hierarchy 1~16. Axis x is the logarithm of degree, and axis y is the logarithm of the number of the nodes

Figure 1. The fitness figures of the degree distribution in different hierarchies.

results under the logarithm coordinate are showed as Figure 1.

The highest coreness of the measurement results in May 2007 is 25, so Internet topology is divided into 25 hierarchies. The distribution on degree of the nodes satisfies power law in outer hierarchies. From outer to inner, the fitness results of the degree distribution become fainter and fainter. And for inner hierarchies, this characteristic is no more satisfied.

Table 1. The monitors and their measurement results in May 2007.

Monitor	Number of links	Number of nodes
arin	381069	286554
cam	371167	282019
champagne	388662	290672
d-roor	371876	282048
e-root	380607	288271
f-root	375229	283454
h-root	366709	275589
i-root	383232	290073
lhr	202611	281534
m-root	367260	151214
neu	397299	266844
riesling	384090	287254
sjc	359032	273192
uoregon	357952	272362
yto	371977	280616

4.2. The Regionally Distribution of the Nodes in Inner Hierarchies

Now we study the characteristics of the nodes in inner hierarchies. By analyzing the distribution of the network addresses in every hierarchy, we find that the nodes in the innermost hierarchy distribute on only a few network addresses. From inner hierarchy to outer hierarchy, the network addresses of the nodes spread more and more expanded (see Figure 2). We can see from Figure 2 that the network addresses of the nodes in outer hierarchies spread expanded, but for the nodes that are in inner hierarchies, their distribution is concentrated.

We can see that the distribution of the network addresses of the nodes in inner hierarchies is concentrated. The higher is the node coreness, the more evident is the concentration. At last they concentrate on only a few

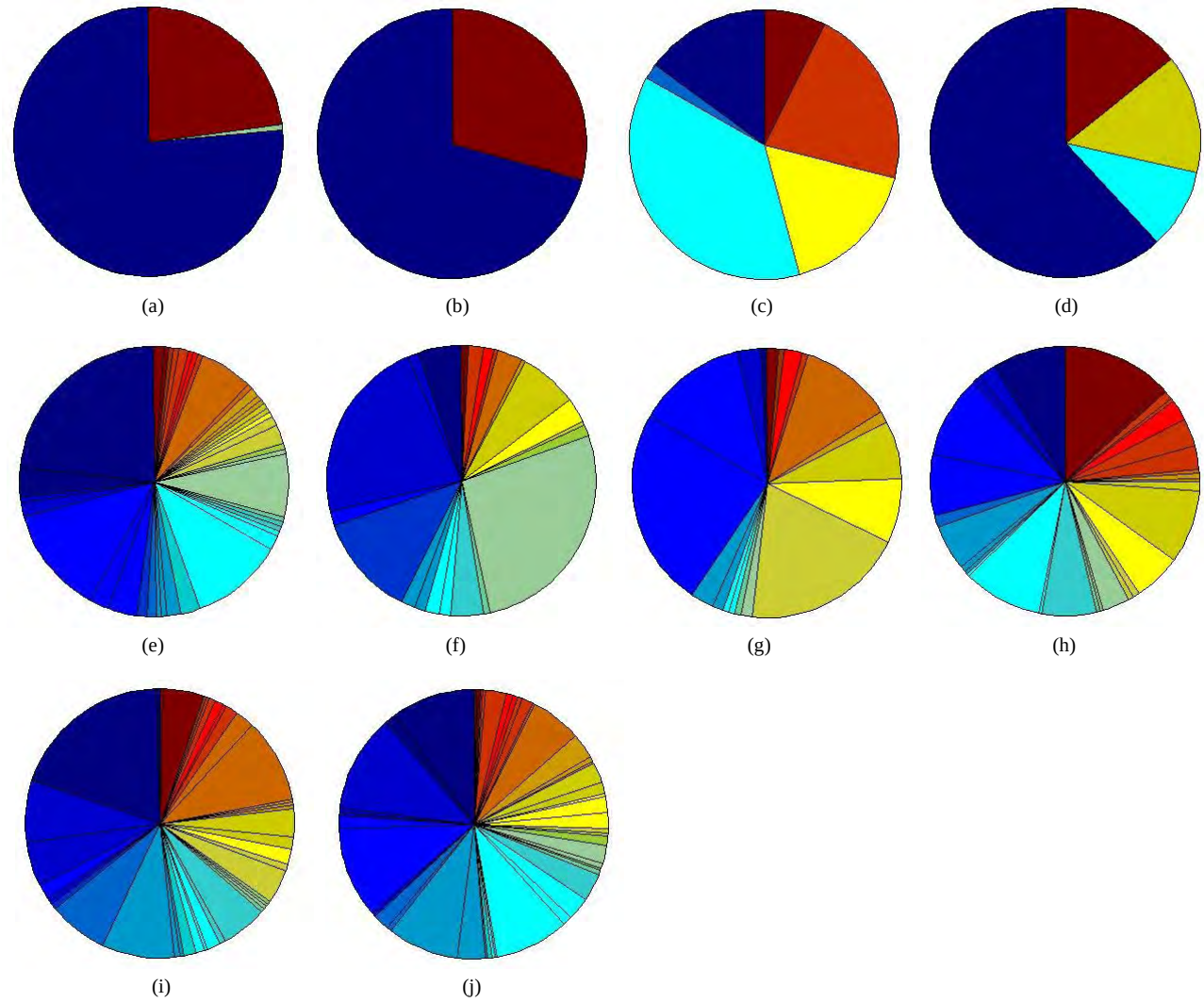

Sub-figures (a)~(j) are corresponding to hierarchy 25~16 respectively. The sectors illuminate how many the nodes distribute on this network address

Figure 2. The network addresses of the nodes in hierarchy 25~16.

Table 2. The number of the nodes in every hierarchy.

Coreness	Nodes	Coreness	Nodes
1	115636	14	778
2	119251	15	750
3	41840	16	360
4	30459	17	267
5	14599	18	275
6	11487	19	143
7	7039	20	230
8	6052	21	171
9	3209	22	21
10	3188	23	107
11	2110	24	17
12	1131	25	157
13	1375		

addresses in the innermost hierarchy. Is the phenomenon related to the number of the nodes in every hierarchy? So we compute the number of nodes in every hierarchy, see Table 2. We found that the number of the nodes decreased with the increment of the coreness in the whole. From lower coreness to higher coreness, the number of the nodes becomes fewer and fewer. But when it reaches the highest coreness, the number of the nodes appears a rebound, remains a certain amount. So we can find that the distribution of the network addresses of the nodes is related with the number of the nodes, but they are not increased with direct proportion. For example, the number of the nodes in hierarchy 25 is more than that in hierarchy 23 and 22, but the distribution of the network addresses in hierarchy 25 is more concentrated than that in hierarchy 23 and 22.

Summarily, from inner hierarchy to outer hierarchy, the nodes distribute from the highest coreness to the lowest. In the innermost hierarchy, the nodes distribute on a few network addresses. From inner to outer, the distribution of the network addresses becomes more and more expanded, and the frequency-degree power law is increasingly finer. To the outmost hierarchy, the distribution of the network addresses is the widest and the power law is the finest.

5. The Visual Description of Internet Topology in Every Hierarchy

The visual description of Internet topology has been being the hot problem for studying on Internet for a long time [16]. How to construct a better topology figure is difficult because of the numerousness of the router-level nodes. In this section, we will describe it in every hierarchy (see Figure 3).

We can see from Figure 3 that the relationship among the nodes is closer in the innermost hierarchy, that is the highest coreness. All the nodes construct two connected figures. From inner to outer, the relationship becomes looser. In hierarchy 24, although the number of the nodes is fewer, the relationship among them is looser. There are two connected figures and several isolated nodes. These isolated nodes have 24 connections with the nodes in the innermost hierarchy. In hierarchy 23, all the nodes are divided into several irrelative figures and some isolated

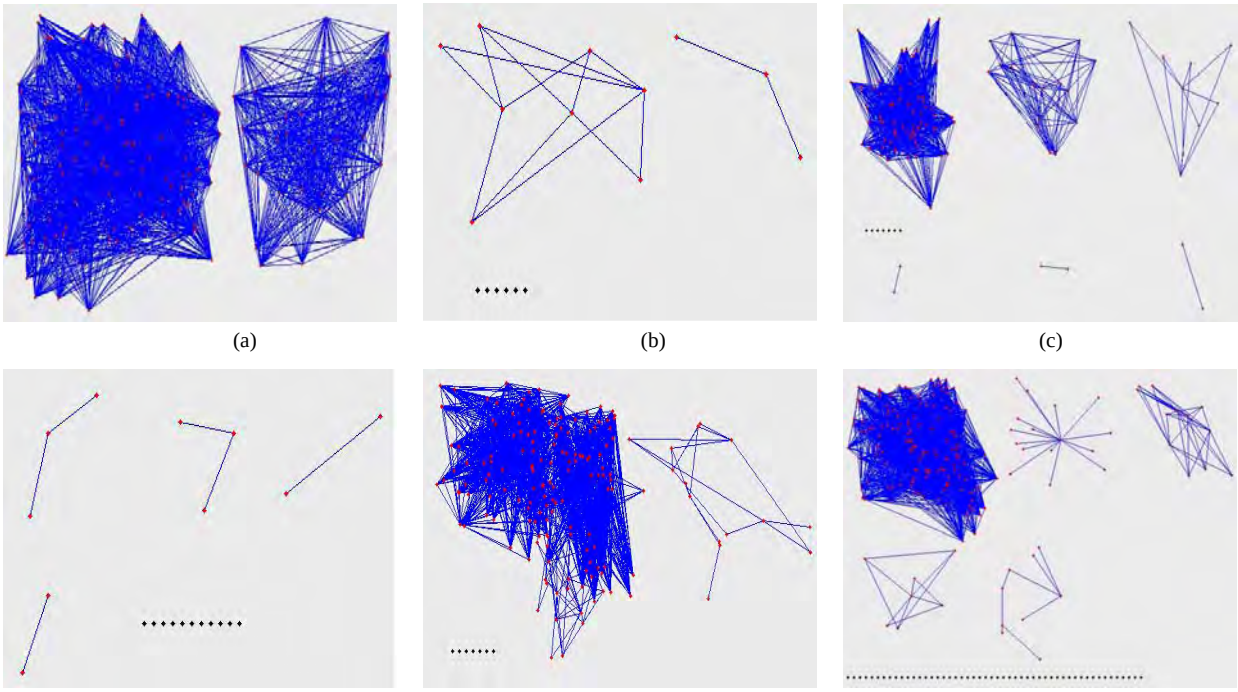

(a) (b) (c) (d) (e) (f)

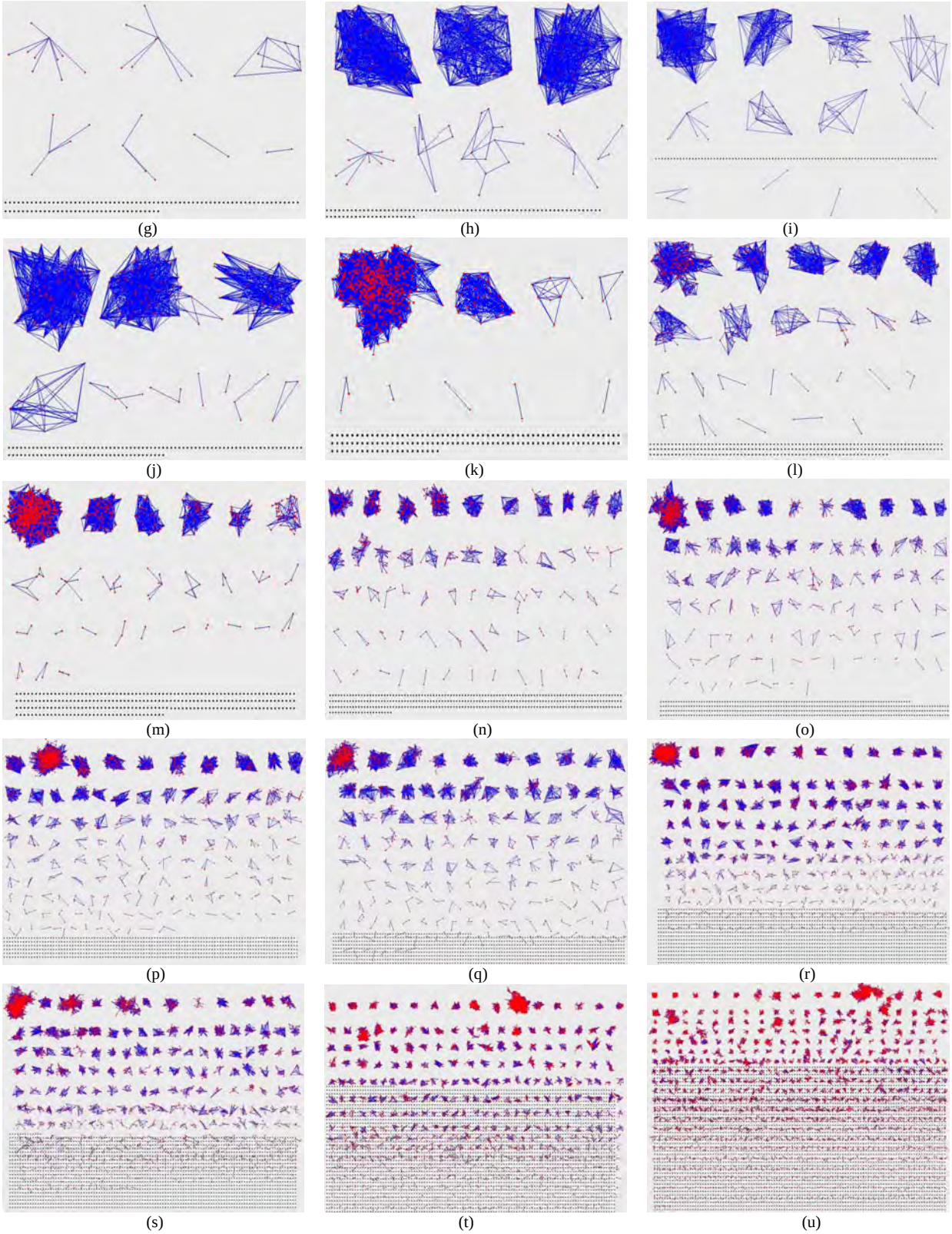

Sub-figures (a)~(u) are the figures of hierarchy 25~5 respectively. The black nodes indicate the isolated nodes, the blue lines indicate the edges among the nodes and the red nodes indicate two nodes of one edge.

Figure 3. The topology figures of hierarchy 25~5.

nodes that have 23 connections with the nodes in the inner hierarchies. From that to outer, the irrelative connected figures become more and more, and the isolated nodes which have *k* connections with the nodes in the inner hierarchies are also more and more. This illustrates that the connections among the nodes in the same hierarchy is smaller, and most connections appear between the hierarchies. Combined with the conclusion that we have got in section 4.2, we find that the nodes in the same network area are prone to connect with each other.

6. Conclusions

The hierarchy of Internet router-level topology is analyzed in the paper. Combining with the actual topology measuring data, we described the characteristics of the hierarchy of Internet router-level topology. We first used the concept of coreness to decompose Internet topology into different hierarchies. Then studied the characteristics of the nodes in inner hierarchies and outer hierarchies respectively. We found that the distribution on degree of the nodes in outer hierarchies satisfied power law. The lower the node coreness is, the better the fitness is. On the other hand, although the number of the nodes in the innermost hierarchy is over hundred, they do not distribute in different areas. On the contrary, they concentrate on only a few network addresses. At last, we described the topology of every hierarchy by giving their figures, and we found that the nodes in the same network area were prone to connect with each other. These descriptions can provide a valuable reference for modeling on Internet topology.

7. References

[1] X. F. Wang, X. Li, and G. R. Chen, "The theory and application of complex network," TsingHua University Press, Beijing, 2006.

[2] D. Magoni and J. J. Pansiot, "Internet topology modeler based on map sampling," Proceedings of the ISCC 2002, Taormina, IEEE, pp. 1021−1027, 2002.

[3] J. Winick and S. Jamin., "Inet-3.0: Internet topology generator," Technical Report, CSE-TR-456-02, Ann Arbor: University of Michigan, 2002.

[4] D. Magoni, "A software for network topology analysis and modeling," Proceedings of the MASCOTS 2002. IEEE Computer Society, pp. 364−371, 2002.

[5] S. Zhouu and R. J. Mondragon, "Accurately modeling the Internet topology," Physical Review Letters, Vol. 70, pp. 106−108, 2004.

[6] S. Zhouu and R J. Mondragon, "Towards modeling the Internet topology-the interactive growth model," Teletraffic science and engineering, Vol. 5, pp. 121−130, 2003.

[7] S. Zhouu and R J. Mondragon, "The rich-club phenomenon in the Internet topology," IEEE Communication Letters, Vol.8, No.3, pp. 180−182, 2004.

[8] S. T. Park, D. M. Pennock, and C. L. Giles, "Comparing static and dynamic measurements and models of the Internet's topology," Proceedings of the 23rd Annual Joint Conference of the IEEE Computer and Communications Societies, pp. 1616−1627, March 2004.

[9] G. Chen, Z. P. Fan, and X. Li, "Modeling the complex Internet topology," Complex Dynamics in Communication Networks, G. Vattay, L. Kocarev (Eds), Berlin, Springer-Verlag, 2005.

[10] D. Vukadinovic, P. Huang, and T. Erlebach, "On the spectrum and structure of Internet topology graphs," Proceedings of the Innovative Internet Computing Systems (I2CS), LNCS 2346, Berlin, Springer-Verlag, pp. 83−95, 2002.

[11] Y. Zhang, H. L. Zhang, and B. X. Fang, "A survey on internet topology modeling", Journal of Software, Vol. 15, pp. 1220−1226, 2004.

[12] Macroscopic Topology Measurements, CAIDA. http://www.caida.org/analysis/topology/macroscopic/

[13] K. Calvert, M. Doar, and E. Zegura, "Modeling Internet topology", IEEE Communication Magazine, Vol. 35, pp. 160−163, 1997.

[14] J. I. Alvarez-Hamelin, et al., "k-core decomposition: A tool for the visualization of large scale networks," Arxiv preprint cs. NI/0504107, 2005

[15] J. Zhang, H. Zhao, and Y. Zhou, "Relationship between degree and core number of Internet nodes at router level," Journal of Northeastern University (Natural Science), Vol. 29, No.5, pp. 653−656, 2008.

[16] B. Cheswick, H. Burch, and S. Branigan, "Mapping and visualizing the Internet," in Proceedings of the 2000 USENIX Ann Technical Conference, San Diego, California, USA, June 2000.

Int. J. Communications, Network and System Sciences, 2009, 4, 249-324
doi:10.4236/ijcns.2009.24033 Published Online July 2009 (http://www.SciRP.org/journal/ijcns/).

Adaptive Backoff Algorithm for IEEE 802.11 MAC Protocol

Maali ALBALT[1], Qassim NASIR[2]
Department of Electrical and Computer Engineering, College of Engineering, University of Sharjah, Sharjah, UAE
Email: {[1]maali, [2]nasir}@sharjah.ac.ae
Received October 4, 2008; *revised December* 28, 2008; *accepted March* 3, 2009

ABSTRACT

A Mobile Ad Hoc Network (MANET) is a collection of mobile nodes that can communicate directly over wireless media, without the need for a pre-configured infrastructure. Several approaches have been suggested to improve Quality of Service (QoS) in IEEE 802.11-based MANETs through modifying some of the IEEE 802.11 Medium Access Control (MAC) algorithms, such as the backoff algorithm that is used to control the packets collision aftermath. In this work, an adaptive IEEE 802.11 backoff algorithm to improve QoS is developed and tested in simulations as well as in testbed implementation. While the Binary Exponential Backoff (BEB) algorithm deployed by IEEE 802.11 reacts based on individual packet transmit trials, the new algorithm takes the history of successive packet transmit trials into account to provide a better QoS performance.

The new algorithm has been tested against the legacy IEEE 802.11 through simulations using QualNet and a Linux-based testbed comprising a number of stations. The performed tests have shown significant improvements in performance, with up to 33.51% improvement in delay and 7.36% improvement in packet delivery fraction compared to the original IEEE 802.11.

Keywords: MANETs, Ad-Hoc Networks, Quality of Service, Backoff Algorithm, IEEE 802.11

1. Introduction

A MANET is a collection of mobile nodes that are connected without any infrastructure or base station [1]. In such networks, nodes are free to enter, leave the network, move and organize themselves; thus, the topology of the network can change unpredictably. Since the wireless medium is shared by all transmitting nodes in range, there should be a mechanism to control medium access among contending stations so as to minimize the effect of collisions on the performance of the network. The famous IEEE 802.11, for instance, adopts a binary exponential backoff (BEB) algorithm that exponentially increases a station's waiting time if the medium is found busy, and resets to a minimum value right after a successful transmission. The BEB algorithm is considered "memory-less" since it resets the Contention Window (CW) value to the minimum right after a successful transmission without taking into consideration the network conditions.

Many researchers were motivated to enhance the performance of the IEEE 802.11 through modifying the BEB algorithm [1–12]. Most of the prior work in this area have changed or modified the BEB algorithm such that it provides relative priority among two or more traffic classes [1–5]. This solves the *intra-class* contention problem since the class with the least specified CW value would access the channel first. However, it does not solve the *inter-class* contention problem since a number of stations wishing to send packets of the same priority class may still contend and collide (in case their backoff timers expire simultaneously). The latter problem is solved by determining what to do until a successful transmission takes place, or simply how to increment the value of the contention window in the case of a busy channel. The suggested backoff algorithms were mostly slight variations or scales of the BEB algorithm for each traffic class. However, the way how to decrement the CW was unaddressed explicitly and hence assumed to remain the same as the original BEB algorithm (the CW would reset to CWmin upon a successful transmission).

It can be said that the above works solved the contention problem from a priority point of view through determining which class should access the medium first.

But that is not enough since the sudden CW reset to CWmin may cause several collisions, which requires addressing the contention problem from a congestion point of view. More specifically, when a station succeeds in transmitting a packet at a given CW, that doesn't mean a decrease in congestion, but it means arriving at a convenient CW value [6].

This finding inspired some researchers to adopt a different approach of looking at the backoff algorithm, which is what to do after a successful transmission takes place, or simply how to decrement the CW. Several works on slowly decreasing the CW value were proposed [6–12]. [7] and [8] suggested an exponential decrease in the CW value upon a successful transmission instead of resetting to CWmin, but they assumed a fixed scale of decrease without taking the network conditions into account. That might result in underutilizing the channel if it was idle or returning to a congestion state if the network had not yet relieved from a previous congestion.

While [6] and [9] suggested slow decrease backoff algorithms to adapt to the network load, there was another proposal to assume a p-persistent MAC protocol in which the station would transmit with a probability p and refrain form transmitting with a probability 1-p [10,11]. That p-value was calculated in runtime and updated after each transmission to reflect the current number of active stations in [10] or the average time the channel is idle or busy in [11] among other conditions that affect the network load. In both the slow decrease and p-persistent cases, complex computations were needed to update the p-value and to estimate the network load, respectively. Complex computations also mean high power consumption, which is in many cases considered unaffordable in the wireless ad hoc networks context.

This work has modified the IEEE 802.11's main mechanism for managing access to the shared wireless medium, which is the Binary Exponential Backoff (BEB) algorithm; it is replaced with a History-Based Adaptive Backoff (HBAB) algorithm that updates the value of the BEB's Contention Window (CW) according to the network conditions with a suitable prediction. The algorithm proposes a novel approach to slowly increase and decrease the CW value based on the busyness of the channel, i.e. MAC layer transmission retrials. In a previous work by the same authors [13] a similar backoff algorithm was introduced under the same name, but it used a different technique to update CW. Besides developing HBAB in theory and testing it in simulation, this work has built a Linux-based MANET to act as a testbed for implementing HBAB. The constructed testbed, which integrates a number of ready-made and customized hardware and software components, implements HBAB as well as the original IEEE 802.11 protocols in real-time. Both simulation and testbed results show significant improvements in QoS related performance measures, especially in delay, when using HBAB over the original IEEE 802.11.

The paper is organized as follows. Section 2 reviews the IEEE 802.11 MAC protocol backoff algorithm and QoS in MANETs. Section 3 presents the HBAB algorithm. Sections 4 and 5 discuss performance evaluation of the proposed HBAB against the standard BEB IEEE 802.11 in simulation and Linux testbed, respectively. Section 6 concludes the paper and provides directions for future work.

2. IEEE 802.11 and Binary Exponential Backoff

The IEEE 802.11 family of standards defines the specifications of both the physical (PHY) and medium access control (MAC) layers to construct a WLAN [14]. While the 802.11 PHY layer defines the signaling and modulation properties of the protocol, the 802.11 MAC layer controls access to the shared wireless medium. In order to accomplish that, the 802.11 MAC defines two medium access functions: a mandatory distributed coordination function (DCF) and an optional point coordination function (PCF) [3]. The DSF function uses BEB to manage access to the medium in the case of packet collisions.

The DCF function uses a carrier sense multiple access with collision avoidance (CSMA/CA) mechanism to control access to the shared wireless medium. This mechanism features the exchange of control packets (Request-To-Send (RTS) and Clear-To-Send (CTS)) before data transmission to minimize the chances of collisions. Furthermore, before initiating that type of RTS/CTS exchange, each STA is required to sense the medium for a time interval consisting of the DCF Interframe Space (DIFS) and the current value of the backoff timer [3]. The value of the backoff timer is randomly picked in the range of the current Contention Window (CW) of the station. CW value is updated by a Binary Exponential Backoff (BEB) algorithm that exponentially increases a station's waiting time if the medium is found busy, and resets to a minimum value right after a successful transmission. A positive Acknowledgment (ACK) is used to notify the sender that the frame has been successfully received. If an ACK is not received within a time period of ACKTimeout, the sender assumes that there is a collision and schedules a retransmission by entering the backoff process again until the maximum retransmission limit is reached [3]. A maximum of 7 retransmissions (4 retransmissions) for short frames (long frames) are allowed before the frame is dropped. The basic access procedure is shown in Figure 1.

The BEB algorithm is used by the IEEE 802.11 to control access to the shared wireless medium among contending stations. This is done through adjusting the contention window size based on the current medium

status. When a station has some data to send, it senses the channel to determine whether it is idle. If the medium remains idle for a time interval equal to DIFS, the station is allowed to transmit. If the medium is busy, the transmission is postponed until the ongoing transmission concludes. Meanwhile, a slotted binary exponential backoff procedure takes place: each slot is equal to DIFS, and the number of such slots is determined by a random value uniformly chosen in [0, CW -1], where CW is the current contention window size.

That random value is used to initialize the backoff timer, which keeps running as long as the channel is sensed idle, paused when data transmission (initiated by other stations) is in progress, and resumed when the channel is sensed idle again for more than DIFS. The time immediately following an idle DIFS is slotted, with each slot equal to the time needed for any station to detect the transmission of a frame (in the IEEE 802.11 term, MAC Service Data Unit (MSDU)) from any other station. When the backoff timer expires, the station attempts to transmit a data frame at the beginning of next slot.

Finally, if the data frame is successfully received, the receiver transmits an acknowledgment frame after a specified interval, called the *short inter-frame space* (SIFS), that is less than DIFS. If an acknowledgment is not received, the data frame is presumed to be lost, and a retransmission is scheduled. The value of CW is set to CW_{min} in the first transmission attempt, and is doubled at each retransmission up to a pre-determined value CW_{max}. Retransmissions for the same data frame can be made up to a pre-determined retry limit, L, times. Beyond that, the pending frame will be dropped [3]. The contention window update can be summarized as follows:

$$CW_{new} = \begin{cases} 2\,CW_{current}, & \text{transmission failure- up to max value} \\ CW_{min}, & \text{transmission success} \end{cases}$$

The metrics used in comparing protocol performance are 1) the Packet Delivery Fraction (PDF), which represents the ratio of the number of the successfully delivered data packets to their destinations versus the number of all data packets being sent; 2) the average end to end delay, which measures the average required time in seconds to receive a packet; and 3) the throughput, which is the amount of data successfully transferred through the channel in a given time period. It is measured in kilo bits per second (kbps) [15].

3. History Based Adaptive Backoff (HBAB) Algorithm

This paper proposes a novel backoff algorithm, the History Based Adaptive Backoff (HBAB) algorithm, in which the history of the past trials for transmission is taken into account. In short, HBAB modifies BEB in such a way that the history of the past trials of transmission is taken into account. In order to do that, HBAB defines three variables: **the contention window size** (***CW***), which holds the current contention window size, **the multiplicative factor**, ***α***, which is used to update *CW* and **the *ChannelState***, which captures a snapshot of the medium (or channel) representing its most recent busy/free states. The first variable is common with BEB whereas the latter two variables are HBAB-specific.

The parameter α is a multiplicative factor used to update CW value. A similar multiplicative factor is implicitly defined in the original IEEE 802.11 BEB to have the value of two since CW is doubled upon each transmission failure, i.e. the current CW is multiplied by two to get the new CW. However, α is different from that implicit definition in two aspects:

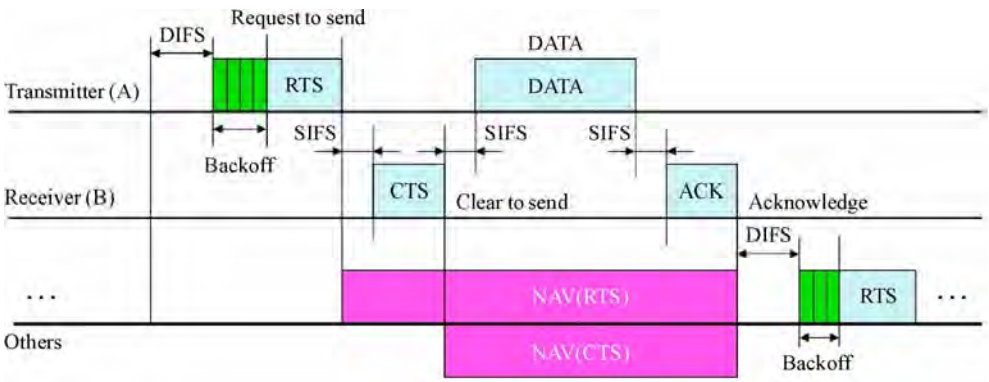

Figure 1. IEEE 802.11 DCF operation.

- Value: theoretically, any positive value greater than 1 can be assigned to α while the multiplicative factor of the original algorithm is fixed at two. The value of α can be either assigned statically, i.e. before runtime and remains constant during runtime or dynamically, i.e. to change according to certain parameters that are sampled during runtime. In this work, only static assignment is implemented.
- Usage: α is used to update CW upon both transmission failures and successes. BEB uses the multiplicative factor only in transmission failure updates since it resets CW upon a transmission success.

In addition to α, HBAB defines another parameter, *ChannelState*, which reflects the most recent history of the medium in terms of its busy/free states. That is, *ChannelState* stores the most recent N states of the medium sensed upon each transmission trial. A free channel state means that the channel is available and no stations are currently transmitting; it is represented by 1. A busy channel state means that there is at least one stations currently transmitting; it is represented by 0. Hence, if N=2 (which is the case in this work), a *ChannelState* of 01 means that the medium had been busy then becomes free. N indicates the depth of this history; the greater N, the deeper captured history of the channel. An obvious tradeoff will be the depth of the channel history versus the available memory to store the states.

The *ChannelState* is updated upon each transmission trial, i.e. each time the station senses the medium trying to transmit a packet. To make room and store the new channel state, the oldest channel state is removed and the remaining stored states are shifted to the left.

When HBAB begins, the three variables, *CW*, α and *ChannelState*, are initialized as follows:

$$CW = CW_{min} \quad \textbf{(1)}$$

$$\alpha = f,\ f > 1 \quad \textbf{(2)}$$

$$ChannelState = 11 \quad \textbf{(3)}$$

where CW_{min} is the minimum value of *CW*, *f* is the chosen value for the multiplicative factor α and *ChannelState* is expressed in binary representation. *f* could be theoretically any positive value greater than one to assure the multiplicative impact on *CW*; in the special case of *f* is exactly one, no updates will take place as the process of updating *CW* involves multiplication or division as will be shown later in this section. If *f* is a positive value less than one, then the multiplicative impact is reversed: multiplying by α decreases the multiplicand whereas dividing by α increases it. Negative values of *f* are meaningless since α is used to update a counter.

If the current transmission trial has failed, *CW* is updated to be the current value of *CW* multiplied by the multiplicative factor α. Thus, the station would wait for a number of time slots equal to the new value of *CW* before attempting transmission again. If, however, the current transmission trial has succeeded, further checks need to be done in order to calculate the updated, namely:

1) If the value of the *ChannelState* represents two consecutive busy states, the new value of *CW* would be the current *CW* divided by α.

2) Otherwise, *CW* is reset to CW_{min}.

Equation (4) illustrates the possible update schemes:

$$\mathrm{CW} = \begin{cases} \mathrm{CW} \cdot \alpha, transmission\ \ failure \\ \mathrm{CWmin,\ transmission\ success,\ ChannelState} \neq 00 \\ \dfrac{\mathrm{CW}}{\alpha},\ \mathrm{transmission\ success,\ ChannelState} = 00 \end{cases} \quad \textbf{(4)}$$

where ChannelState is expressed in binary representation.

Table 1 shows the suggested CW updating method per state check (0 indicates a busy channel and 1 indicates a free channel):

Compared to BEB adopts a similar incrementing approach. While BEB doubles the value of *CW* upon a transmission failure, HBAB multiplies the value of *CW* by α. As for the decrementing approach, it is somehow different. Instead of resetting *CW* to CW_{min} all the time as in BEB, HBAB first checks the value of the *ChannelState* is not busy for two consecutive times provided that the current channel state is free (the latter condition is indicated by the transmission success). In case the channel state is busy for two consecutive times (which indicates a congested medium), *CW* is divided by α instead of resetting to CW_{min}. In other words, a slow decrease in

Table 1. Possible CW update values based on HBAB operation.

Current state	State	CW value
0 (busy)	00(busy, busy) 01 (busy, free) 10 (free, busy) 11 (free, free)	CW = CW *(α)
1 (free)	11 (free, free) 01 (busy, free) 10 (free, busy)	CW = CW_{min}
	00(busy, busy)	CW = CW / (α)

CW is preferred in this case since a congested medium (for at least two states) is unlikely to be free upon a single success.

As for the overhead that comes with implementing HBAB, it is due to two factors: extra memory space for new variables and extra computations for additional operations. As for memory, the extra storage space is needed for the new variables: ChannelState and eight other utility variables. As for computations, five additional operations are needed to determine the next value of CW, which are multiplication, shifting, 'if' conditional statement, memory read and memory write operations (to update the hardware registers). An implicit power overhead is associated with the additional operations.

4. Simulation Results

This section shows the performance of HBAB-based IEEE 802.11 against the BEB-based IEEE 802.11 under different network loads. The simulation is carried out in QualNet network simulator version 4.0 [17]. Each point on every graph represents the average of 10 trials using different SEED values to minimize the effect of outliers. The SEED value is used to initialize the random number generator, which is used for node placement and mobility among other usages. Each SEED was used twice: once for an IEEE 802.11 simulation run and the other for the corresponding HBAB simulation run under the same parameters. That ensures the testing has been conducted under the exact conditions, including any random-based parameter.

4.1. Simulation Environment

Our simulation modelled a network of 50 mobile nodes placed randomly within a 1000 × 1000 meters area. Radio propagation range for each node is 250 meters and channel capacity is 2 Mbits/sec. As for node mobility, the random waypoint model is used. In this model, a node chooses a random point in the network, and moves towards that point at a constant speed. The speeds are uniformly chosen between the minimum and maximum speeds set to 0 m/s and 10 m/s, respectively. When the node reaches its destination, it stays there for a certain pause time (fixed to be 20 seconds in this paper), after which it chooses another random destination point and repeats the process.

All simulations last for 600 seconds. The data traffic is generated by Constant Bit Rate (CBR) sessions initiated between random source and destination pairs. Each session lasts until the end of the simulation. Table 2 shows the common simulation parameters.

Table 2. Simulation parameters.

Parameter	Value
Area	1000×1000m
Number of nodes	50
Simulation time	600s
Packet size	512 bytes
Packet rate (per connection)	4 packets/s
Mobility pattern	Random waypoint with max speed of 10m/s and pause time of 20s
Traffic type	Constant bit rate (CBR)
CW_{min}, CW_{max}	31, 1023

Simulation results are shown in Table 3 and Figures 2 through 4. Table 3 shows a detailed percentage improvement of HBAB averaged for all connections loads per values of α (compared to IEEE 802.11). Figures (2)–(4) show the individual PDF, throughput and average delay comparisons between HBAB (for selected values of α) and IEEE 802.11. It was noted that for all values of α and under most of the tested networks loads, HBAB had outperformed IEEE 802.11 for all of the three performance metrics. The only exception was the lowest network load (the ten connections) for higher values of α. In general, performance improvement tended to be higher for smaller values of α; in other words, as the value of α increases, the percentage improvement in HBAB performance compared to IEEE 802.11 decreases.

As for each of the performance metrics, the PDF maintained a descending pattern of improvement as the value of α increased (with the highest improvement at α = 1.1), while the average delay showed a different behavior; it reached the peak at α = 1.2 and recorded another increase at α = 1.4. Throughput showed similar behavior to PDF. Overall, the best performance improvement was obtained for α = 1.2 (with 33.51% improvement in delay and 7.36% improvement in PDF compared to IEEE 802.11).

Table 3. Performance improvement of HBAB.

α value	Improvement (compared to IEEE802.11)		
	PDF	Average delay	Throughput
1.1	8.60%	12.13%	8.56%
1.2	7.36%	33.51%	7.40%
1.3	7.70%	14.43%	7.57%
1.4	5.73%	17.48%	5.71%
1.5	5.33%	9.28%	5.32%
1.6	5.04%	6.95%	4.93%
1.7	5.69%	3.38%	5.68%
1.8	5.87%	0.89%	5.89%
1.9	5.36%	1.33%	5.46%
2	3.59%	-16.39%	6.46%

5. Linux Testbed Results

The testbed that was used to test HBAB for real time performance comprises 4 Linux-based stations: 3 desktops and 1 laptop configured to work in the ad-hoc mode. The backoff algorithm itself was loaded on an Atheros-based wireless adapter [18] running the Madwifi driver [19]. All of the four stations ran Fedora 7 distribution [20] and the Linux kernel version 2.6.21. Although Atheros chipset and Madwifi driver offer a level of coding flexibility not present in other chipsets, implementing the backoff algorithm fully was not possible because packet

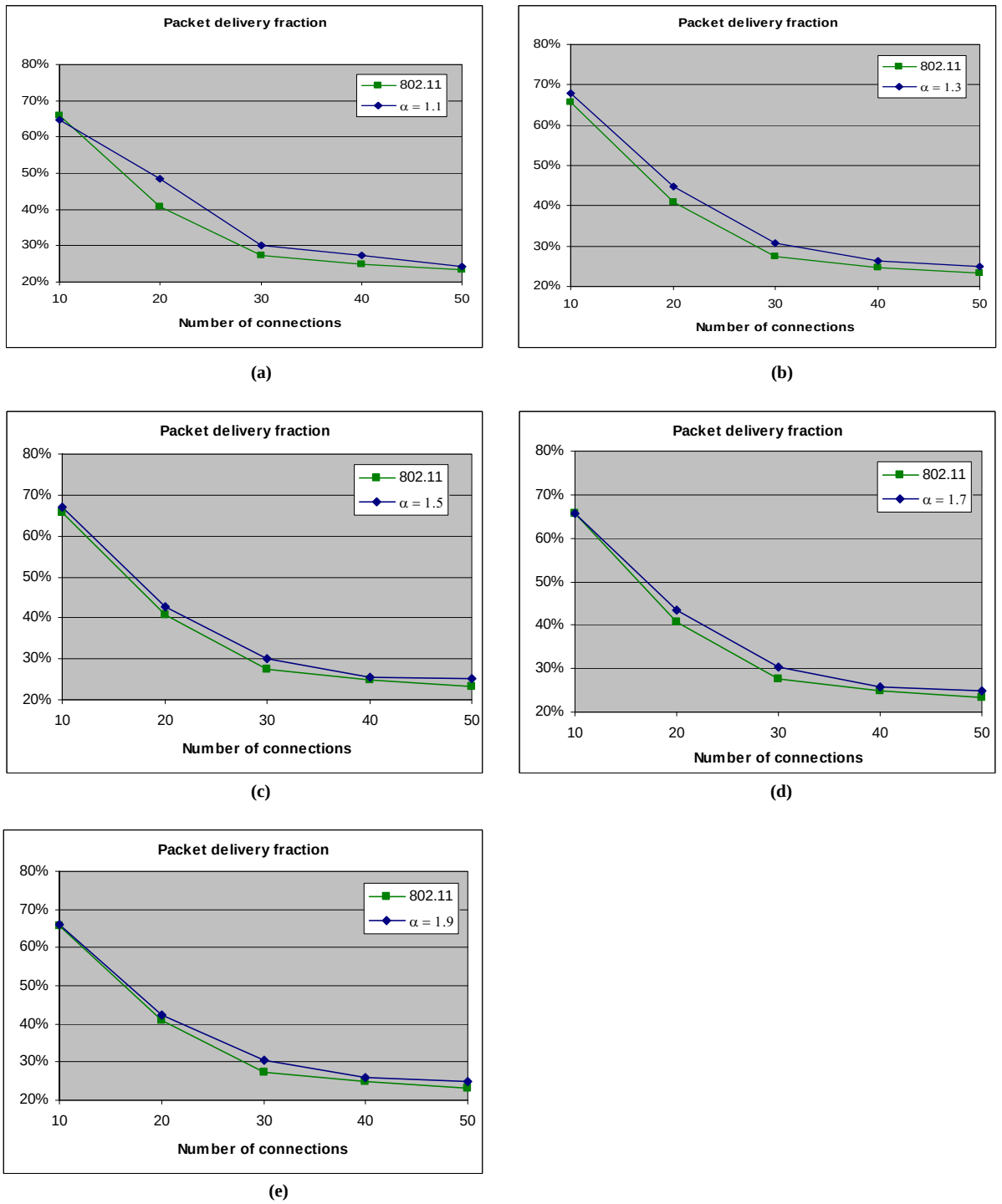

Figure 1. PDF of HBAB (α= 1.1, 1.3, 1.5, 1.7 and 1.9) vs BEB-simulation.

transmission trial handling is done per-packet, not per transmission. That is, a packet success in Madwifi means that a packet has been delivered to the destination regardless the number of retransmissions it had encountered. Similarly, a packet failure means that the packet had failed all the possible transmission trials (until hit-ting the maximum retry limit). Not being able to access the packets per retransmission means that implementing a backoff algorithm per transmission is not possible. Alternatively, a per-packet variant of HBAB has been pro-

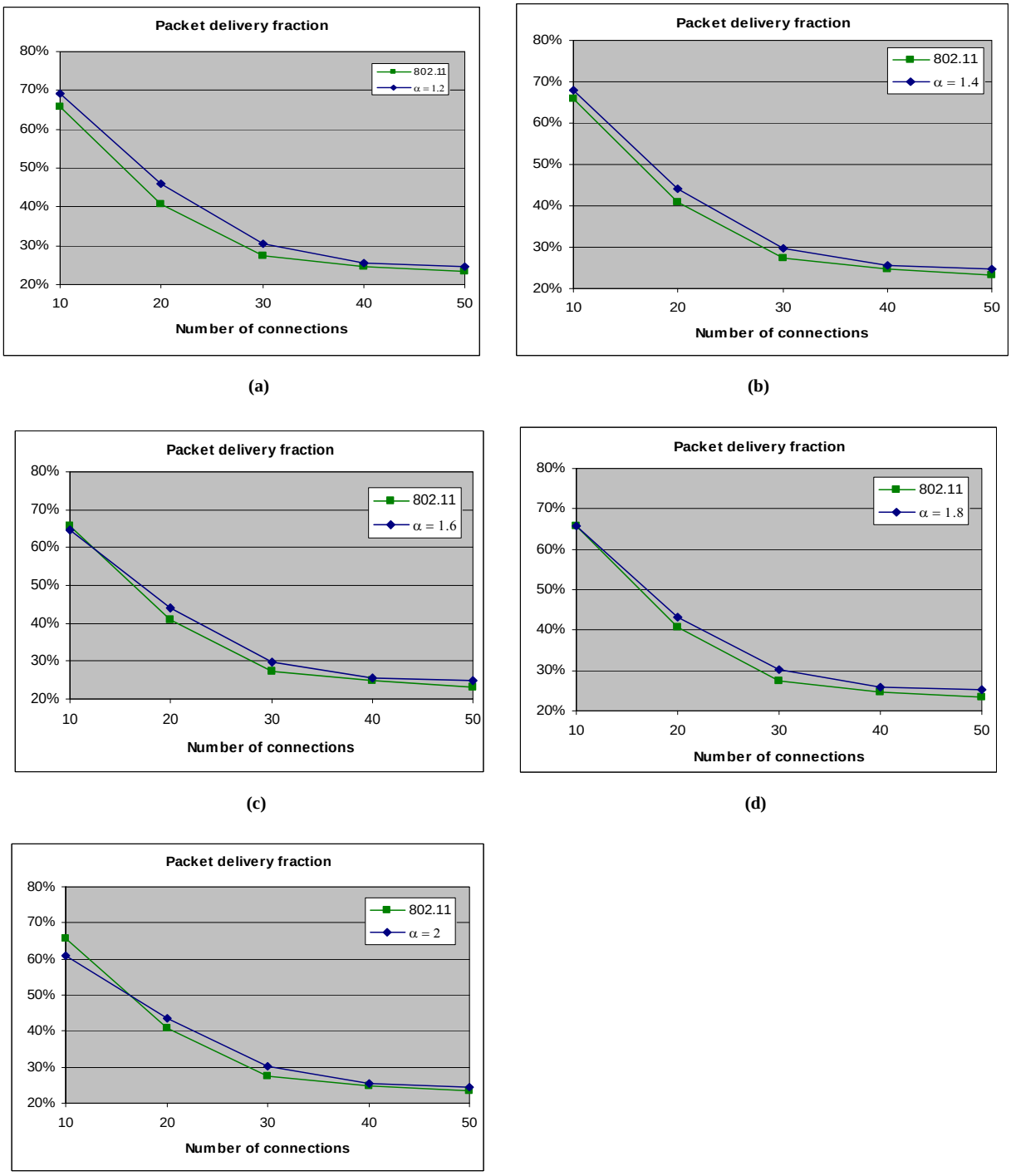

Figure 2. PDF of HBAB (α = 1.2, 1.4, 1.6, 1.8 and 2) vs BEB-simulation.

posed to demonstrate the new backoff algorithm. Table 4 shows the wireless adapters used in this work along with their specifications.

A number of Linux-compatible software tools were used to implement and evaluate HBAB. The network load traffic was generated using the Multi-Generator (MGEN) tool, which is open source software that provides the ability to perform IP network performance tests and measurements using UDP/IP traffic [21]. The TRace Plot Real-time (TRPR) software tool was used to analyze the output files generated by MGEN and calculate the performance metrics used in this work [22]. In order to

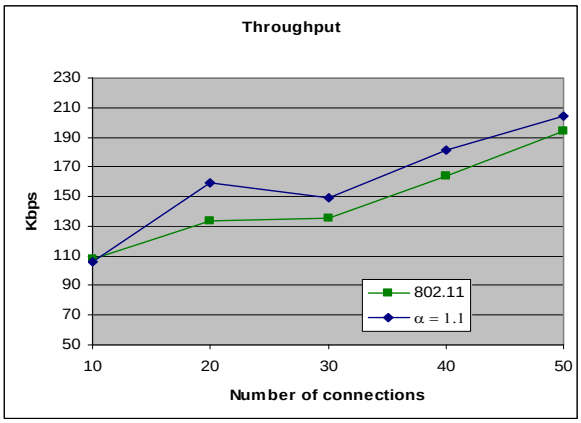

(a)

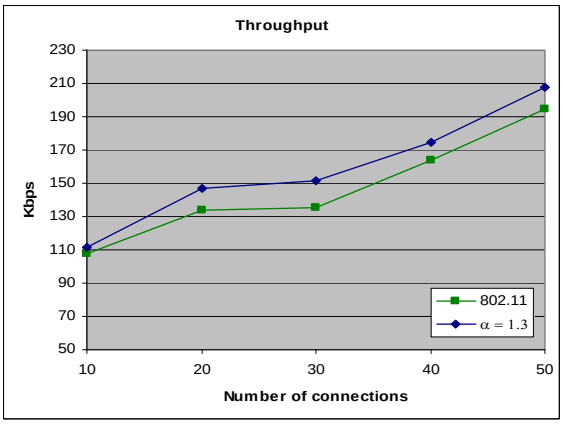

(b)

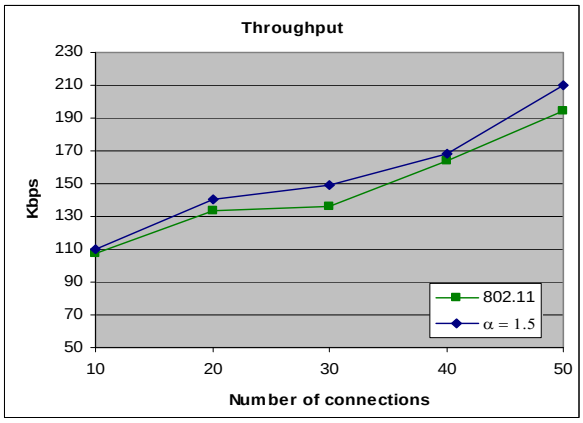

(c)

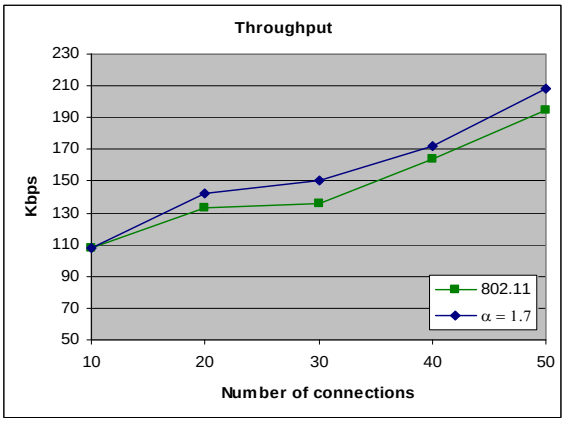

(d)

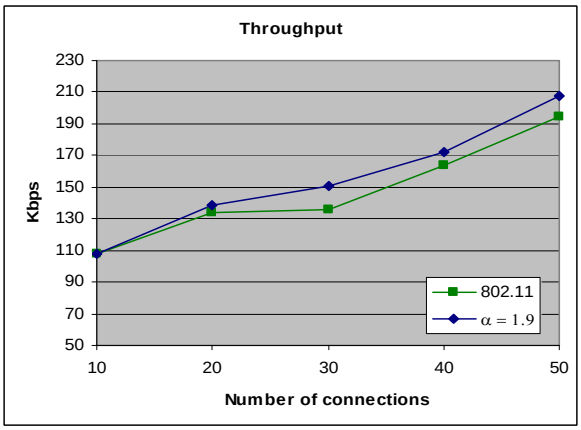

(e)

Figure 3A. Throughput of HBAB (α = 1.1, 1.3, 1.5, 1.7 and 1.9) vs BEB-simulation.

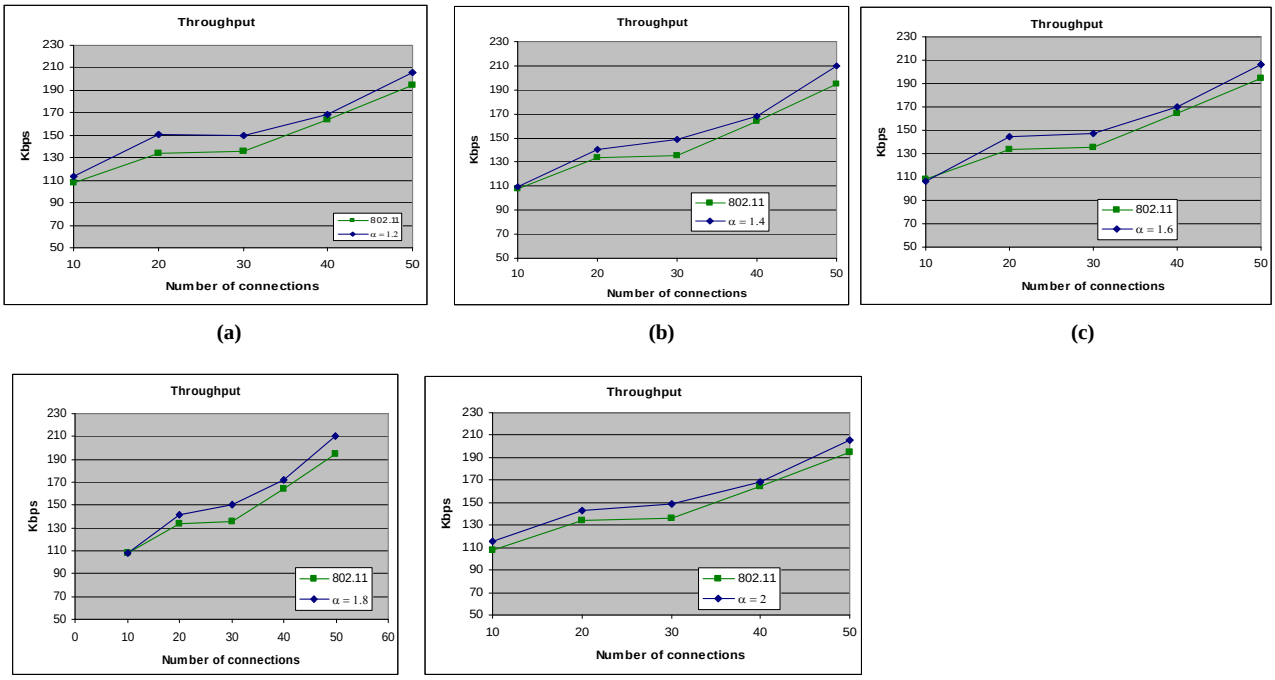

Figure 3B. Throughput of HBAB (α = 1.2, 1.4, 1.6 and 1.8) vs BEB-simulation.

monitor the network and capture live packets as experiments were conducted, Wireshark network protocol analyzer was used [23]. Forming a MANET needed a suitable routing protocol, which was the DSR routing protocol in this work (DSR-UU implementation) [24].

In order to evaluate HBAB real-time performance, a number of testing scenarios were conducted in both simulation and Linux testbed environments. In all testing scenarios, the main connection that was used to evaluate HBAB performance, i.e. to generate the fore ground traffic, was established between Station 2 (source; HBAB-loaded) and Station 4 (destination). The packet generation rate was changed per testing scenario. Other connections were established between Stations 1 and 3 as well as Stations 2 and 4 to generate background traffic, whose packet generation rate also varied per testing scenario. The performance measures (average delay, loss fraction and throughput) were extracted from the log files produced at Station 4 after each testing scenario. Traffic generation rate was changed from 100 to 200 packets/s per station in steps of 20. All testbed scenarios were conducted using the special per-packet variant of HBAB (with varying the multiplicative factor α from 1.1 to 2.0 in steps of 0.1). Table 5 further shows the parameters of the testing scenarios.

The results of the Linux testbed experiments are shown in Table 6 and Figures (5)–(7). Table 6 shows a detailed percentage improvement of HBAB averaged for all connections loads per values of α (compared to IEEE 802.11), whereas Figures (6)–(8) show the individual PDF, throughput and average delay comparisons between HBAB (for selected values of α) and IEEE 802.11. Since HBAB implementation in the Linux testbed was a bit different from simulation, performance results were different as well. In general, there was no consistent performance improvement pattern in the testbed experiment results as illustrated in simulation. HBAB outperformed IEEE 802.11 for almost all values of α (except α = 1.1) with respect to the average delay, and for half of the values of α with respect to the PDF and throughput. Overall, the best performance improvement was obtained for α = 1.7 (with 34.30% improvement in delay and 1.40% improvement in PDF compared to IEEE 802.11).

6. Conclusions

A MANET is an infrastructure-less network connecting a number of mobile nodes via wireless media. The special characteristics of MANETs, such as mobility and absence of centralized control, have made the provisioning of end-to-end QoS guarantees a very challenging problem.

In this work, an adaptive backoff algorithm was developed based on the IEEE 802.11 MAC to provide better QoS performance (especially delay) in MANETs. In

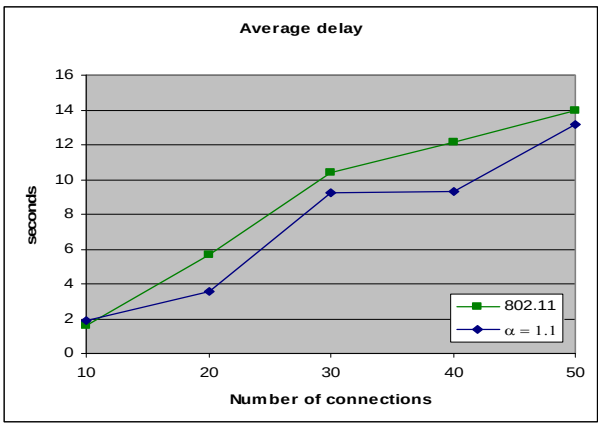

(a)

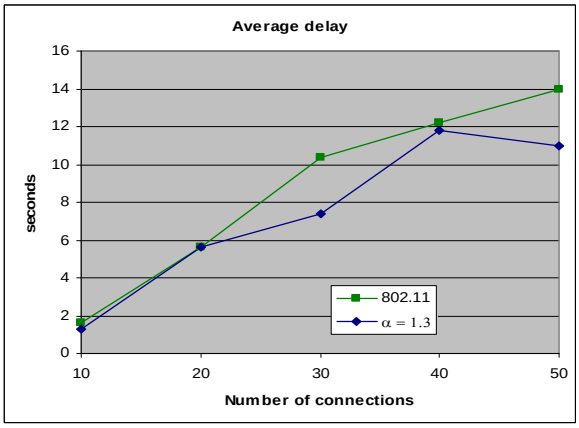

(b)

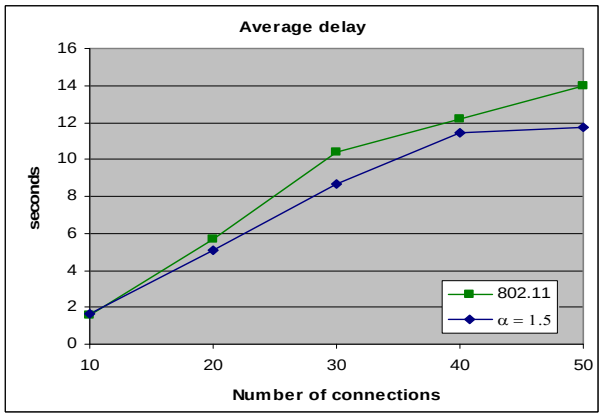

(c)

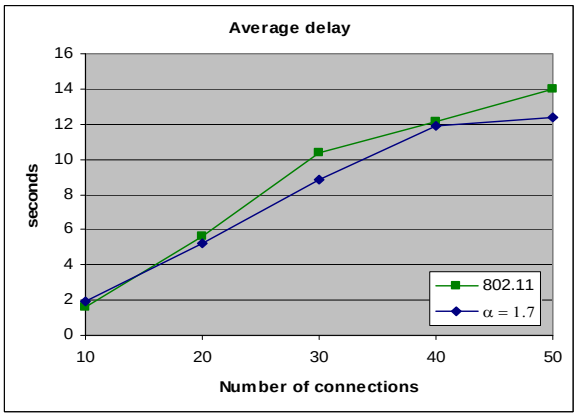

(d)

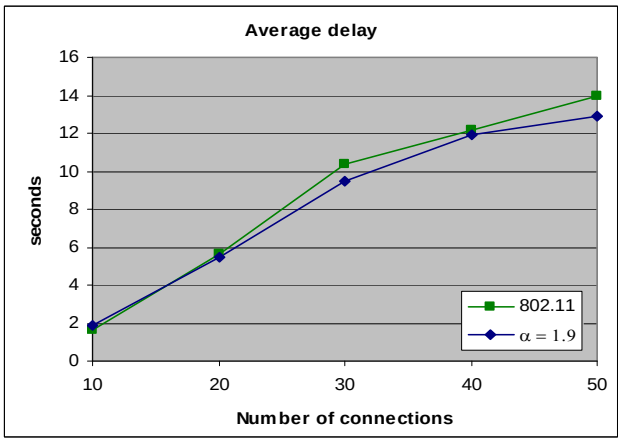

(e)

Figure 4A. Average delay of HBAB (α = 1.1, 1.3, 1.5, 1.7 and 1.9) vs BEB-simulation.

particular, the IEEE 802.11's Binary Exponential Back off (BEB) algorithm was replaced with a History-Based Adaptive Backoff (HBAB) algorithm that updated the value of the BEB's Contention Window (CW) according to the channel state over a period of time. In addition to the channel state, HBAB utilized a multiplicative factor, α, to increase or decrease CW value.

HBAB was tested by simulation (using QualNet simulation package) and implemented in a Linux-based testbed. The simulation environment featured fifty nodes moving in random way-point fashion within 1000 square meters area, whereas the Linux testbed comprises four

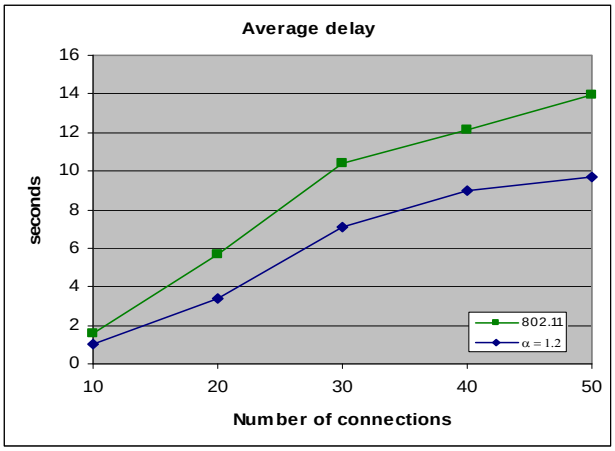

(a)

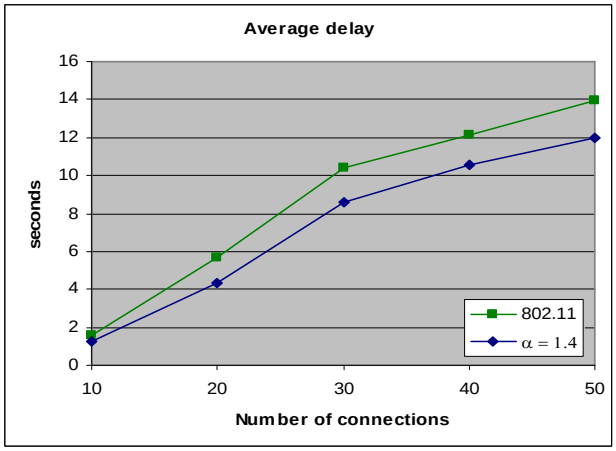

(b)

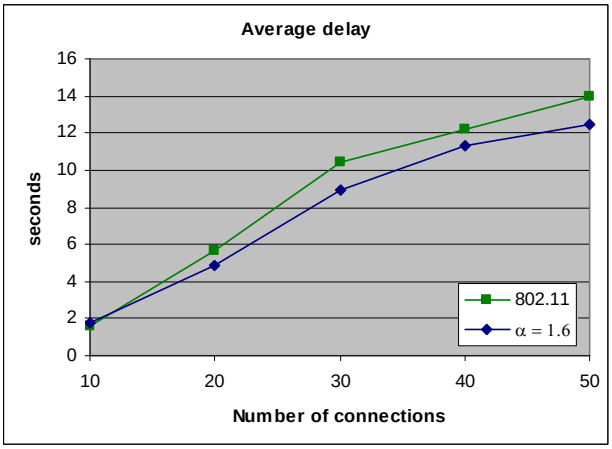

(c)

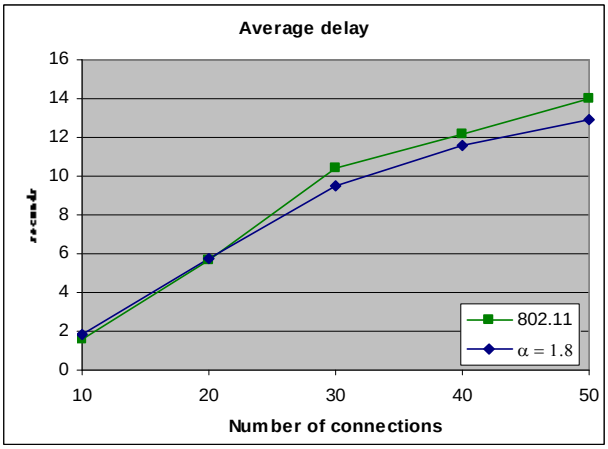

(d)

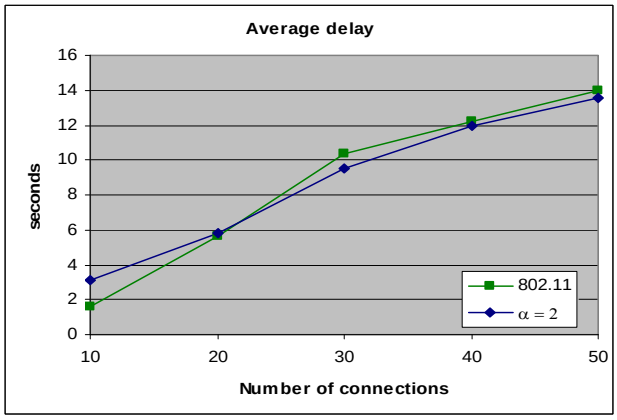

(e)

Figure 4B. Average delay of HBAB (α = 1.2, 1.4, 1.6, 1.8 and 2) vs BEB-simulation.

Table 4. Wireless cards specifications.

Make and model	Dlink DWL-122	Netgear WPN-511	Dlink DWA-110
Chipset	Intersil Prism II	Atheros AR5002 (AR5212)	Ralink RT2501U
Network standards	802.11 b	802.11 b and g	802.11 b and g
Host interface	USB	PCMCIA	USB
Wireless adapter driver	Linux-wlan-ng 0.2.8	Madwifi 0.9.3.1	rt73 1.1.0.0

Table 5. Testbed parameters.

Parameter	Value
Area	4×4m
Number of stations	4
Testing scenario duration	Average of 2 trials, each of 60 s
Packet size (foreground and background traffic)	512 bytes
Packet rate (foreground and background traffic)	100, 120, 140, 160, 180, 200 packets/s (per station)
Background traffic type	UDP Constant Bit Rate (CBR)

Table 6. HBAB performance improvement (compared to IEEE 802.11) for the hardware testbed experiments.

α value	Improvement (compared to IEEE 802.11)		
	PDF	Average delay	Throughput
1.1	1.50%	-0.51%	1.50%
1.2	-1.49%	6.10%	-1.49%
1.3	0.74%	1.11%	0.74%
1.4	0.72%	13.11%	0.73%
1.5	0.33%	14.75%	0.32%
1.6	-2.47%	10.95%	-2.48%
1.7	1.40%	34.30%	1.40%
1.8	0.29%	13.37%	0.29%
1.9	-1.37%	17.57%	-1.37%
2	-3.75%	4.35%	-3.75%

stationary nodes equipped with the necessary hardware and software to form a MANET. Due to some hardware limitations, it was not possible to implement HBAB in the Linux-based testbed with its original design as im plemented in simulation. Therefore, a special variant of HBAB was developed for that purpose as detailed in Section 5.

Simulation results have shown significant improvement in IEEE 802.11 performance measures upon using HBAB over BEB. For HBAB (α = 1.2), the average improvements in PDF and average delay were 7.36% and 33.51%, respectively. The Linux-based testbed results for α = 1.7 showed 1.40% and 34.30% improvement in PDF and average delay, respectively. Based on those results, it could be concluded that the lower values of α (which are associated with lower delay) combined with HBAB's novel approach in updating CW provided better channel utilization and eliminated unnecessary waiting time. That was revealed as a decrease in the average delay and increase in PDF and throughput. The overhead associated with implementing HBAB is due to two factors: extra memory space for nine new variables and extra computations for five additional operations.

There are a number of open issues for future development. For instance, HBAB can be applied to different Access Categories (ACs) in IEEE 802.11e instead of only one category as in the legacy IEEE 802.11. Also, the multiplicative factor α can be implemented in such a way that it can be dynamically modified according to the network load and/or medium status.

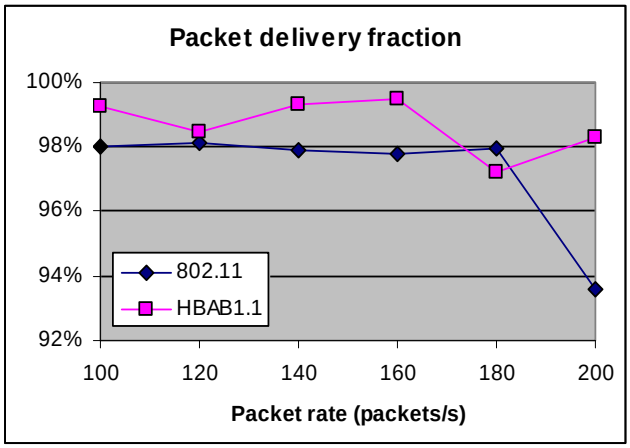

(a)

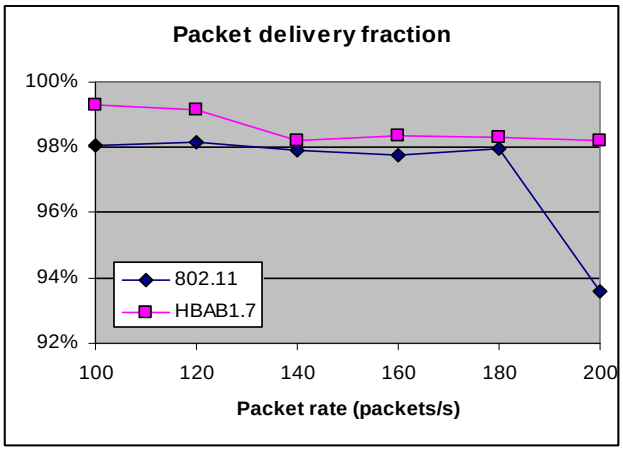

(b)

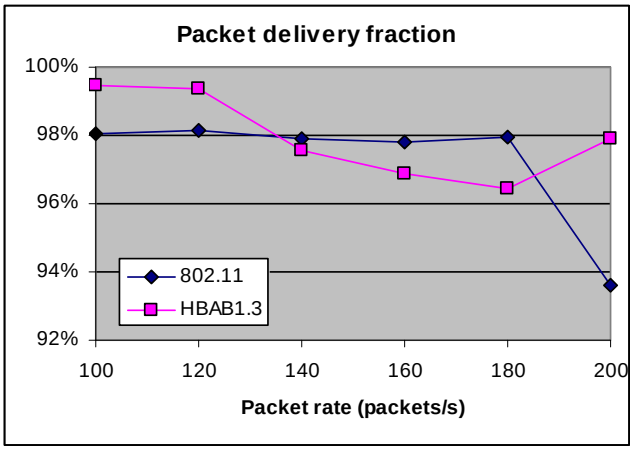

(c)

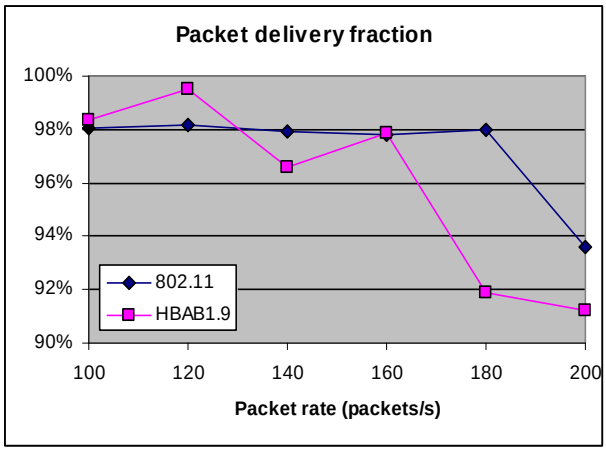

(d)

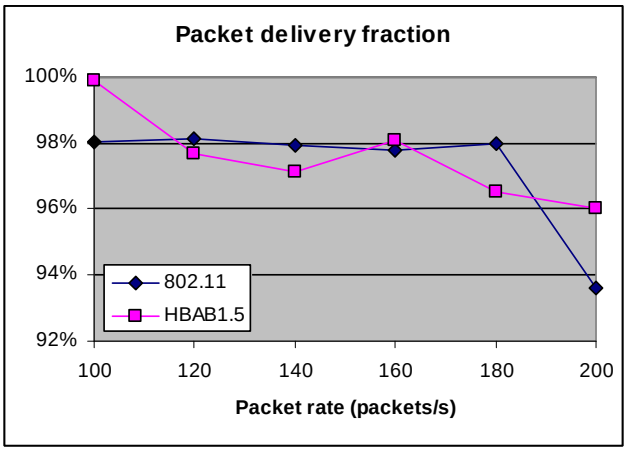

(e)

Figure 5A. PDF of HBAB (α = 1.1, 1.3, 1.5, 1.7 and 1.9) vs BEB-Linux implementation.

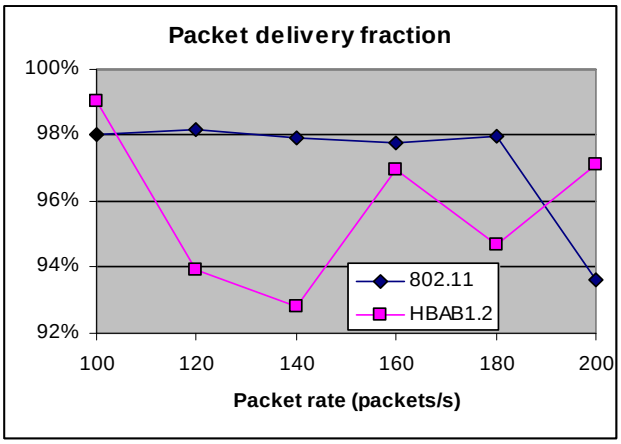

(a)

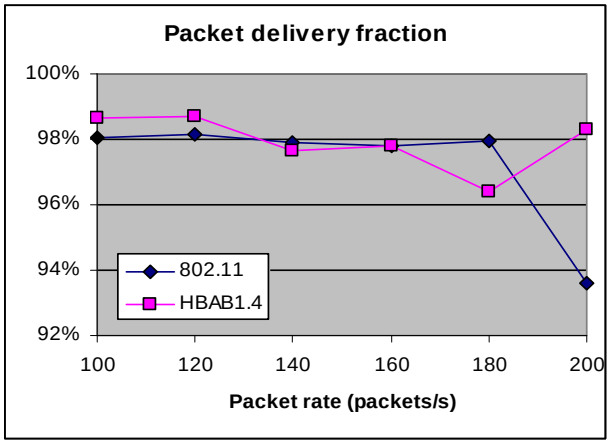

(b)

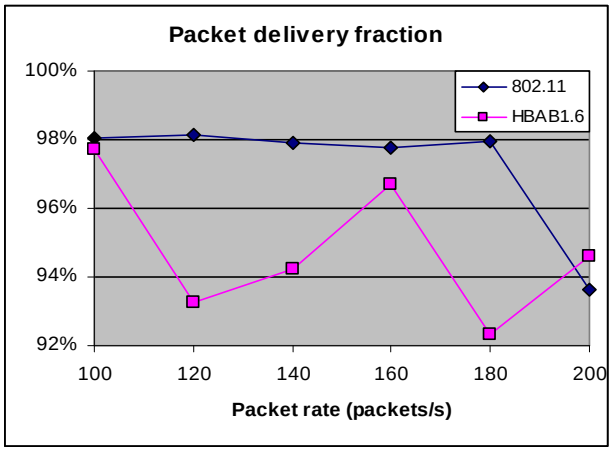

(c)

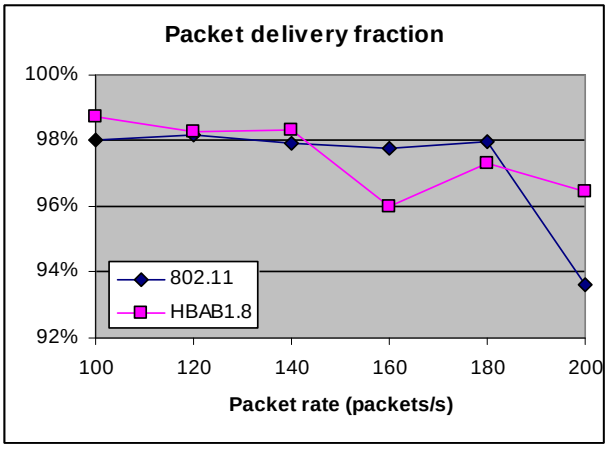

(d)

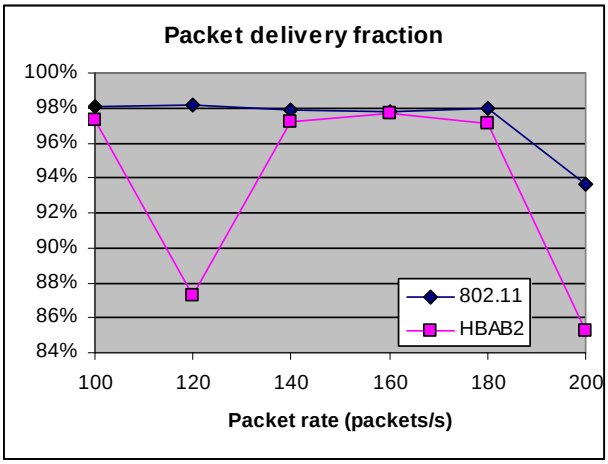

(e)

Figure 5B. PDF of HBAB (α = 1.2, 1.4, 1.6, 1.8 and 2) vs BEB-Linux implementation.

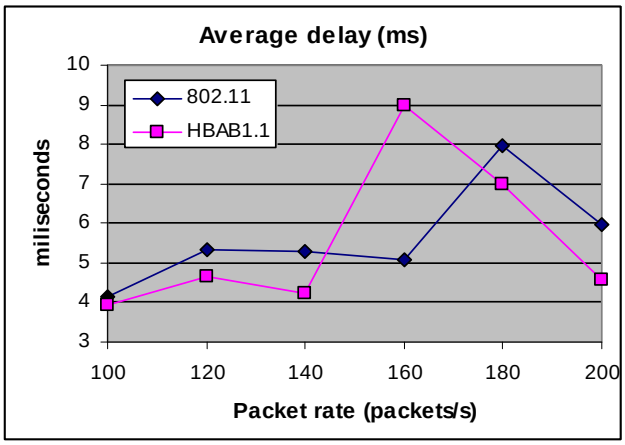

(a)

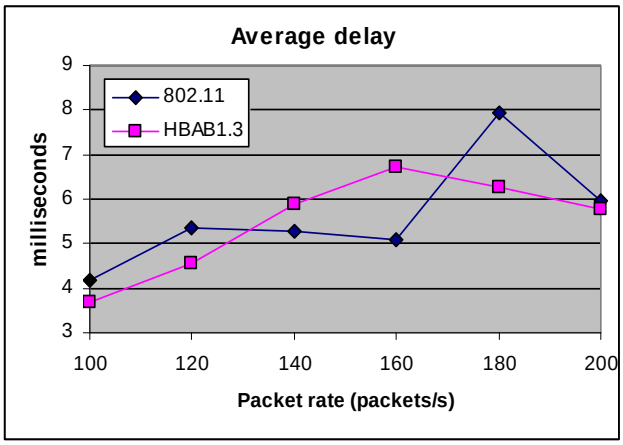

(b)

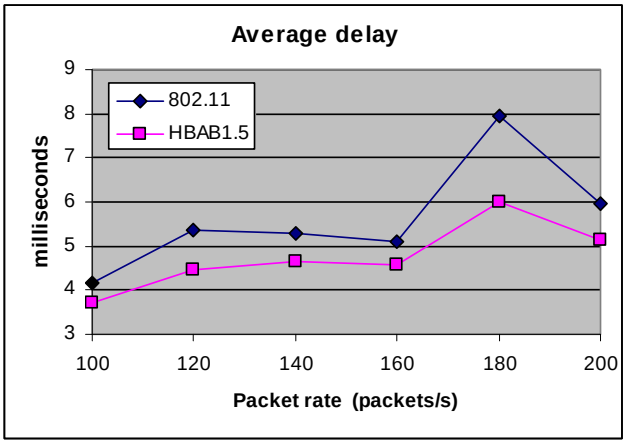

(c)

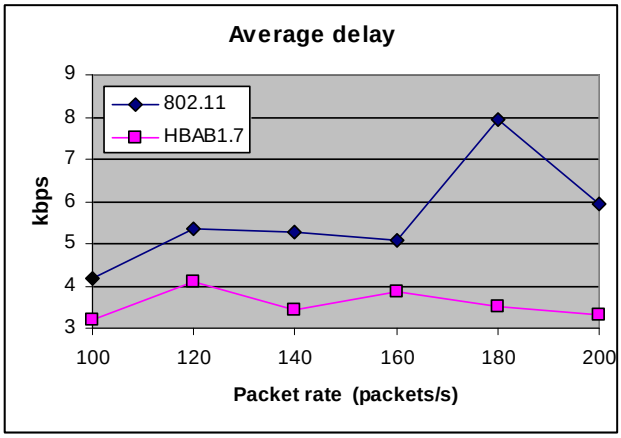

(d)

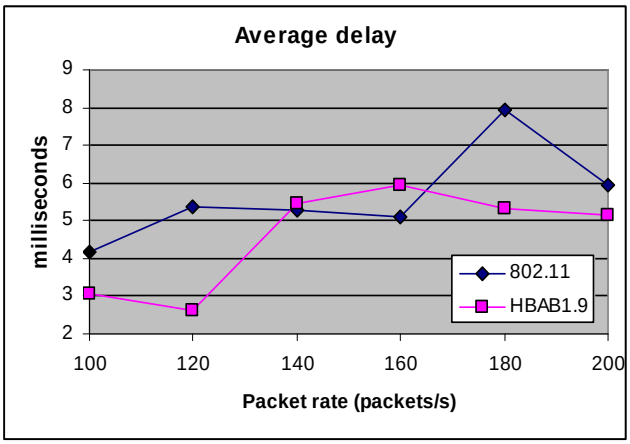

(e)

Figure 6A. Average delay of HBAB (α = 1.1, 1.3, 1.5, 1.7 and 1.9) vs BEB-Linux implementation.

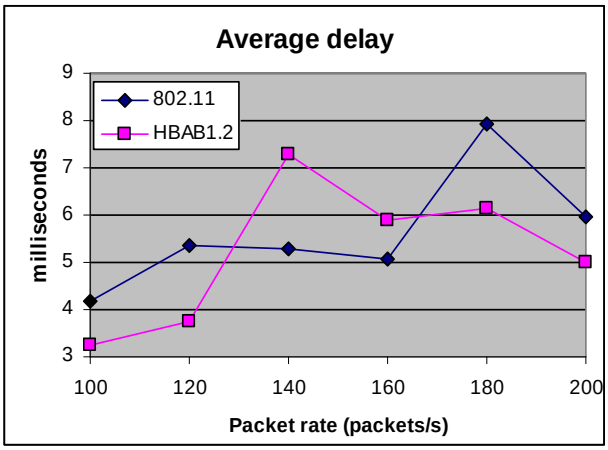

(a)

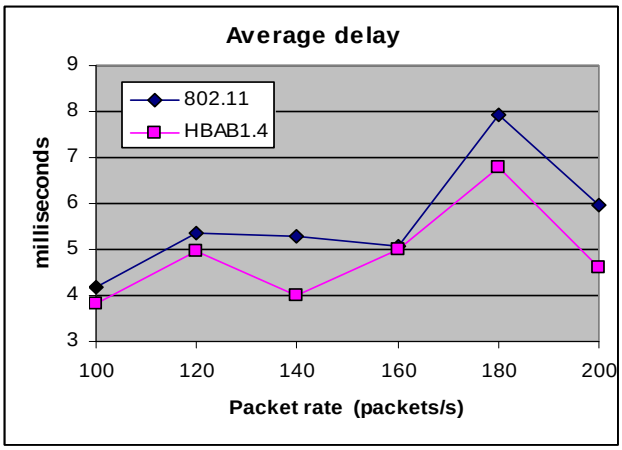

(b)

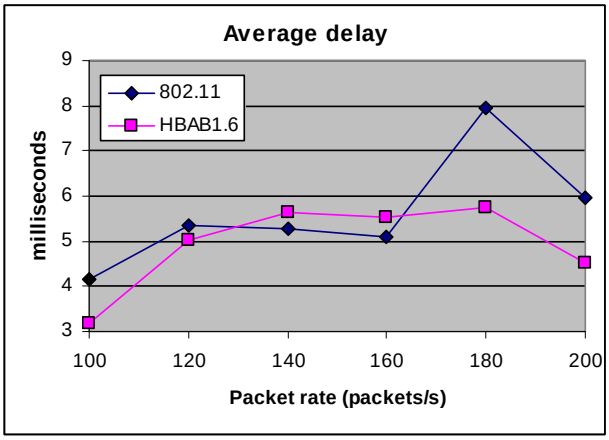

(c)

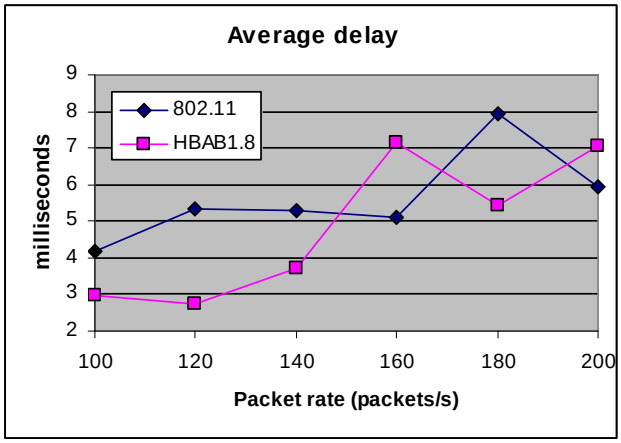

(d)

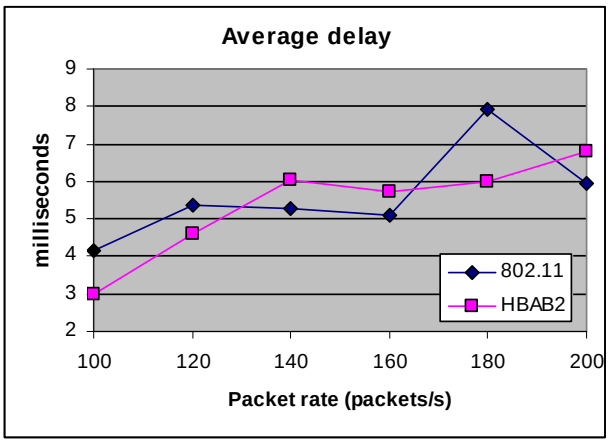

(e)

Figure 6B. Average delay of HBAB (α = 1.2, 1.4, 1.6, 1.8 and 2) vs BEB-Linux implementation.

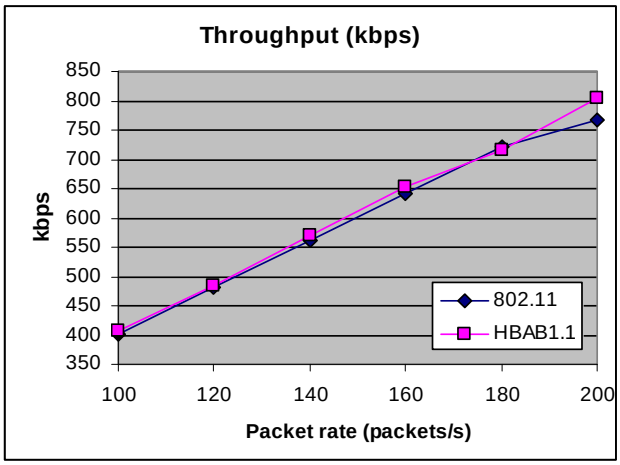

(a)

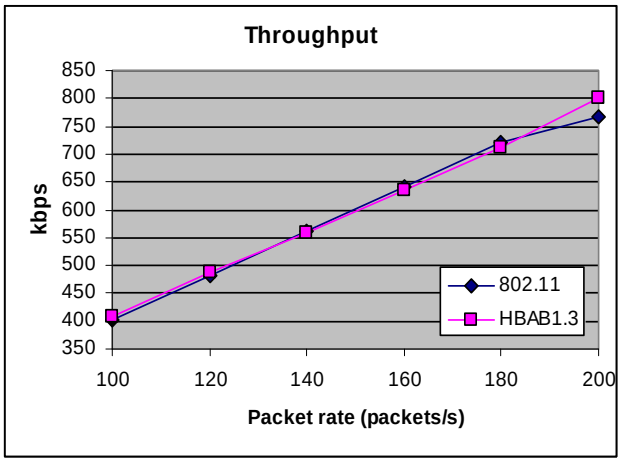

(b)

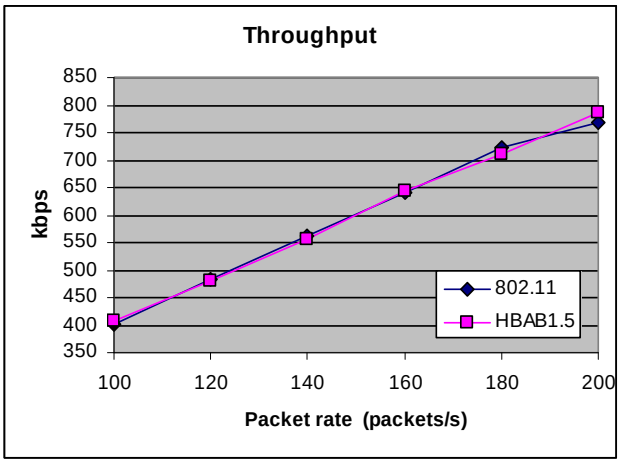

(c)

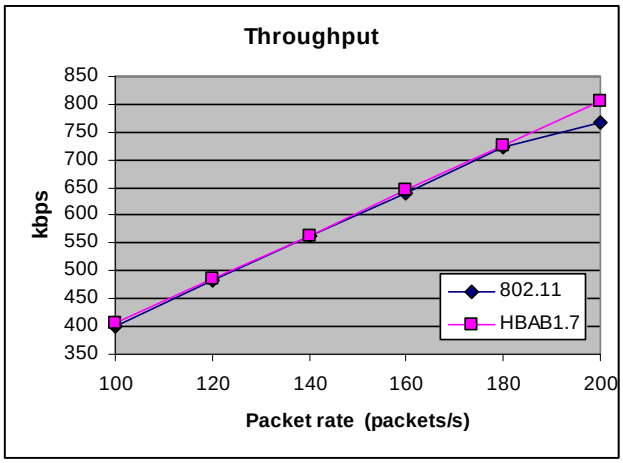

(d)

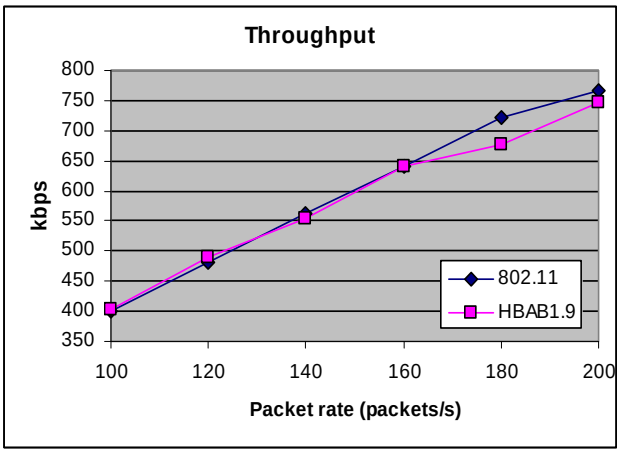

(e)

Figure 7A. Throughput of HBAB (α = 1.1, 1.3, 1.5, 1.7 and 1.9) vs BEB-Linux implementation.

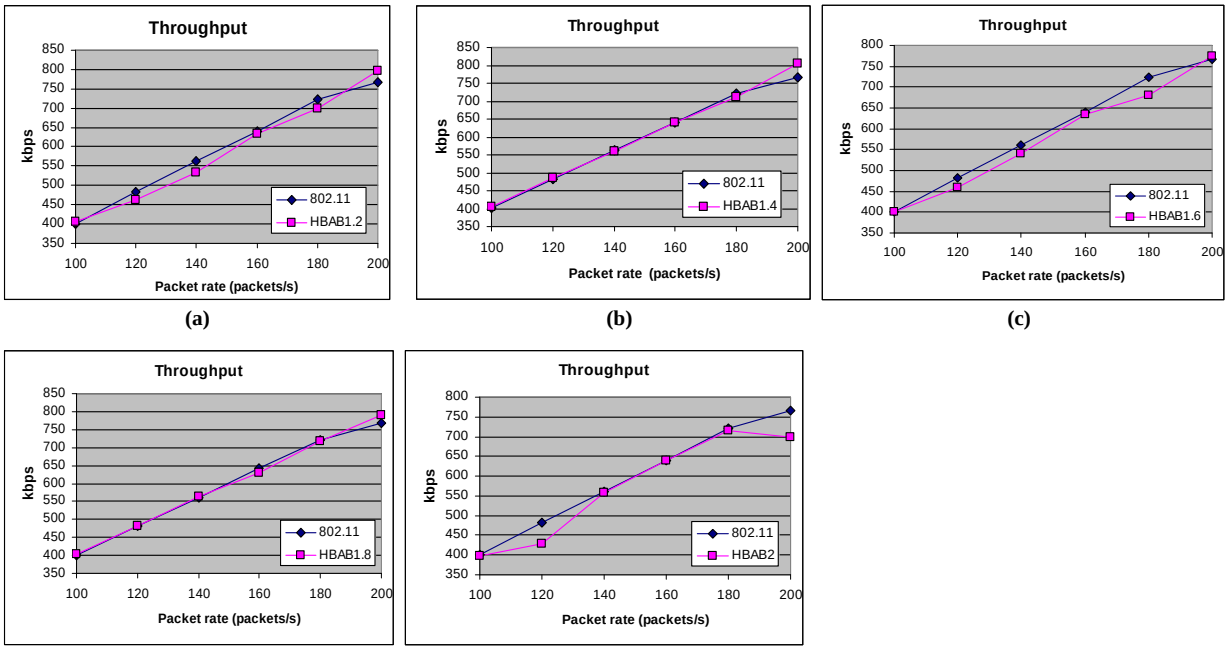

Figure 7B. Throughput of HBAB (α = 1.2, 1.4, 1.6, 1.8 and 2) vs BEB-Linux implementation.

7. References

[1] C. Jones, "A survey of energy efficient network protocols for wireless networks," Wireless Networks, Vol. 7, No. 4, pp. 343–358, 2001.

[2] D. Deng and R. Chang, "A priority scheme for IEEE 802.11 DCF access method," IEICE Transactions on Communications, Vol. E82-B, No. 1, pp. 96–102, 1999.

[3] M. Barry, A. Campbell, and A. Veres, "Distributed control algorithms for service differentiation in wireless packet networks," Proceedings of INFOCOM 2001, Anchorage, AK, USA, April 2001.

[4] V. Kanodia, C. Li, A. Sabharwal, B. Sadeghi, and E. Knightly, "Distributed multi-hop scheduling and medium access with delay and throughput constraints," Proceedings of MobiCOM 2001, Rome, Italy, July 2001.

[5] I. Aad and C. Castelluccia, "Differentiation mechanisms for IEEE 802.11," Proceedings of INFOCOM 2001, Anchorage, AK, USA, April 2001.

[6] Q. Ni, I. Aad, C. Barakat, and T. Turletti, "Modeling and analysis of slow CW decrease for IEEE 802.11 WLAN," Proceedings of PIMRC 2003, Beijing, China, September 2003.

[7] P. Chatzimisios, et al., "A simple and effective backoff scheme for the IEEE 802.11 MAC protocol," Proceedings of CITSA 2005, Orlando, FL, USA, July 2005.

[8] J. A. Moura and R. N. Marinheiro, "MAC approaches for QoS enhancement in wireless LANs," Proceedings of JETC 2005, Lisbona, Portugal, November 2005.

[9] B Li and R. Battiti, "Achieving optimal performance in IEEE 802.11 wireless LANs with the combination of link adaptation and adaptive backoff," Computer Networks Journal, Elsevier Science BV, Vol. 51, No. 6, pp. 1574–1600, 2007.

[10] F. Calì, M. Conti, and E. Gregori, "IEEE 802.11 protocol: Design and performance evaluation of an adaptive backoff mechanism," IEEE Journal on Selected Areas in Communications, Vol. 18, No. 9, pp. 1774–1786, 2000.

[11] R. Bruno, M. Conti, and E. Gregori, "A simple protocol for the dynamic tuning of the backoff mechanism in IEEE 802.11 networks," Computer Networks Journal, Elsevier Science BV, Vol. 37, No. 1, pp. 33–44, 2001.

[12] T. B. Reddy, J. P. John, and C. S. R. Murthy, "Providing MAC QoS for multimedia traffic in 802.11e based multi-hop ad hoc wireless networks," Computer Networks: The International Journal of Computer and Telecommunications Networking, Vol. 51, No. 1, pp. 153–176, 2007.

[13] Q. Nasir and M. Albalt, "History based adaptive backoff (HBAB) IEEE 802.11 MAC protocol," Proceedings of CNSR 2008, Nova Scotia, Canada, May 2008.

[14] Q. Ni, "Performance analysis and enhancements for IEEE 802.11e wireless networks," IEEE Networks, Vol. 19, No. 4, pp. 21–27, 2005.

[15] K. Farkas, D. Budke, B. Plattner, O. Wellnitz, and L. Wolf, "QoS extensions to mobile ad hoc routing supporting real-time applications," Proceedings of AICCSA 2006, Sharjah, UAE, March 2006.

[16] T. Reddy, J. John, and C. Murthy, "Providing MAC QoS for multimedia traffic in 802.11e based multi-hop ad hoc wireless networks," Computer Networks, Vol. 51, No. 1, pp. 153–176, 2007.

[17] Scalable Network Technologies, Inc., QualNet 4.0 product tour, 2006.

[18] Atheros Communications, AR5002 product bulletin, 2007.

[19] Madwifi driver webpage: www.madwifi.org, retrieved on April 15, 2008.

[20] Fedora Linux distribution webpage: www.fedoraproject.org, retrieved on April 15, 2008.

[21] MGEN webpage: http://cs.itd.nrl.navy.mil/work/mgen/, retrieved on April 15, 2008.

[22] TRPR webpage: http://pf.itd.nrl.navy.mil/protools/trpr.html, retrieved on April 15, 2008.

[23] Wireshark webpage: http://www.wireshark.org/, retrieved on August 15, 2008.

[24] DSR-UU webpage: http://core.it.uu.se/core/index.php/DSR-UU, retrieved on August 15, 2008.

Int. J. Communications, Network and System Sciences, 2009, 4, 249-324
doi:10.4236/ijcns.2009.24034 Published Online July 2009 (http://www.SciRP.org/journal/ijcns/).

Design and Implementation for Ladder Diagram in Hydropower Simulation System Based on All Paths Searching Algorithm

Bo LI, Hai ZHAO, Chun-He SONG, Hui LI, Jun AI
College of Information Science and Engineering, Northeastern University, Shenyang, China
Email: *Libokkkkk_0_0_0@yahoo.com.cn, zhhai@neuera.com*
Received August 13, 2008; *revised November* 18, 2008; *accepted January* 29, 2009

ABSTRACT

An approach to design and implement the control function of LD (Ladder Diagram) in the hydropower simulation system based on all paths searching algorithm is proposed in this paper. LD is widely used as a programming language for PLC (Programmable Logic Controller), but it doesn't be executed automatically in the hydropower simulation system which is a software system, and there is no compiler or interpretation for LD in it. The approach in this paper is not only to present a graphical interface to design LD, but also implement its control function through trans-forming it to a corresponding undigraph, in which, all paths between two vertexes (live wire and null line) are searched by the proposed algorithm. An application example is presented to verify the validity of the algorithm and shows that the algorithm is correct and practicable. In addition, how to implement the control function based on object-oriented thought is introduced.

The running time is shown at last, which proves that the system with the algorithm can meet the real-time request in the hydropower simulation system.

Keywords: Ladder Diagram, Object-oriented Thought, Undigraph

1. Introduction

Recently, great changes have arisen in the electrical virtual instruments, e.g. the hydropower simulation system [1–4]. It is a comprehensive system including hydraulic, water conservancy, mechanics and autocontrol. LD control system plays an important role in the system, so an user friendly design interface component-based should be developed for users, and meanwhile, unlikely in the PLC, the control function of LD must be implemented without compiler or interpretation.

Reference [5] proposed a control modeling approach using PNs, an automated CNC lathe door interlocking control program is used as an example, for which model is constructed and validated via PNs. Reference [6] proposed a method to design an LD based on a PN modeling approach. A general method for mapping PNs to LDs is implemented. But converting LDs to PNs can not solve the problem in the hydropower simulation system. Reference [7] converts from a ladder diagram to a native code directly, and a benchmark test in an automotive manufacturing process shows that the translation method fairly speeds up execution in comparison with existing interpretation methods, but there is no interpretation for the code in the software system. Reference [8] extracts the relations of control elements in LD, it presents a transformation method that is achieved by traversing AOV digraph, which is mapped from LD. This method obtains logic relations in the LD by predefining meaning of graphical symbols. It can't be obviously applied in our system since there need an interpretation for the relations.

Fengman hydroelectric power station is the earliest large hydropower station in china, the simulation system in it has run more than 10 years, the work in this paper is based on the system of the next version.

2. Problem Description

Figure 1 shows the accident control circuit of high pressure compressor. Its control principle is that: When the

pressures of the first, second, and third stages are higher than the specified value, pressure relays 2YX1, 3YX1and 4YX1 are open respectively, signal relay coils 2XJ1 (controlled by relay 2YX1), 3XJ1(controlled by relay 3YX1),and 4XJ1(controlled by relay 4YX1) are excited, and then, contacts 2XJ1(controlled by relay coil 2XJ1), 3XJ1(controlled by relay coil 3XJ1), and 4XJ1 (controlled by relay coil 4XJ1) are open,BCJ1 is excited, leading to the accident shutdown.

When the pressure of the third stage is lower than the specified value, pressure relay 5YX1 is open, the signal relay coil 5XJ1 is excited, the contact 5XJ1 is open, BCJ1 is excited, leading to the accident shutdown.

In a word, all paths between the live wire and the null line should be searched to find out which controls are in the same path between the live wire and the null line, e.g. the pressure relay 2YX1 and the signal relay coil 2XJ1,the Pressure Relay 5YX1 and the signal relay coil 5XJ1, etc.

There are few elements, e.g. the signal relay coil 5XJ1 and the contact 5XJ1, are not in the same path, their control relations can be achieved through adding member variables respectively. There are many other types of circuit elements of which control functions are as similar as ones mentioned above in the ladder diagram.

Firstly, a graphical interface to design LD must be presented, as demonstrated in the following sections.

3. The Graphical Interface for LD

In the hydropower simulation system, which is developed with Microsoft c#.net, each circuit element is an user control. The relay coil and the contact, which are the main elements in LD, are taken as examples to illustrate the class structure of the circuit elements. Figure 2 shows the class diagram of the voltage relay coil and the current relay coil.

IRelay is the interface of all the types of the relay coils. VoltageRelay and CurrentRelay are two subclasses, The main attributes and methods of the Voltage- Relay are as follows:

_isExciting; // the excitation state of the coil

_standardVoltage; // the standard induced voltage of the coil

_currentVoltage; // the current voltage of the coil

_title; // an attribute to determine which contact is controlled by it SetState(); // set _isExciting of the coil

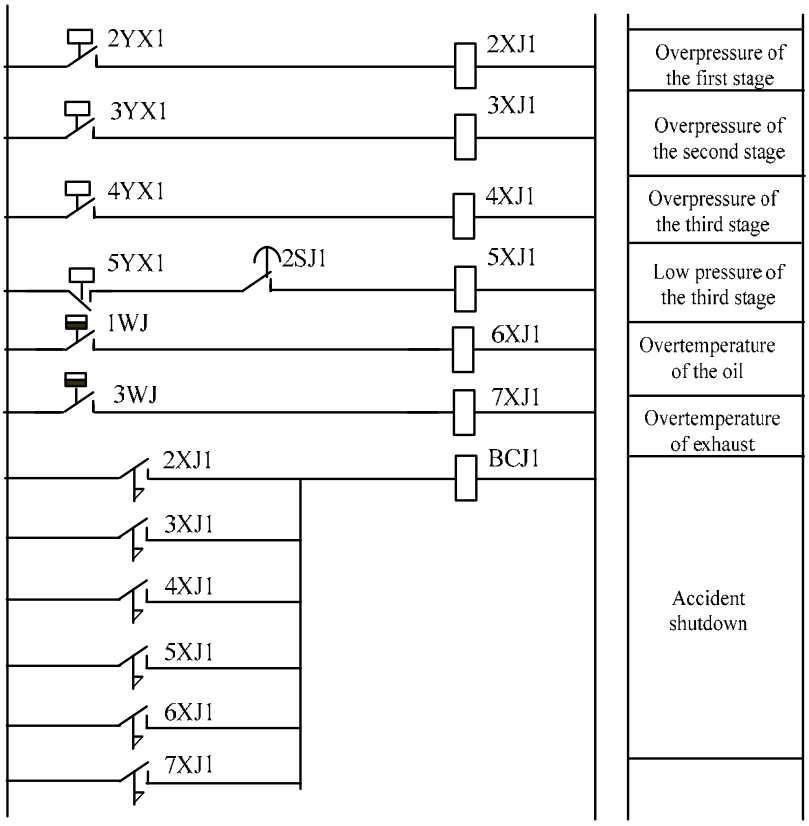

Figure 1. Accident shutdown control circuit of high-pressure compressor.

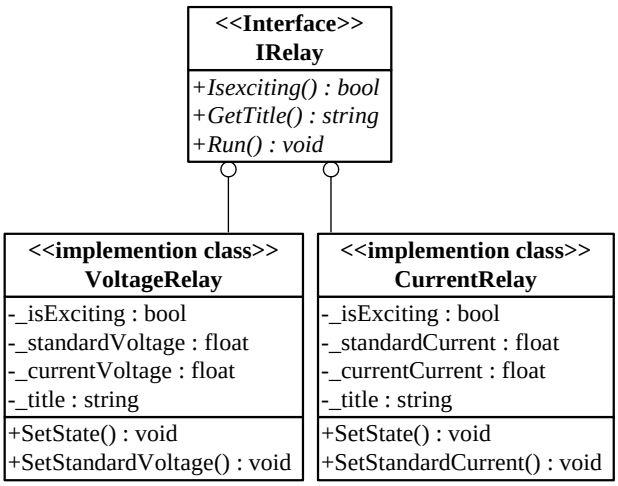

Figure 2. The class diagram of the relay coil.

SetStandardVlotage(); // set _standardVoltage of the coil

IsExciting(); // return the excitation state of the coil

GetTitle(); // return _title

Run(); // to judge whether the coil should be excited

The attributes and methods of CurrentRelay are similar to VoltageRelay. Figure 3 shows the class diagram of the contact. Its main attributes and methods are as follows:

_isConnect: // the state of the contact(open or closed)

_type: // the type of the contact(normally open or normally closed)

_title: // an attribute corresponding to the one in the relay coil, when they are equal,the contact is controlled by the coil

SetState(): // set _isConnect of the coil

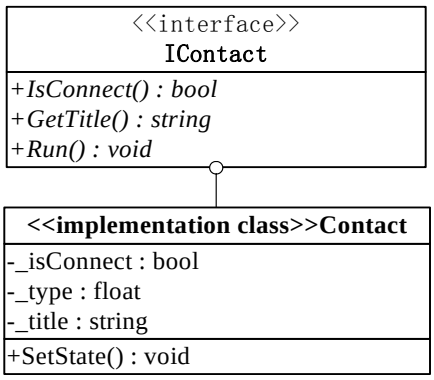

Figure 3. The class diagram of the contact.

The line is a special user control, connects two user controls, which are the member variables of the line: control1 and control2.These two member variables are also used in the all paths searching algorithm, as demonstrated in Section 4.

Besides the graphical interface of the circuit elements, the edit function for LD is also presented, of which the class diagram is shown in Figure 4. It is developed based on the command pattern, which encapsulates the detail of processing the messages. The functions of the controls such as adding, copying, cutting, moving and plastering can be performed through the menu or the shortcut keys. The function Add() of the menu is to add the user controls to the panel. Clicked() is to select an user control and generates the corresponding instance of the Command subclass, then call the function Execute() and sends the requirements to the control, which determines what to do. As mentioned above, based on the Command pattern, the details of the execution after sending a message is transparent for the menu.

Figure 5 shows the graphical interface corresponding to Figure 1, The right part of the interface is the library of circuit elements. After designing the interface, the control function of LD should be implemented, as presented in Section 4.

4. All Paths Searching Algorithm

As mentioned in Section 2.The main task to achieve the control function of LD is to search all the paths between and the live wire(LW) and the null line (NL), which can be implemented through conforming LD to an undigraph, as shown in Figure 6. ((R) represents the relay coil,(C) represents the contact). Each user control in the undigraph can be seemed as a vertex except the line, which is seemed as an edge. The line varible previousLine doesn't

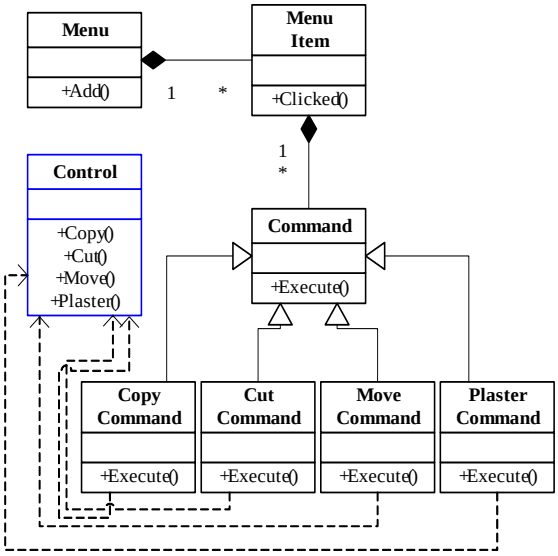

Figure 4. The class diagram of edit functions.

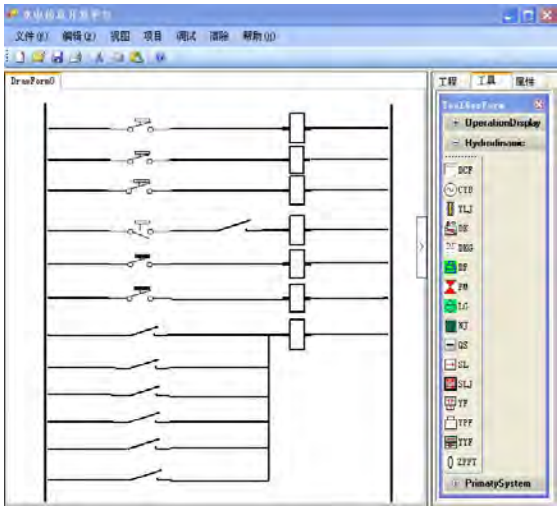

Figure 5. The graphical interface.

exist, but only for the algorithm.

Important variables and functions during the algorithm execution are as follows:

1) myStack: A stack variable, insert, remove and return the line varible at the top of itself (Its corresponding member functions are mystack. push(), mystack. pop() and mystack. peek()).

2) myHashtable: A hashtable variable, add or remove an element with the specified key and value (Its corresponding member functions are myHashtable.-add(), myHashtable.remove()), here the key and value are all line variables. The value is the immediate predecessor of the key which has been visited during the algorithm, each path can be extracted from myHashtable.

3) lineVisited: A table variable,includes two fields: the former is the line in the stack,the lattter is the immediate successor of the former and has been visited during the algorithm.The line variables can be inserted into or removed from lineVisited ((Its corresponding member functions are lineVisited.add(), lineVisited.re- move()).

4) tempControl: An user control variable,represents the user control being visited during the algorithm execution.

5) previousLine: A line variable, it doesn't exist in the LD but for the algorithm (previousLine. control1= null, previousLine.control2 = LW), as shown in Figure 6.

6) refresh (line, tempcontrol): Return an user control variable. The parameter line is a line varible, the parameter tempcontrol is an user control varible.If line.control1 = tempcontrol, return line.control2; else return line.control1.

The implementation of the algorithm is:

Step 1. Initialize the variables: myStack.push (previousLine), tempControl=LW. Goto Step2.

Step 2. If myStack is empty, then the algorithm ends, all paths are searched, else goto Step3.

Step 3.Search the immediate successor of myStack.-peek(), the successor must be not in myStack and not in lineVisited as the second field value with the first field value of myStack.peek(), if it exist (we suppose it named as templine), goto step4; else goto step7.

Step 4. lineVisited.Add (mystack.peek(), templine), myHashtable.add(templine, mystack.peek()), myStack. push (tempLine), tempControl=refresh(templine, temp-Control). Then if tempControl is LW,goto step5, else if tempControl is NL, goto step6, else goto step2.

Step 5. Remove the elements from lineVisited with the first field value of mystack.peek(),and if mystack. peek() isn't previousLine, remove the elements from myHash-table with the key of myStack.peek().Refresh (myStack. peek(), tempControl), myStack.pop(), go to step2.

Step 6. A path is searched and can be extracted from myHashtable, if myStack.peek() isn't previousLine, remove the elements from myHashtable with the key of myStack.peek(). tempControl = Refresh(mystack.peek(), tempControl), myStack.pop(), go to step2.

Step 7. Remove the elements from lineVisited with the first field value of mystack.peek(), and if mystack. peek() isn't previousLine, remove the elements from myHashtable with key of myStack.peek(). tempControl =Refresh (mystack.peek(), tempControl), mystack.pop(), go to step2.

5. The Application Example and Analysis

As mentioned that the control function of LD should be implemented based on object-oriented thought. The running module which is irrelated to the edit environment, receiving the messages from the circuit elements, is to implement the control function.

The edit environment transfers all the paths searched with the algorithm to the running module, and when the state of the circuit element changes, it sends the corresponding message (including some attributes) to the module. After transformed to an undigraph in Figure 6, LD in Figure 1 is taken as an example to illustrate the whole process. Paths searched between live wire and null line with the algorithm are as follows:

Path1: LW-2YX1-2XJ1(R)-NL.
Path2: LW-3YX1-3XJ1(R)-NL.
Path3: LW-4YX1-4XJ1(R)-NL.
Path4: LW-5YX1-2SJ1-5XJ1(R)-NL.
Path5: LW-1WJ-6XJ1(R)-NL.
Path6: LW-3WJ-7XJ1(R)-NL.
Path7: LW-2XJ1(C)-BCJ1(R)-NL.
Path8: LW-3XJ1(C)-BCJ1(R)-NL.
Path9: LW-4XJ1(C)-BCJ1(R)-NL.
Path10: LW-5XJ1(C)-BCJ1(R)-NL.
Path11: LW-6XJ1(C)-BCJ1(R)-NL.
Path12: LW-7XJ1(C)-BCJ1(R)-NL.

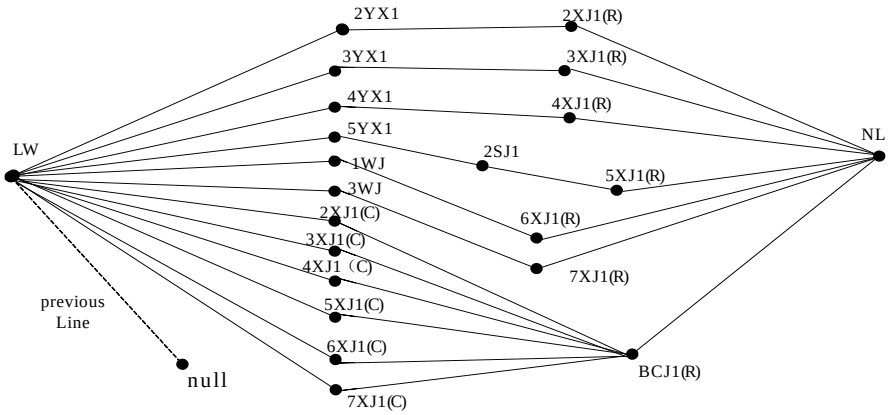

Figure 6. The undigraph corresponding to LD in Figure 1.

Table 2. The Longest Running Time According to the Number of the Control Elements.

The Number of the Control Elements	30	40	50	60	70	80	90
The Max Number of the Paths Searched	14	17	29	44	69	73	76
The Longest Running Time/ms	21.5	28.7	39.2	57.4	79.8	111.5	144.1

When the pressures of the first stage is higher than the specified value, the pressure relay 2YX1 is open and sends a message including three attributes: its name (2YX1), control type(pressure relay) and state (open) to the running module. After receiving the message including some attributes, operations of the module are that: finds the path 2YX1 is in(path1), if there is an relay coil in path1(2XJ1(R)), it should be excited, and then, 2XJ1 (R) sends a message including its name, control type, state and _title, the module finds out the contact controlled by 2XJ1(R) from the user controls of all the paths: 2XJ1(C)(If there are many contacts controlled by 2XJ1(R), they all send messages to the running module), 2XJ1(C) sends a message, the module finds out 2XJ1(C) is in path7 and judges whether other contacts in path7 are all open, here there is only one and is open, the relay coil in path7(BCJ1) should be excited, send a message to the module, and lead to the accident shutdown. What should be noticed is that if there are many messages received, the module complies with FIFO rule.

From the process above, it proves the validity of the algorithm and its essence is to search all the paths between two vertices. The algorithm excludes the loops with the table varible: lineVisited, and store the paths with the hashtable varible: myHashtable. Generally, there are 30-90 control elements in the LD. Table 2 shows the longest running time with the proposed algorithm according to the maximum number of the paths searched with different number of control elements. (It runs on a platform of Core (TM)2 CPU with 512 Megabytes memory). When there are 90 control elements and 76 paths, the longest running time is no more than 150ms, so it can be concluded that the LD system can meet the real-time request in the hydropower simulation system.

6. Conclusions

In this paper, a method to design an interface for LD is presented with typical class diagrams and the graphical interface, then an algorithm is proposed to implement the control function of LD through transforming LD to an undigraph and search all the paths between LW and NL. The application example and the analysis verify the validity of the algorithm. The running time is shown at last, it proves that the LD system with the algorithm can meet the real-time request in the Hydropower simulation system.

7. Acknowledgements

The authors are grateful to the support of the Cultivation Fund of the Key Scientific and Technical Innovation Project, Ministry of Education of China (NO.708026) and would like to thank personnel of Embedded Key Lab at Northeastern University for their help.

8. References

[1] P. Sanderson, W. B. L. Wong, S. Choudhury, and R. Memisevic, “Hydro scheme control in a deregulated en-

vironment: Cognitive work models and design implications," Annual Meeting of the Human Factors and Ergonomics Society, Santa Monica, CA, 2003.

[2] J. R. Hajdukiewicz and K. J. Vicente, "What does computer- mediated control of a thermal-hydraulic system have to do with moving your jaw to speak?" Ecological Psychology, Vol. 16, No. 4, pp. 255−285, 2004.

[3] R. Memisevic, P. Sanderson, S. Choudhury, and W. Wong, "A low-cost, easy-to-use, real-time power system simulator," in Proceedings of International Conference on Power and Energy Systems, Clearwater Beach, FL, 2004.

[4] Y. Su, H. Zhao, W. J. Su, and Y. Xu, "GHS: Research and application of grid based hydroelectrical simulation system platform," Journal of System Simulation, Vol. 17, No. 5, pp. 1230−1233, 2004.

[5] E, R. R. Kato, O. Morandin Jr., P. R. Politano, and H. A. Camargo, "A modular modeling approach for CNC machines control using Petri nets," in Proceedings of International Conference on Systems, Man and Cybernetics, Nashville, TN, Vol. 5, pp. 3417−3152, 2000.

[6] J.-L. Chirn and D. C. Mcfarlane, "Petri net based design of ladder logic diagram," Working paper, Institute for manufacturing, University of Cambridge, UK, 2000.

[7] H. S. Kim, W. H. Kwon, and N. Chang, "A translation method for ladder diagram with application to a manufacturing process," in Proceedings of International Conference on Robotics and Automation, Vol. 1, pp. 793−798, 1999.

[8] X. L. Cui and Z. C. Zhou, "The algorithm of transformation between the ladder language and the sentence table language of PLC," Microelectronics and Computer, China, Vol. 1, No. 17, pp. 26−30, 2000.

Appendix

The algorithm excution in another complex undigraph with two loops is demonstrated as follows: the thick edges represents the lines in myStack, the white vertex represents the variable tempControl.

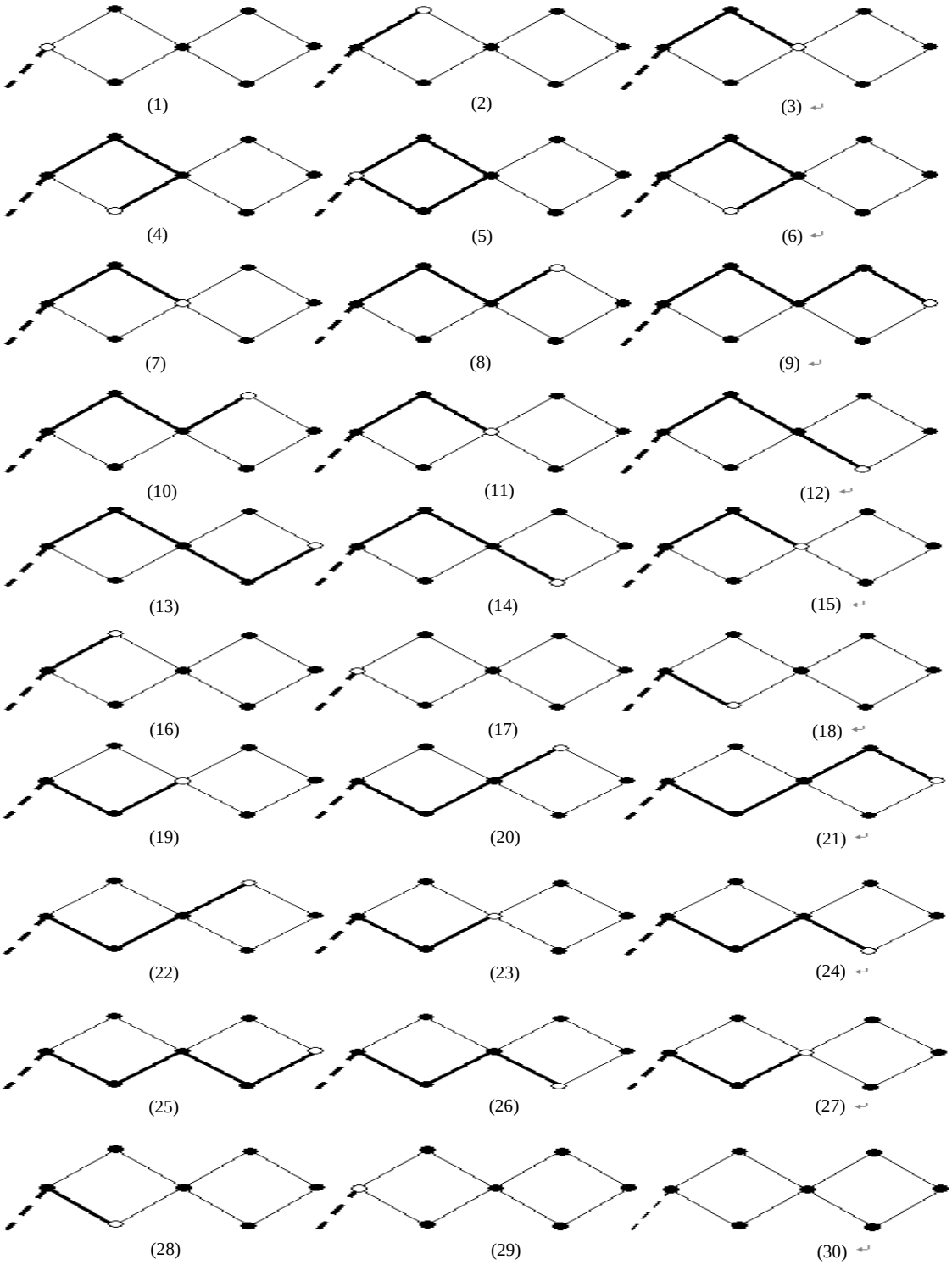

The 6th International Conference on Wireless Communications, Networking and Mobile Computing

September 23–25, 2010, Chengdu, China
http://www.wicom-meeting.org/2010

Call For Papers

WiCOM serves as a forum for wireless communications researchers, industry professionals, and academics interested in the latest development and design of wireless systems. In 2010, **WiCOM** will be held in **Chengdu**, China. You are invited to submit papers in all areas of wireless communications, networking, mobile computing and applications.

Wireless Communications

- B3G and 4G Technologies
- MIMO and OFDM
- UWB
- Cognitive Radio
- Coding, Detection and Modulation
- Signal Processing
- Channel Model and Characterization
- Antenna and Circuit

IMPORTANT DATES

Paper due:	March 10, 2010
Acceptance Notification:	May 10, 2010
Camera-ready due:	May 31, 2010

Network Technologies

- Ad hoc and Mesh Networks
- Sensor Networks
- RFID, Bluetooth and 802.1x Technologies
- Network Protocol and Congestion Control
- QoS and Traffic Analysis
- Network Security
- Multimedia in Wireless Networks

Services and Application

- Applications and Value-Added Services
- Location based Services
- Authentication, Authorization and Billing
- Data Management
- Mobile Computing Systems

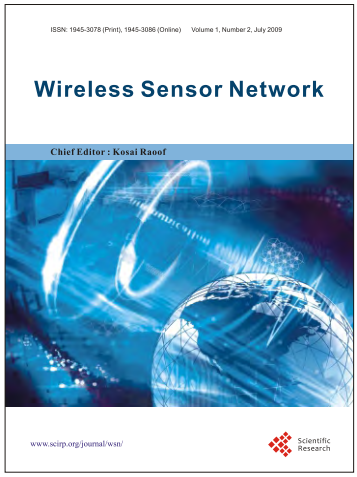

Wireless Sensor Network (WSN)

Call For Papers

http://www.scirp.org/journal/wsn

ISSN 1945-3078 (Print) ISSN 1945-3086 (Online)

WSN is an international refereed journal dedicated to the latest advancement of wireless sensor network and applications. The goal of this journal is to keep a record of the state-of-the-art research and promote the research work in these areas.

Editor-in-Chief

Dr. Kosai Raoof , GIPSA LAB, University of Joseph Fourier, Grenoble, France

Subject Coverage

This journal invites original research and review papers that address the following issues in wireless sensor networks. Topics of interest are (but not limited to):

- Network Architecture and Protocols
- Self-Organization and Synchronization
- Quality of Service
- Data Processing, Storage and Management
- Network Planning, Provisioning and Deployment
- Integration with Other System
- Software Platforms and Development Tools
- Routing and Data Dissemination
- Energy Conservation and Management
- Security and Privacy
- Developments and Applications
- Network Simulation and Platforms

We are also interested in short papers (letters) that clearly address a specific problem, and short survey or position papers that sketch the results or problems on a specific topic. Authors of selected short papers would be invited to write a regular paper on the same topic for future issues of the WSN.

Notes for Intending Authors

Submitted papers should not have been previously published nor be currently under consideration for publication elsewhere. Paper submission will be handled electronically through the website. All papers are refereed through a peer review process. Authors are responsible for having their papers checked for style and grammar prior to submission to WSN. Papers may be rejected if the language is not satisfactory. For more details about the submissions, please access the website.

Website and E-Mail

http://www.scirp.org/journal/wsn

Email: wsn@scirp.org

Call for Papers

International Journal of

Communications, Network and System Sciences (IJCNS)

ISSN 1913-3715 (Print) ISSN 1913-3723 (Online)

http://www.scirp.org/journal/ijcns/

IJCNS is an international refereed journal dedicated to the latest advancement of communications and network technologies. The goal of this journal is to keep a record of the state-of-the-art research and promote the research work in these fast moving areas.

Editors-in-Chief

Subject Coverage

This journal invites original research and review papers that address the following issues in wireless communications and networks. Topics of interest include, but are not limited to:

MIMO and OFDM technologies	Sensor networks
UWB technologies	Ad Hoc and mesh networks
Wave propagation and antenna design	Network protocol, QoS and congestion control
Signal processing and channel modeling	Efficient MAC and resource management protocols
Coding, detection and modulation	Simulation and optimization tools
3G and 4G technologies	Network security

We are also interested in:

- Short reports—Discussion corner of the journal:
  2-5 page papers where an author can either present an idea with theoretical background but has not yet completed the research needed for a complete paper or preliminary data.
- Book reviews—Comments and critiques.

Notes for Intending Authors

Submitted papers should not have been previously published nor be currently under consideration for publication elsewhere. Paper submission will be handled electronically through the website. All papers are refereed through a peer review process. For more details about the submissions, please access the website.

Website and E-Mail

http://www.scirp.org/journal/ijcns ijcns@scirp.org

Int. J. Communications, Network and System Sciences, 2009, 4, 249-324
Published Online July 2009 in SciRes (http://www.SciRP.org/journal/ijcns/).

TABLE OF CONTENTS

Volume 2 Number 4 **July 2009**

ISSN: 1913-3715
9771913371005 08